BioMed Research International

Conventional and Unconventional Use of Lasers in Skin Disorders

Guest Editors: Silvia Moretti, Michael S. Kaminer, Anne Le Pillouer-Prost, and Piero Campolmi

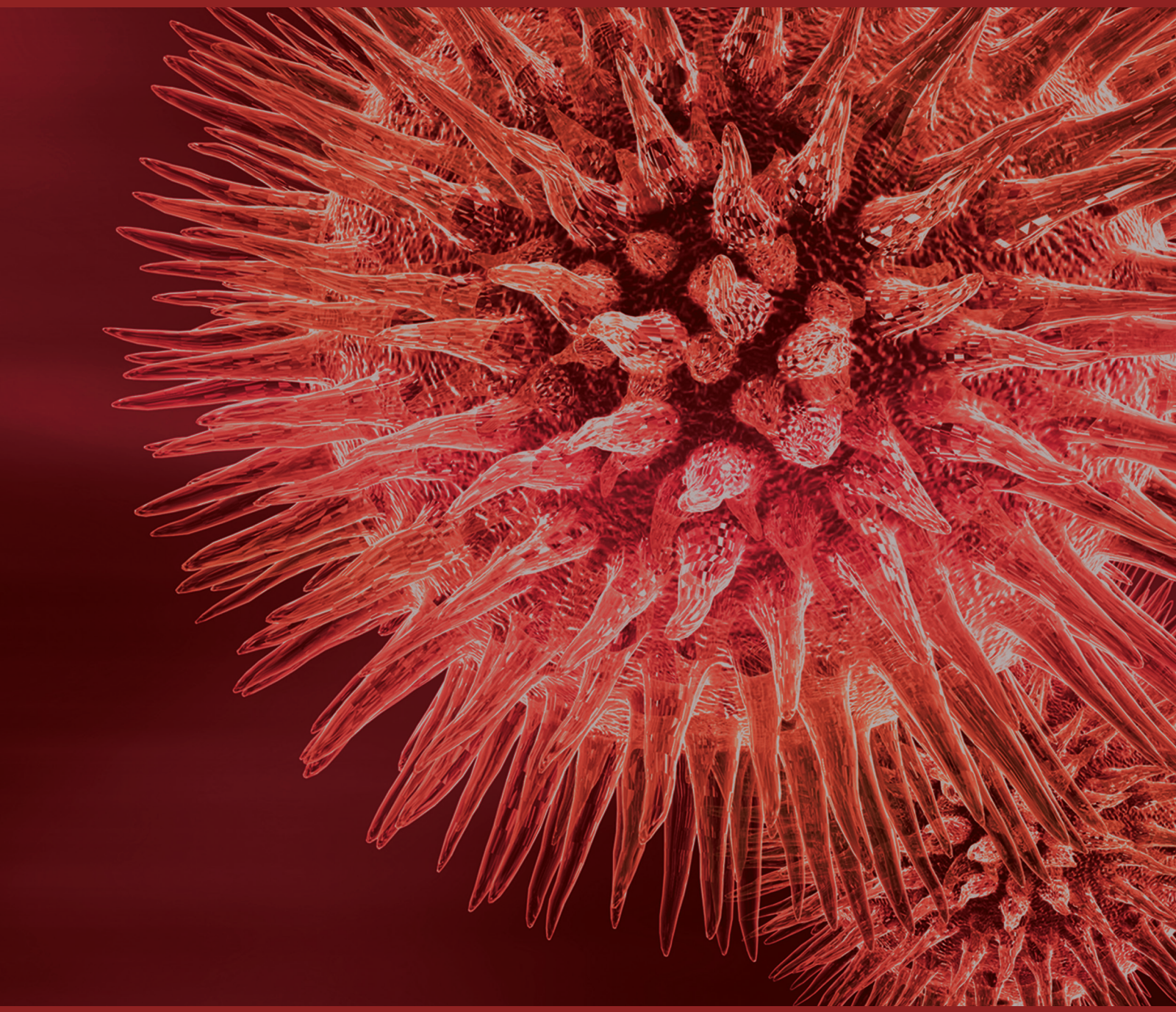

Conventional and Unconventional Use of Lasers in Skin Disorders

BioMed Research International

Conventional and Unconventional Use of Lasers in Skin Disorders

Guest Editors: Silvia Moretti, Michael S. Kaminer, Anne Le Pillouer-Prost, and Piero Campolmi

Contents

Hindawi Publishing Corporation
BioMed Research International
Volume 2015, Article ID 934931, 2 pages
http://dx.doi.org/10.1155/2015/934931

Editorial

Conventional and Unconventional Use of Lasers in Skin Disorders

Silvia Moretti,[1] Michael S. Kaminer,[2,3] Anne Le Pillouer-Prost,[4] and Piero Campolmi[5]

[1]*Section of Dermatology, Department of Surgery and Translational Medicine, University of Florence, Ospedale Piero Palagi, Viale Michelangelo 41, 50125 Florence, Italy*
[2]*SkinCare Physicians, Inc., 1244 Boylston Street, Chestnut Hill, MA, USA*
[3]*Yale School of Medicine, New Haven, CT 06510, USA*
[4]*Hôpital Prive Clairval, 317 boulevard du Redon, 13009 Marseille, France*
[5]*Dermatology Clinic, Department of Surgery and Translational Medicine, University of Florence, Ospedale Piero Palagi, Viale Michelangelo 41, 50125 Florence, Italy*

Correspondence should be addressed to Silvia Moretti; silvia.moretti@unifi.it

Received 14 December 2014; Accepted 14 December 2014

Over the last 50 years, laser sources have been used in many skin diseases, and their role has been increasing in most fields of dermatology. At present, laser technology allows us to treat a variety of skin conditions, either inflammatory or neoplastic, in addition to aesthetic problems.

Hence, in the last few years, surgical, vascular, selective, and other lasers have become more popular. A significant advantage of lasers is their ability to provide "noncontact surgery," since lesion vaporization occurs without any physical contact between skin and the device. This assures sterilization and helps avoid possible infections.

The different types of laser treatments have been expanding as well as laser technology.

A better understanding of interactions between laser radiation and tissues has made lasers more powerful and selective for each type of lesion and aesthetic problem. Due to the specific properties of selective photothermolysis, lasers exert effects strictly limited to the treated area, avoiding any damage to the surrounding skin. This unique attribute of lasers allows physicians to treat even very small skin lesions with excellent aesthetic results.

In particular, in the vascular field, dye lasers have become the gold standard in treating superficial vascular disease and are excellent for treating large lesions such as port wine stains. Pulsed dye lasers are also useful tools for the so-called unconventional treatments, such as hypertrophic scars, keloids, superficial basal cell carcinoma, and common warts. ND-Yag lasers are used for treating deep vascular lesions and hair removal. In addition, these two lasers can also be employed effectively in combination on difficult lesions, as reported by K. Vas et al., showing that sequential combined treatment with both dye and ND-Yag lasers is satisfactory for surgical scars.

Another popular device is the Q-switched laser, which is effective and safe for removal of benign pigmented lesions and tattoos since it interacts with the dermal structures holding exogenous pigment.

Tattoo removal may be associated with a number of cutaneous side effects, such as inflammatory or rare neoplastic skin reactions, which are described by A. Bassi et al. They highlight that early diagnosis is essential for proper treatment. Intense pulsed light is a versatile tool suitable for many different skin conditions thanks to its wide range of wavelengths, and unconventional uses are exhaustively discussed by D. Piccolo et al.

The constant improvement in laser devices and technology results in the need for continuous training and evolving knowledge. For example, A. Soriani et al. highlight this concept with a study that examines the power loss of laser beams induced by various types of tissue. Since laser penetration is closely related to laser settings such as wavelength and spot diameter, they evaluate these variables in order to accurately

determine the fraction of released energy in order to obtain better clinical results.

Due to the increasing need for noninvasive technology for diagnosis, therapy, and follow-up, high resolution tools such as nonlinear optical microscopy and two-photon fluorescence microscopy are in depth presented by R. Cicchi et al. They evaluate possibilities to monitor the effect of therapy and topical absorption.

Since the 1970s, photodynamic therapy aroused a growing interest in treating several skin diseases. E. Filonenko et al. evaluate the effectiveness of this treatment for penile in situ carcinoma, obtaining satisfactory oncological results without affecting patient quality of life. In addition, X. Wang et al. emphasize that these therapies may require long application times so that the use of an automatic medical manipulator system can increase the radiation uniformity and ensure a better therapeutic result.

Due to the growing importance of laser techniques in dermatologic practice, ongoing multicenter studies will be valuable in helping us develop precise standardization of parameters used for each laser and each disease. This will improve the effectiveness of the tools and allow physicians to obtain better and more reproducible results.

Silvia Moretti
Michael S. Kaminer
Anne Le Pillouer-Prost
Piero Campolmi

Hindawi Publishing Corporation
BioMed Research International
Volume 2015, Article ID 245080, 4 pages
http://dx.doi.org/10.1155/2015/245080

Research Article

Own Experience in Treatment of Patients with Penile Cancer Using Photodynamic Therapy

Elena Filonenko, Andrey Kaprin, Boris Alekseev, and Antonina Urlova

P.A. Herzen Moscow Cancer Research Institute, 2nd Botkinskiy Proezd 3, Moscow 125284, Russia

Correspondence should be addressed to Elena Filonenko; derkul23@yandex.ru

Received 24 April 2014; Revised 7 August 2014; Accepted 26 August 2014

Academic Editor: Michael S. Kaminer

Penile cancer is a rare pathology. For penile cancer surgical treatment, radiotherapy, chemotherapy, and combined modality treatment are available. Because of great importance of this organ for mental condition of patient, the development of organ-preserving methods allowing to minimize impact on patient's quality of life without compromising of oncological results is desirable. In the Center of Laser and Photodynamic diagnosis and treatment of tumors in P.A. Herzen Moscow Cancer Research Institute the methods of photodynamic therapy in patients with penile cancer have been developed. From 2011 to 2013 the treatment was conducted in 11 patients with precancer and cancer of penile. The average age was 56.6. According to morphological diagnosis photodynamic therapy (PDT) was performed using two methods. One method included topical application of agent for PDT and the second intravenous administration of photosensitizer. For topical application alasens was used and for intravenous injection we applied radachlorine. All patients had no complications. Complete regression was achieved in 9 patients, and partial regression in 2. Thus, the results showed that photodynamic therapy for penile cancer stage Tis-1N0M0 permits performing organ-preserving treatment with satisfactory oncological results and no impairment of patient's quality of life.

1. Introduction

Penile cancer is a rare pathology [1]. In 2012 in Russia 493 new cases were registered [2]. The average age of patients accounts for 62.3. Increase of incidence occurs from 45 years with maximal rates in patients of 60–64 years old. For penile cancer surgical treatment, radiotherapy, chemotherapy, and combined modality treatment are available. Due to its rarity and the consequent lack of randomized trials, current therapy is based on retrospective studies and small prospective trials [3]. Surgical treatment includes resection, amputation at the level of pubic symphysis with perineal urethrostomy, emasculation, degloving, and Ducuing surgery for regional lymph node metastases. Penile amputation with following reconstruction becomes widespread. A partial and glans-sparing penectomy provides psychosocial benefits, preserves sexual function, and is generally feasible for a T1 tumor [4]. Total penectomy is preferred for ≥T2 tumors, although some T2 tumors are amenable to partial penectomy based on location. Penile-sparing surgical modalities including Mohs' micrographic surgery and laser ablation are considered for small tumors, particularly if located on the glans and margins ≥3 mm can be attained [5]. Radiotherapy is used as option of organ-preserving treatment. Chemotherapy is performed in combination with other methods. For radiotherapy there is a high risk of radiation-induced effects; surgery is also associated with risk of postoperative complications. Because of great importance of this organ for mental condition of patient, the development of organ-preserving methods allowing to minimize impact on patient's quality of life without compromising of oncological results is desirable. Penile preservation is superior in functional and cosmetic outcomes and should be offered as a primary treatment modality in men with low stage penile cancer [6].

2. Material and Methods

In the Center of Laser and Photodynamic diagnosis and treatment of tumors in P. A. Herzen Moscow Cancer Research Institute the methods of photodynamic therapy in patients with penile cancer have been developed. From 2011 to 2013 the treatment was conducted in 11 patients with precancer and

Table 1: Patients' distribution according to age.

Number of patients	Age of patients, y.o.						Total
	20–30	31–40	41–50	51–60	61–70	71–80	
Abs.	1	0	3	2	3	2	11
%	9.0	0	27.3	18.2	27.3	18.2	100%

Table 2: Patients' distribution according to histological type of tumor.

Morphological diagnosis	Number of patients	
	Abs.	%
Dysplasia grade III	1	9.1
Erythroplasia of Queyrat	4	36.4
Squamous cell carcinoma T1-2N0M0	5	45.4
Paget's cancer	1	9.1
Total	**11**	**100%**

cancer of penile. The age of patients accounted for 25 to 74 y.o. The average age was 56.6 (Table 1).

Prior to photodynamic therapy all patients had biopsy of penile lesions. According to histological type of tumor there were the following diagnoses: dysplasia grade III was in 1 patient, erythroplasia of Queyrat in 4, squamous cell carcinoma in 5 (stage T1N0M0 in 4, T2N0M0 in 1), and Paget's cancer of root of penis and scrotal skin in 1 (Table 2).

Erythroplasia of Queyrat ($n = 2$ patients) and squamous cell carcinoma of glans penis stages I-II ($n = 2$ patients) were diagnosed at first presentation in 4 patients; in the other 7 patients the interval between first presentation and accurate diagnosis accounted for up to 1 year (in 5 patients), up to 2 (in 1), and 3.5 (in 1). All 7 patients underwent nonefficient treatment with ointment by dermatologists or urologists with no morphological diagnosis during the interval. All patients had negative inguinal lymph nodes.

Primary, untreated tumor occurred in 9 patients, continued growth after chemoradiotherapy in 2, and recurrence 1 year after circumcision in 1. Eight patients had single lesion and in 3 from 2 to 3 lesions.

In 2 patients with continued growth after chemoradiotherapy, one had 1 tumor lesion 2.5 cm in size and with area of 3.75 cm^2; the second had 3 tumor lesions with maximal size of 1.8 cm and total area of 4.5 cm^2. One patient with recurrent tumor after circumcision had a single lesion with maximal size of 4.0 cm and area of 8 cm^2.

For group of patients ($n = 6$) with previously untreated single tumor, in 3 patients maximal size of lesion was from 1 to 2 cm and in 3 from 3.0 to 4.5 cm. The area of tumor accounted for 1 cm^2 to 1.5 cm^2 in 2 patients; from 3 to 4.5 cm^2 in 1; and from 7 to 11.3 cm^2 in 3. For group of patients ($n = 2$) with previously untreated 2 and 3 lesions, maximal size of the largest lesion was 3.0 and 4.0 cm and total area of all lesions 10.4 cm^2 and 7 cm^2, respectively (Table 3).

In 9 patients penile lesion was the only cancer disease and in 2 one of primary multiple metachronous oncological processes. One of them had previous successful treatment for Kaposi's sarcoma and another one prostate cancer stage II.

Seven of 11 patients had various comorbidities: chronic obstructive lung disease, previous myocardial infarction and postinfarction cardiosclerosis, asthma, essential hypertension 1 degree, asthma combined with gastric ulcer, multiple hepatic haemangioma and bilateral renal cysts, chronic gastritis, renal cysts, and nerve deafness.

According to morphological diagnosis photodynamic therapy (PDT) was performed using two methods. One method included topical application of agent for PDT and the second intravenous administration of photosensitizer. For topical application alasens was used (agent based on 5-aminolevulinic acid) (NIOPIK, Russia) and for intravenous injection we applied radachlorine (photosensitizer based on chlorine e6) (Radapharma, Russia). After the completion of exposure time specific for each photosensitizer (for alasens-induced PPIX and for radachlorine—3 h), a session of fluorescence diagnostics with evaluation of area of tumor and planning of laser irradiation fields was performed.

Fluorescence diagnosis was performed by visual assessment and by local fluorescence spectroscopy. For visual assessment of fluorescence image video-assisted fluorescence device (BioSpec, Russia) was used. After registration the fluorescence image was recorded in computer for subsequent analysis of type and boundaries of tumor lesion for planning of laser fields for PDT [7]. After visual assessment of fluorescence image local fluorescence spectroscopy was performed using laser electronic spectrum analyzer for fluorescence diagnosis LESA-01-BioSpec (BioSpec, Russia). Accumulating levels of photosensitizer in tumor and normal tissue and value of tumor/normal tissue fluorescence contrast were measured (Figure 1).

Then PDT session was performed. In all cases laser irradiation of tumor was performed after premedication and spinal anaesthesia. Laser irradiation was performed using macrolenses and lasers with wavelength according to peak of photosensitizer absorption: for alasens-induced PPIX—630 nm and for radachlorine—662 nm (Figure 2). The light dose accounted for 200 to 350 J/cm^2. To prevent urinary retention because of edema in the treatment area urinary catheter was placed in all patients and was removed within 1-2 days after treatment.

3. Results

All patients had no complications. There were no urinary retention after removal of catheter and no complications related to skin photosensitivity.

Complete regression was achieved in 9 patients (all 8 patients with primary tumor and 1 with recurrence) and

Table 3: Patients' distribution according to tumor characteristics and lesion area.

Tumor characteristics	Area of lesion, cm^2			Total, abs. (%)
	≤1.5	3–4.5	7–11.3	
Untreated tumor	2	1	5	8 (72.7)
Recurrent/residual tumor	0	2	1	3 (27.3)
Total, abs. (%)	**2 (18.2%)**	**3 (27.3)**	**6 (54.5)**	**11 (100%)**

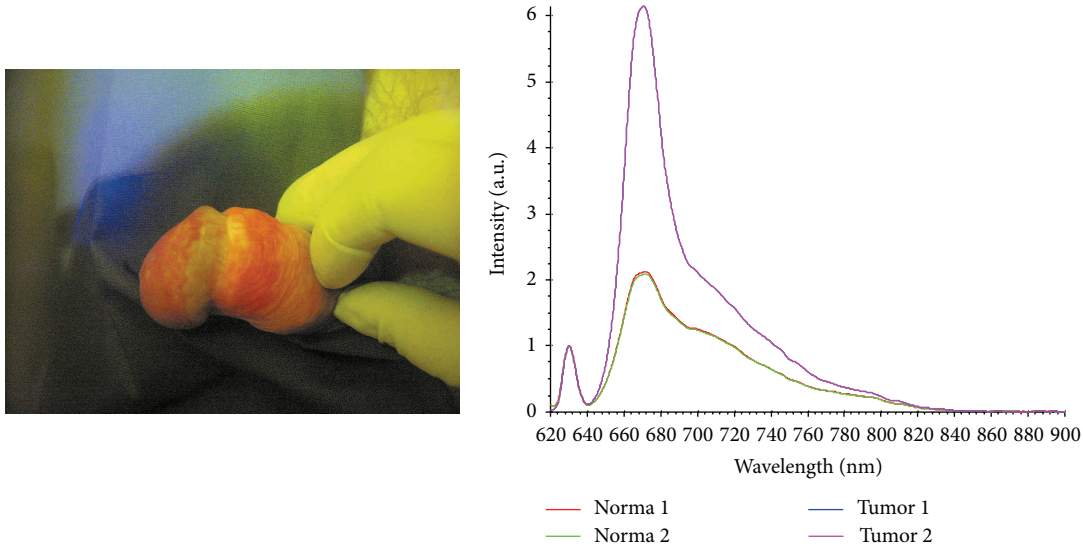

(a) (b)

Figure 1: Session of fluorescence diagnosis: (a) visual assessment of fluorescence image; (b) local fluorescent spectroscopy (red curve—tumor fluorescence profile; green—normal tissue).

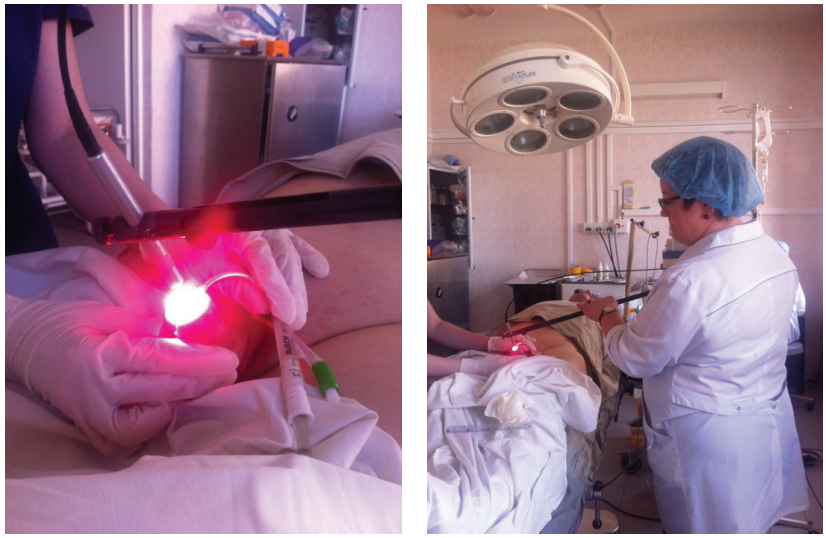

(a) (b)

Figure 2: PDT session (a, b).

partial regression in 2. Two patients with recurrent tumors after external radiotherapy and partial regression after PDT underwent surgical treatment 3 months after PDT.

In other 9 patients the follow-up period was from 5 to 32 months. All patients underwent physical examination, biopsy of lesion, ultrasonography of penis, and regional lymph nodes every 3 months for the first year, every 6 months for the second year, and then annually. Recurrence occurred 20 months later in PDT area in one patient who had first PDT for recurrent tumor after surgical treatment. Another patient had

recurrence of disease as new lesion beyond PDT area which was diagnosed and successfully treated with PDT 9 months after first course of treatment. For 11 months the patient had no recurrence after second course of PDT.

4. Conclusion

Thus, photodynamic therapy for penile cancer stage Tis-1N0M0 permits to perform organ-preserving treatment with satisfactory oncological results with no impairment on patient's quality of life. We suggest that photodynamic therapy should be recommended for Tis tumors. Because of small case number our recommendations for photodynamic therapy in patients with T1 tumors require further investigations.

Conflict of Interests

The authors declare that there is no conflict of interests regarding the publication of this paper.

References

[1] M. C. G. Bleeker, D. A. M. Heideman, P. J. F. Snijders, S. Horenblas, J. Dillner, and C. J. L. M. Meijer, "Penile cancer: epidemiology, pathogenesis and prevention," *World Journal of Urology*, vol. 27, no. 2, pp. 141–150, 2009.

[2] A. D. Kaprin, V. V. Starinskiy, and G. V. Petrova, Eds., *Malignant Neoplasms in Russia in 2012 (incidence and mortality)*, Moscow, Russia, 2014.

[3] M. Shabbir, R. Barod, P. K. Hegarty, and S. Minhas, "Primary prevention and vaccination for penile cancer," *Therapeutic Advances in Urology*, vol. 5, no. 3, pp. 161–169, 2013.

[4] A. S. Feldman and W. S. McDougal, "Spatio-temporal variation of $PM_{2.5}$ concentrations and their relationship with geographic and socioeconomic factors in China," *Journal of Urology*, vol. 186, no. 4, pp. 1303–1307, 2014.

[5] G. Sonpavde, L. C. Pagliaro, C. Buonerba, T. B. Dorff, R. J. Lee, and G. di Lorenzo, "Penile cancer: Current therapy and future directions," *Annals of Oncology*, vol. 24, no. 5, pp. 1179–1189, 2013.

[6] P. K. Hegarty, I. Eardley, A. Heidenreich et al., "Penile cancer: organ-sparing techniques," *BJU International*, 2013.

[7] V. B. Loschenov, K. G. Linkov, T. A. Savelieva, M. V. Loschenov, S. S. Model, and A. V. Borodkin, "Hardware and tool equipment for fluorescence diagnostics and photodynamic therapy," *Photodynamicheskaya Terapiya i Photodiagnostika*, vol. 1, pp. 17–25, 2013.

Hindawi Publishing Corporation
BioMed Research International
Volume 2014, Article ID 151969, 5 pages
http://dx.doi.org/10.1155/2014/151969

Research Article

Physical and Dosimetric Optimization of Laser Equipment in Dermatology: A Preliminary Study

A. Soriani,[1] D. D'Alessio,[1] V. Cattelan,[1] N. Cameli,[2] M. Mariano,[2] S. Ungania,[1] M. Guerrisi,[3] and L. Strigari[1]

[1] *Medical Physics Laboratory, Regina Elena National Cancer Institute, 00144 Rome, Italy*
[2] *Department of Dermatology, San Gallicano Institute, 00144 Rome, Italy*
[3] *Department of Physics, Tor Vergata University, 00173 Rome, Italy*

Correspondence should be addressed to A. Soriani; soriani@ifo.it

Received 25 April 2014; Revised 30 July 2014; Accepted 30 August 2014; Published 15 September 2014

Academic Editor: Silvia Moretti

The aim of this preliminary study is to investigate the correlation between clinical set-up at present used in the treatment of specific skin conditions and laser beam absorbed power in the tissue. This study focused on the CO_2 and Nd-Yag laser equipment used in the daily clinical practice in the Department of Dermatology of San Gallicano Institute in Rome. Different types of tissue-equivalent material with various water and haemoglobin concentrations were tested to evaluate laser beam attenuation power. In particular, thinly sliced pork loin, of uniform consistency and without fat, was selected for its high content of haemoglobin to mimic human tissues. An optical power meter was used to measure the power or energy of a laser beam. During measurements, the tissue equivalent phantoms were positioned on the detector head and the laser beam was orthogonally oriented. The results of two experimental set-ups are reported here. The dependence of residual power (W) as a function of *ex vivo* tissue thickness (mm) for different laser output powers was studied. Data were fitted by a parametric logistic equation. These preliminary data allow for more accurately determining the energy fraction released from lasers to the tissues in order to improve clinical outcomes.

1. Introduction

Over the last 50 years, lasers have been used to treat a large variety of skin conditions, either inflammatory or neoplastic, in cosmetic and aesthetic dermatology.

These treatments use different laser types classified according to their tissue target and/or tissue interaction. On the basis of this classification, the most commonly used lasers in dermatology are ablative lasers (CO_2-Erbium), vascular lasers (Nd-Yag, KTP, and PDL), and pigment lasers (Q-switched Nd-Yag, Rubino, and Alexandrite). Through their selective targeting of skin chromophores these lasers have become the treatment of choice for a wide range of cutaneous lesions including angiomas, telangiectasias, lentigo, tattoos, and acne scars and wrinkles [1, 2].

The ever improving design and technology of lasers result in increased safety and efficacy for patients; nonetheless, continuous training and an evolving knowledge are needed. In fact, the penetration of radiation is closely linked to the laser characteristics and to operative conditions. Short-pulse high-peak power (Q-switched or mode-locking) lasers produce high irradiance in a short time, while traditional continuous or long pulsed lasers imply shorter exposures repeated over prolonged time periods. These different mechanisms are likely to produce, on the irradiated tissues, different biological effects that should be taken into consideration to avoid irreversible damage as well as to reduce any potential hazard.

In daily clinical practice, the wavelength alone is perhaps less of a determining factor as far as depth of penetration is concerned—with respect to type of emitter and operating mode, physical design of the applicator, and adopted technique. A working knowledge of tissue targets and light-tissue interaction is essential to use laser appropriately as well as to interpret clinical laser parameters. As a matter of fact, the clinical applications of the laser depend on wavelength

peaks of the laser light, pulse durations, and target skin tissue absorption. Furthermore, histological tissue types (muscle, adipose, and bone), lesion location, and skin phototype are critical parameters for determining the effects of laser interaction [3–6].

The aim of this study is to define the correlation between clinical set-up at present used in the treatment of specific skin conditions and laser beam absorbed power in the tissue. An experimental set-up has been performed using different samples simulating human tissues. Measurements of energy-power at different depths in the tissue have been carried out in order to fully understand the effects of tissue-laser interaction for the optimization of clinical outcomes.

It is to be stressed that *ex vivo* tissue used for the tests has rather different characteristics from those of human tissue, being less vascularized and hydrated. At any rate, the information obtained from these experiments can help us better understand the power and energy release mechanisms in irradiated tissues.

2. Material and Methods

2.1. Lasers. Our attention was devoted to the laser equipment used in the daily clinical practice in the Department of Dermatology of San Gallicano Institute in Rome, namely, traditional CO_2 laser, and Nd-Yag laser.

Carbon dioxide (CO_2) lasers were considered for their prominent role and broad spectrum of possible uses in dermatologic surgery. In particular, SmartXideDOT (DEKA M.E.L.A. Calenzano, Italy), in the two modes of laser beam delivery ($7''$ handpiece or fractional CO_2), is utilized in our clinical practice. In this latter mode the system generates perfectly controlled energy pulses (DOTs) by managing the energy per pulse parameter and the DOT spacing between two microscopic wounds (about 0.5 mm). This mode was not analyzed in this preliminary study but will be dealt with in the future. The spot size for the traditional mode, under examination in this study, is 6.5 mm.

Nd-Yag laser (neodymium-doped yttrium aluminum garnet) with a wavelength of 1064 nm long pulsed mode and 5 mm beam diameter was also investigated.

2.2. Tissue-Like Phantoms. Different types of tissue-equivalent material with various water and haemoglobin concentrations were used to evaluate laser beam attenuation power. Haemoglobin concentrations are important because of the presence of red chromophores. In particular, beef was selected for its high content of haemoglobin (about 0.1 mg/mL in beef muscle [7]) to mimic well-vascularised tissues (with human muscle-like chromophores); however, due to its lack of uniformity, it proves difficult to repeat the experiments, affecting reproducibility. All the *ex vivo* material tested was sliced and, slice by slice, accurately measured with a caliper in the incident areas. Loin (fat-free pork loin), characterized by high haemoglobin concentration (red chromophores) and low water concentration (about 37% in fat [8] and 58% in dry-cured loin [9]), was selected as test tissue because of its consistency.

2.3. Detection System. The detection system (Laser 2000 Ltd, UK) used in this study had two measuring heads (A-2-D12-HCB and A-200-D60-HPB) for the evaluation of the effective power or energy of the incident laser beam. Through conversion of absorbed energy into heat, the thermal head sensor (thermopile) registered the potential differences (V_{output}) produced by the thermal gradient generated by lasers and proportional to the incident energy or power.

For nonintensive powers, A-2-D12-HCB air cooling system head turned out to be compatible with different laser types allowing high resolution studies for medium power lasers. The power ranges from 1 mW to 2 W, while energy ranges from 0.5 mJ to 2 J. It has a diameter of 12 mm and a spectral range from 0.25 to 11 μm.

The A-200-D60-HPB air forced cooling system head, characterized by a low reflection index, results to be more resistant. The power ranges from 100 mW to 40 W, while energy ranges from 1 to 200 J. It has a diameter of 60 mm and a spectral range varying from 0.25 to 11 μm. However, A-200-D60-HPB head resolution is lower than A-2-D12-HCB. All systems are calibrated (3% accuracy) according to NIST (National Institute of Standards and Technology) and/or PTB (Physikalisch-Technische Bundesanstalt).

The electronic processing system retrieves all necessary data elaborated by the software interface LP-EXPLORER. The software, connected to the head of detection, automatically recognizes the head and, through a control panel, allows the measurements to be selected and made. All data collected and recorded are useful to verify the stability of the signal in CW lasers and any anomalies in PW laser, directly in the GUI (graphical user interface).

2.4. Experimental Set-Up. Since in clinical applications laser hand piece is generally located next to the patient skin (about 3–5 mm), during measurements the laser beam was positioned orthogonally to the system head, in contact with the tissue-equivalent phantoms executing continuous circular movements.

Power measurements with CO_2 laser were performed for different thickness (without tissue, 1.6 mm, 3.2 mm, and 4.8 mm). Each set of measurements was repeated with three different powers in CW mode (0.5 W, 0.6 W, 0.8 W). To obtain more accurate incident power detection, a smaller detector head (A-2-D12-HCB) was used (Figure 1).

For CO_2 laser measurements values of maximum, minimum, and mean power (W), tissue thickness (mm) and residual power (W) were recorded.

Energy measurements with Nd-Yag were performed at five different thicknesses (1.6 mm, 3.2 mm, 4.8 mm, 6.4 mm, and 8.0 mm) with the same phantom (Figure 2). An energy fluence of 125 J/cm^2 was used. The A-200-D60-HPB head is used in this case. The values of maximum, minimum, and mean power (J), energy fluence (J/cm^2), tissue thickness (mm), and residual energy (J) were as well recorded.

Laser set-up parameters were chosen, in agreement with clinicians, in order to simulate clinical protocols. The maximum experimental thickness had to be higher than the range ($d_{\max}$) reducing the residual measured power/energy

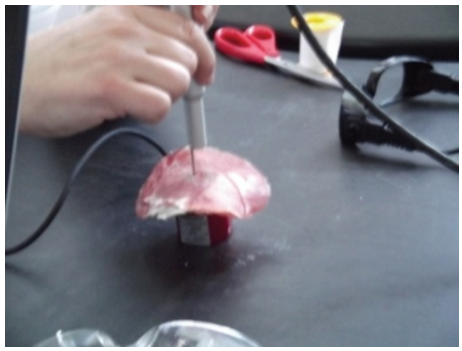

Figure 1: Experimental set-up used for the *ex vivo* phantom and small head measurements.

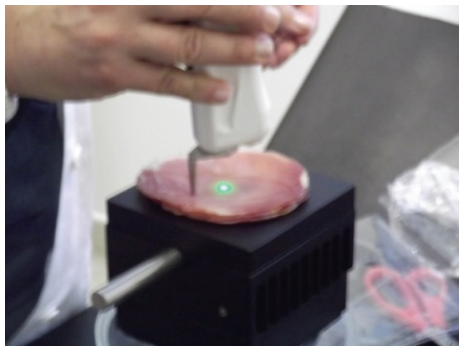

Figure 2: Experimental set-up used for the *ex vivo* phantom and larger head measurements.

at a constant value, determined by the measuring head (saturation value).

The net residual energy ΔE can be calculated for different tissue thickness as the measured energy value minus the determined saturation value.

For each measuring point a different laser position on the tissue was selected to obtain independent measurements.

2.5. Fitting Function. The following empirical function was used to fit the experimental data of power and energy against thickness (x):

$$y = \frac{Kae^{-bx}}{1 + ae^{-bx}}, \quad (1)$$

where K is the maximum measured intensity, "a" represents a scale factor, and "b" determines the curve slope.

The curve was selected being the logistic behaviour representative of the expected physical phenomena.

3. Results and Discussion

Figure 3 shows residual power (W) dependence as a function of tissue thickness (mm) for three experimental output powers using CO_2 laser. A fit with the expected curves is also reported (blue, red, and green lines).

It is to be underscored that for thickness >2 mm the delivered radiation results in being totally absorbed inside

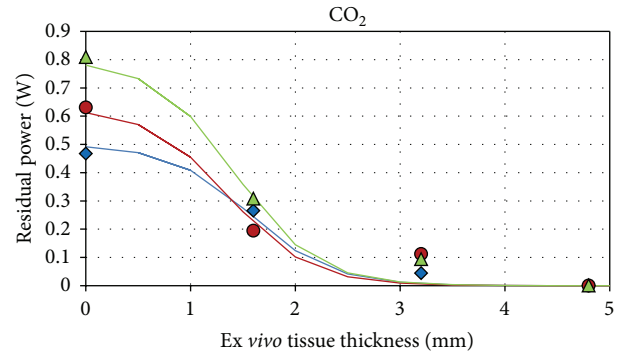

Figure 3: Dependence of the residual power (W) as a function of equivalent-tissue thickness (mm) for three experimental output powers for CO_2 ((blue diamond) 0.5 W, (red circle) 0.6 W, and (green triangle) 0.8 W).

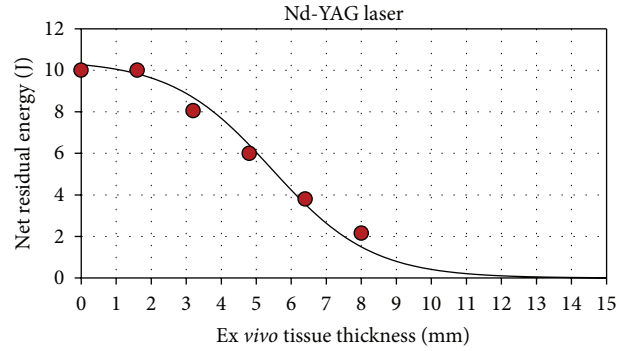

Figure 4: Dependence of the net residual energy ΔE (J) as a function of equivalent-tissue thickness (mm) for Nd-Yag ((red circle) 125 J/cm^2).

the dedicated phantom for all levels of power between the experimental error.

The parameters of each power fitted curve are reported in Table 1.

As regards measurements with the Nd-YAG laser, a certain amount of energy is not absorbed in the first centimeter of tissue and therefore does not contribute to interaction phenomena.

Figure 4 represents the dependence of the net residual energy (ΔE) in function of the phantom thickness. A fit of experimental data is also shown (black line).

The saturation level is located next to the 15 J energy value. This effect is probably overestimated due to the rather different characteristics of *ex vivo* and human tissue.

It is worth noting that the energy was obtained by converting the selected energy fluence (125 J/cm^2) with the following expression: $125 \times \pi \times r^2$, where $r = 2.5$ mm is the radius of laser applicator. The theoretical value of energy thus obtained was 24.5 J while the experimental value was 26.5 J. We could then verify that the average energy value revealed by the power meter head does not differ for more than 10% from that of the set value.

The parameters of the net residual energy fitted curve are reported in Table 1.

Table 1: Parameters of each power fitted curve related to the experimental measurements.

Laser type	Unit	Measured value (W or J)	a	b	K	Point symbol*
CO_2	Power	0.5	60	2.6	0.50	◆
CO_2	Power	0.6	35	2.6	0.63	●
CO_2	Power	0.8	40	2.6	0.80	▲
Nd-Yag	Energy	24.5	45	0.7	10.5	●

*Point symbols used in Figures 3 and 4.

Other equivalent tissues—ham or chicken (data not shown)—were tested in order to mimic different biological tissues. Low haemoglobin concentration and high water concentration strongly affected the measurements because of the scatter fraction increasing against depth. As a matter of fact, in such cases the detected power was below the detection system sensitivity level because of the generated high scatter fraction.

Data show that only a small fraction of the incident energy is absorbed by the tissues.

In the CO_2 laser it is important to establish proper measurement duration and to acquireat least five measurements to check the reproducibility of beam. In this case, the 10.600 nm wavelength emitted as continuous beam destroys tissue by rapidly heating and vaporizing intracellular water. It should however be considered that measurements are affected by an error due to the intrinsic response time of electronics, higher than tissues response. This leads to a general overestimation of values.

As for the potential application of similar studies in the clinical practice, they could be carried out in collaboration with clinicians with limited costs and relevant time-sparing. Our results show that the beam spreading thermal front is one of the source physical parameters characterizing the mechanisms that induce either tissue damage or proper tissue heating, depending on thermal tolerance.

Thin superficial lesions, on the order of hundreds of microns in thickness, receive about the same amount of light throughout their volume due to incident as well as backscattered light reflected from the underlying tissues. This behaviour is a localized effect of laser therapy due to the light administered on the tissue surface, irradiance in (W/cm^2) or fluence in (J/cm^2).

In the thick tumour case the aim is to treat the lesion to some desired depth. To treat a volume homogeneously, efficacy ends up to be proportional to the light penetration depth which can be obtained by choosing a proper wavelength. In both cases the knowledge of the beam planar size plays an important role.

In particular, prolonged exposure to moderate (CW) or long pulsed levels of light (PW) produces an absorption effect and relative irreversible local or peripheral tissue damage, depending on the spreading thermal front. These biological effects are different from those associated with the short-pulse high-peak power in which, because of thermal expansion, tissues damage is generated far from the absorbing area. Thus, in the Q-switched lasers, the spreading effect does not occur in the absorbing area.

Moreover, geometrical distortion, the ability to reproduce the real dimensions of the focused beam spots at working distance, is another important parameter. Accuracy out of the acceptable limits of the geometrical distortion affects heterogeneity in power/energy delivery.

4. Conclusion

The experimental set-ups analyzed in this study are just a few examples of laser applications in dermatology obtained using standard parameters routinely applied in clinical practice. These preliminary data stress the importance to more accurately know the fraction of released energy from the system to the tissues, to improve the treatment strategy. The main point is the correlation between physical design of the hand piece, the technique used to apply it, wavelength, and laser power in determining clinical outcome. Our team of physicists and physicians will further investigate this relevant topic to improve therapeutic procedures.

Conflict of Interests

The authors have no potential conflict of interests.

Acknowledgment

The authors are grateful to Ing. Tiziano Zingoni for his kind and meaningful contribution.

References

[1] N. Cameli, M. Mariano, M. Serio, and M. Ardigò, "Preliminary comparison of fractional laser with fractional laser plus radiofrequency for the treatment of acne scars and photoaging," *Dermatologic Surgery*, vol. 40, no. 5, pp. 553–561, 2014.

[2] G. Ma, P. Wu, X. Lin et al., "Nd: YAG laser for "fractional" treatment of angiofibromas," *International Journal of Dermatology*, vol. 53, no. 5, pp. 638–642, 2014.

[3] E. A. Edwards and S. Q. Duntley, "The pigments and color of human skin," *American Journal of Anatomy*, vol. 65, no. 1, pp. 1–33, 1939.

[4] R. R. Anderson and J. A. Parrish, "The optics of human skin," *Journal of Investigative Dermatology*, vol. 77, no. 1, pp. 13–19, 1981.

[5] M. J. C. Van Gemert, S. L. Jacques, H. J. C. M. Sterenborg, and W. M. Star, "Skin optics," *IEEE Transactions on Biomedical Engineering*, vol. 36, no. 12, pp. 1146–1154, 1989.

[6] Z. Q. Zhao and P. W. Fairchild, "Dependence of light transmission through human skin on incident beam diameter at

different wavelengths," in *Proceedings of the SPIE, Laser-Tissue Interaction IX*, vol. 3254, pp. 354–360, 1998.

[7] P. D. Warriss and D. N. Rhodes, "Haemoglobin concentrations in beef.," *Journal of the Science of Food and Agriculture*, vol. 28, no. 10, pp. 931–934, 1977.

[8] A. Papp, E. Romppanen, T. Lahtinen, A. Uusaro, M. Härmä, and E. Alhava, "Red blood cell and tissue water content in experimental thermal injury," *Burns*, vol. 31, no. 8, pp. 1003–1006, 2005.

[9] B. M. Popkin, K. E. D'Anci, and I. H. Rosenberg, "Water, hydration, and health," *Nutrition Reviews*, vol. 68, no. 8, pp. 439–458, 2010.

Hindawi Publishing Corporation
BioMed Research International
Volume 2014, Article ID 204532, 8 pages
http://dx.doi.org/10.1155/2014/204532

Clinical Study

Effects of the Combined PDL/Nd:YAG Laser on Surgical Scars: Vascularity and Collagen Changes Evaluated by *In Vivo* Confocal Microscopy

Krisztina Vas,[1] Magdolna Gaál,[1] Erika Varga,[1] Réka Kovács,[1] Balázs Bende,[1] Ádám Kocsis,[1] and Lajos Kemény[1,2]

[1] *Department of Dermatology and Allergology Clinic, University of Szeged, Korányi Fasor 6, Szeged 6720, Hungary*
[2] *MTA-SZTE Dermatological Research Group, Korányi Fasor 6, Szeged 6720, Hungary*

Correspondence should be addressed to Krisztina Vas; krisztina.vas@mail.derma.szote.u-szeged.hu

Received 16 April 2014; Accepted 3 August 2014; Published 9 September 2014

Academic Editor: Piero Campolmi

The aim of this study was to investigate the efficacy of the sequential combined 585 nm PDL and the 1064 nm neodymium:yttrium-aluminium-garnet laser (PDL/Nd:YAG) in the treatment of surgical scars and to evaluate the short-term effects by *in vivo* confocal microscopy (RCM) and the long-term effects by clinical assessment of the scars. Twenty-five patients were enrolled with 39 postoperative linear scars; each scar was divided into two fields. One half was treated with the combined PDL/Nd:YAG laser, whereas the other half remained untreated. Each scar was treated three times at monthly intervals. Scars were evaluated by an independent examiner, using the Vancouver Scar Scale. The combined PDL/Nd:YAG laser significantly improved the appearance of the scars. In order to study the short-term effects of combined laser treatment, six additional patients were enrolled with 7 postoperative linear scars. One half of scars was treated once with the combined PDL/Nd:YAG laser. One week after this laser treatment, both the treated and the nontreated parts of the scars were examined by dermoscopy and RCM. The dermoscopic pictures revealed improvements even in treated areas. In conclusion, the combined PDL/Nd:YAG laser was found to be effective in improving the quality and appearance of the surgical scars.

1. Introduction

Despite modern suturing techniques, operations may be followed by the development of nonesthetic scars. Surgical scars often remain red in color, firm, and elevated to the touch. Some scars may persist in a hyperpigmented form or may become hypertrophic or keloid. These nonesthetic scars may come to be regarded as permanent stigmas and often cause considerable esthetic and psychological problems for patients. Various therapeutic modalities have been attempted with the aim of improving the clinical appearance of scars, with differing degrees of success, for example, corticosteroid injection, dermabrasion, surgical revision, chemical peeling, silicone gel application, vitamin E-based remedies, pressure therapy and X-ray irradiation, cryosurgery, 5-fluorouracil (a pyrimidine analog), and certain antitumor agents (e.g., Bleomycin) [1–6].

Lasers have also been applied to improve the appearance of such scars. The first lasers utilized for this purpose were ablative, nonselective lasers: carbon dioxide (CO_2) or erbium:yttrium-aluminium-garnet (Er:YAG) laser [7–11].

Nouri et al. recently studied the use of the pulsed dye laser (PDL) at different wavelengths (585 nm and 595 nm) and with different pulse durations (short and long), and Conologue and Norwood demonstrated that the cryogen-cooled 595 nm PDL treatment is effective in improving the wound healing [12–15].

Investigations of the therapeutic efficacy of different laser and light source combinations (e.g., the combination of the PDL and the Nd:YAG laser) are important in view of their complementary nature. The skin contains a number of light-absorbing substances (chromophores) such as water, melanin, hemoglobin, and exogenous pigments. An initial low PDL pulse selectively increases the local blood temperature to

Table 1: Patients' data: 25 participants between the ages of 17 and 50 years with Fitzpatrick skin types I–IV and linear scars greater than 3 cm were enrolled into the study.

Patient	Sex	Age (years)	Scars (number of pieces)	Fitzpatrick skin types	Location
1	F	40	1	II.	Abdomen
2	F	20	1	III.	Scapula
3	F	35	1	II.	Abdomen
4	F	26	2	II.	Back
5	M	25	3	II.	Back
6	M	25	2	III.	Neck
7	M	25	1	II.	Neck
8	F	39	2	III.	Abdomen
9	F	17	1	II.	Back
10	F	23	1	I.	Waist
11	F	38	1	II.	Mons pubis
12	F	23	1	I.	Abdomen
13	F	24	1	II.	Leg
14	F	27	1	II.	Leg
15	F	30	2	III.	Back and arm
16	F	21	1	IV.	Back
17	F	30	3	II.	Neck, back, and upper arm
18	F	26	2	II.	Abdomen
19	F	25	3	II.	Abdomen
20	F	50	1	III.	Back
21	F	25	1	III.	Back
22	F	19	1	II.	Back
23	F	19	2	III.	Back
24	F	21	2	II.	Mons pubis and back
25	F	32	2	II.	Back

62–80°C, resulting in oxyhemoglobin-methemoglobin conversion. A recent study revealed that the light of the Nd:YAG laser is preferentially absorbed by methemoglobin rather than by oxyhemoglobin. The high temperature attained induces blood coagulation in the vessels of the treated area. The combination of these lasers functions via selective photothermolysis, which targets the blood vessels with minimal damage to the surrounding tissues.

As sequential combined PDL/Nd:YAG laser treatment has been shown to be highly effective for the treatment of acne vulgaris, cutaneous photoaging, and leg veins, the aim of our present study was to investigate the efficacy of combined PDL/Nd:YAG laser treatment on the appearance of scars, when used immediately after suture removal [16–18].

In this study, treatment was performed on regular scars after surgery starting right after the removal of sutures. Our results conclude that combined PDL/Nd:YAG laser therapy starting on the day of suture removal is safe and effective in improving the quality and cosmetic appearance of surgical scars in patients with skin types I–IV; the improvement was confirmed at structural level by dermoscopy, *in vivo* confocal microscopy, and VSS. RCM permits the real-time imaging of human skin including various skin disorders. It is a noninvasive high-resolution imaging technique which allows the structural and cellular visualization and analysis of the skin to a depth up to 250 μm. This technique can be used in a wide range of dermatological settings. Objective data can be obtained on the skin structure and its alterations in various conditions. It is also widely used to evaluate almost any kind of superficial skin lesions. The RCM assist of the diagnosis and differential diagnosis of skin diseases can be refined and a more specific opinion can be provided without or before a surgical biopsy. It can help in the assessment of lesions with a clinical and dermoscopic suspicion of malignancy eliminating the performance of unnecessary surgical biopsies or confirming a previous diagnosis in order to plan the optimal surgical solution [19–21].

2. Methods

2.1. Effects of the Combined PDL/Nd:YAG Laser on the Clinical Appearance of the Scars. Twenty-five (22 female and 3 male) participants between the age of 17 and 50 years, with Fitzpatrick skin types I–IV and linear scars greater than 3 cm originating from nevus removal, were enrolled into the study (Table 1). The patients had been operated on at the Plastic Surgery Unit of the Department of Dermatology and Allergology Clinic in Szeged. All of the patients involved in the study had otherwise healthy skin and were not suffering from major medical illnesses. Exclusion criteria were pregnancy, lactation, medicines that increase sensitivity to light, anticoagulant medication, a history of malignancy, and susceptibility to keloids and hypertrophic wound healing. All surgical procedures had been carried out by the same group of plastic surgeons, and wound closure had been performed with standardized suturing techniques

(two-layer intracutaneous running, one deeper absorbable suture and one superficial nonabsorbable suture). The sutures were removed 14 days after the operation.

The patient's informed consent was obtained in all cases before laser treatment was started immediately after suture removal, followed by repeat treatments 4 and 8 weeks later.

Twenty-five patients with 39 postoperative linear scars were treated three times at monthly intervals with the combined 585 nm PDL and 1064 nm Nd:YAG laser (Cynergy, Cynosure Inc., Westford, MA, USA).

Each scar was divided into two fields; one half of each scar was treated with the combined PDL/Nd:YAG laser and the other half remained untreated. The treated and the control halves were selected randomly.

The 585 nm PDL was used with a spot size of 10 mm with 10% overlap and a pulse duration of 0.5 ms at a fluence of 4.5 J/cm^2, in combination with treatment with the 1064 nm Nd:YAG laser with a spot size of 10 mm and a pulse duration of 15 ms at a fluence of 60 J/cm^2, with 500 ms time delay between the delivery of the two wavelengths. Specific safety eyeglasses were worn during the treatment. The skin surface was cooled with a continuous flow of cold air. The patients reported only minimal pain during treatment; erythema appeared around the scar 1-2 days after the laser treatment. No serious side-effects of the treatment were observed. All photographs were taken by one photographer with a *Nikon D200* camera, under identical conditions of illumination and patient positioning. Analysis was performed on 39 scars in a blind study by an independent examiner one month after the last treatment (third laser irradiation).

The level of improvement of the scars was evaluated by using the Vancouver Scar Scale (VSS) one month after the final treatment. This scale is the internationally accepted method for the description of scars. The VSS consists of four variables: vascularity, height (thickness), pliability, and pigmentation. Each variable has four to six possible scores. A total score ranges from 0 to 13, where the score of 0 reflects normal skin.

Statistical analysis was performed with the SPSS 15.0 software.

The Wilcoxon test chosen for the evaluation allows determination of the degree of improvement based on the VSS (pigmentation, vascularity, pliability, and height) scores of the scars in both the treated and the untreated parts.

2.2. Effects of the Combined PDL/Nd:YAG Laser Treatment on Blood Vessels and on Collagen Fibers. To determine the effects of the combined PDL/Nd:YAG laser therapy on scar microcirculation, dermoscopy and *in vivo* confocal microscopic analyses were performed.

Half of each scar in 6 patients (5 female and 1 male) with 7 postoperative linear scars was treated immediately after suture removal once with the combined PDL/Nd:YAG laser, and, one week later, both parts of the scar were examined by dermoscopy and reflectance-mode *in vivo* confocal microscopy (RCM).

One week after the combined laser treatment, the dermoscopic and RCM images of the 7 scars of the 6 patients were analyzed with the LUCID VivaScope 1500 Multilaser (MAVIG GmbH, Munich, Germany) equipment, using the 785 nm wavelength laser of the machine. Our objectives were to analyze the microcirculation and the structures of the epidermis and collagen bundles and to assess the differences between the treated and untreated areas. Images were made first of the combined PDL/Nd:YAG laser-treated and then of the control areas. The captured areas also contained the neighboring normal skin. The first step was to obtain a dermoscopic picture of the examined area with the RCM machine camera. The zero level was then determined and this level was marked relative to the surface of the scar tissue. The first image was intended to be taken at the level of the stratum granulosum-spinosum. We captured the stratum corneum of the scar as the zero level and then defined the first level which was usually 25–30 μm deeper than the zero one. Three further images were next obtained, each 25 μm deeper than the previous one. Due to the above mentioned surface irregularity, we often had to make an additional fifth layer to visualize the deeper structures appropriately. The maximum area of 8 × 8 mm was captured at each level. We also made two Vivastack captures at representative parts of the scar and a comparative one at the normal skin area. These Vivastack images were taken from the level of the stratum granulosum-spinosum down to 150 μm in 1.5-μm steps. Vessels were detected and compared on the basis of the dermoscopy and RCM images.

3. Results

3.1. Effects of the Combined PDL/Nd:YAG Laser on the Clinical Appearance of the Scars. The combined PDL/Nd:YAG laser treatment resulted in a significant clinical improvement of the scars (Figures 1 and 2). The surgical scar is depicted from the day of suture removal to the final combined laser treatment. One month after the third combined laser treatment, the final analysis revealed a significant difference in favor of the treated parts of the scar.

The VSS parameters (n = 39 scars) demonstrated a significant dermoscopic improvement relative to the control (Figure 3). A worsening status of wound healing after laser treatment was detected only in one patient, where we observed pink vascularity, hyperpigmentation, supple, and 2–5 mm heightened parts of the scar at the treated region.

Each of the four parameters (pigmentation, vascularity, pliability, and height) was improved significantly 1 month after the final combined laser treatment (Figure 4). There were no significant complications during this study. Both patients and doctors were satisfied with the cosmetic appearance of the surgical scars after final combined laser therapy. Three months after the last laser treatment, further improvement in the clinical appearance of the laser treated scars was observed (not shown).

3.2. Effects of the Combined PDL/Nd:YAG Laser Treatment on Blood Vessels and on Collagen Fibers. Concerning each of the investigated parameters, the combined PDL/Nd:YAG laser significantly improved the appearance of the scars; thus, we set out to enroll further 6 subjects in order to study the short-term effect of combined laser treatment.

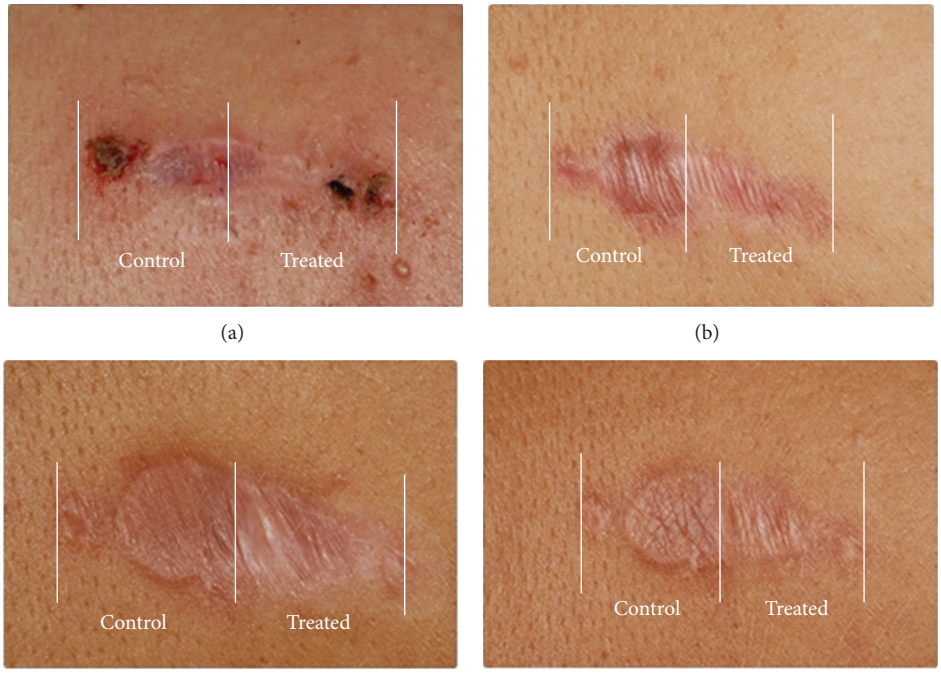

Figure 1: Effects of combined 585/1064 nm laser treatment on the clinical appearance of the scar back of in the patient number 16 (Fitzpatrick skin type IV) on the day of suture removal (a), 1 month after the first treatment (b), 1 month after the second treatment (c), and at the final assessment (d). The treated half (Treated) and the control half (Control) of the scar are indicated.

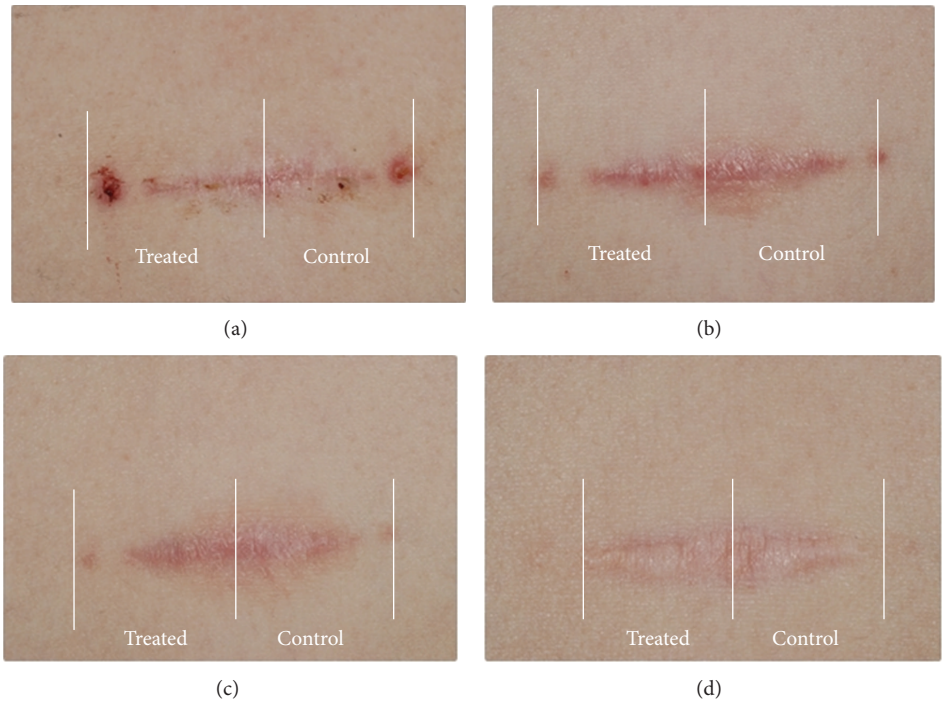

Figure 2: Effects of combined 585/1064 nm laser treatment on the clinical appearance of the scar waist of in the patient number 10 (Fitzpatrick skin types I) on the day of suture removal (a), 1 month after the first treatment (b), 1 month after the second treatment (c), and at the final assessment (d). The treated half (Treated) and the control half (Control) of the scar are indicated.

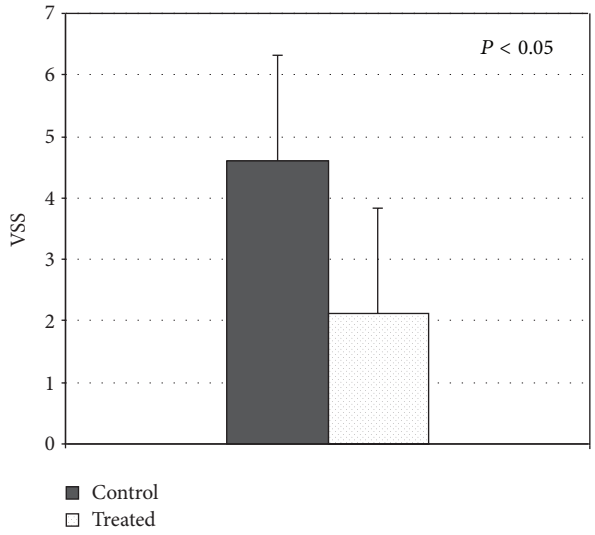

Figure 3: VSS score 1 month after final treatment and final evaluation ($n = 25$); $P < 0.05$ was regarded as a significant change.

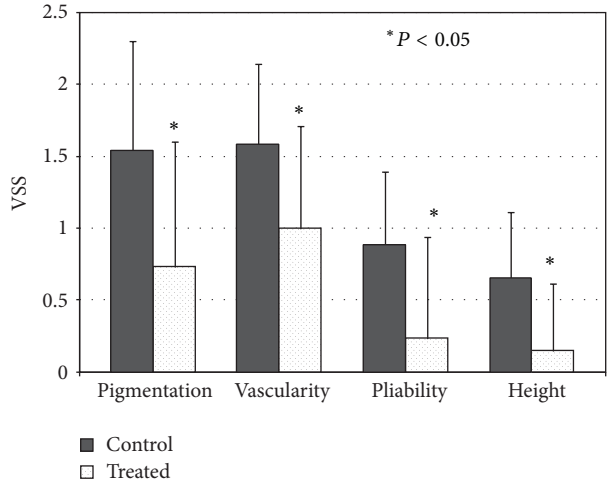

Figure 4: Improvement in individual VSS parameters 1 month after the final combined PDL/Nd:YAG laser treatment ($n = 25$); $^*P < 0.05$ was regarded as a significant change.

One week after the combined PDL/Nd:YAG laser treatment, the dermoscopic pictures of the control, untreated area displayed marked parallel or lace-like vascularity (Figure 5), which was pronounced not only in the scar area but also around it. In several cases, the scar appeared to be slightly elevated; however, more often a depressed characteristic was detectable.

The epidermis exhibited a regular or broadened honeycomb pattern according to the RCM investigation, although some areas revealed atypical keratinocytes as well. The dermoepidermal junction showed nonspecific pattern without papillary contours. Parallel, rough, coarse collagen bundles were detected in the upper dermis, whereas the vessels were dilated and horizontal.

The treated area of the dermoscopic pictures revealed a narrower scar with notably decreased vascularity. The vessels were more delicate and situated apparently haphazardly compared to the untreated part. The treated scars were usually depressed. In some cases, the surroundings of the scar displayed more vascularity than the scar itself. The epidermis also had a broadened honeycomb pattern with a low number of atypical keratinocytes and some dendritic inflammatory cells. At the dermoepidermal junction, the pattern was nonspecific, without papillary contours similar to the untreated area. The collagen fibers were comparably coarse; however, they were not numerous and their orientation was not uniformly parallel. Only low numbers of narrow horizontal vessels were observed.

4. Discussion

Different techniques are used to enhance wound healing, but, thanks to the rapid advances in laser technology, a new method has emerged with a promising future for modern wound healing.

The flashlamp-pumped PDL, which emits light at a wavelength of 585 nm, has become the gold standard in the treatment of port-wine stains and also an effective treatment modality for superficial vascular lesions, including those associated with photoaging, such as facial telangiectasias. The Nd:YAG laser emits light at a wavelength of 1064 nm, which allows deep penetration into the dermis and vascular specificity due to a broad absorption peak of oxyhemoglobin above 800 nm [17, 18].

PDL and Nd:YAG lasers of different wavelengths have been incorporated in the novel dual laser device built into the same console. Laser and light source combinations are currently being examined for their complementary, additive, or sometimes synergistic action.

The abnormal blood vessels in the scar tissue area are occluded and absorbed, which results in artificial ischemia, inhibiting nutrient supply to the wound. The laser treatment enhances wound contraction, the remodelling of collagen fibers by thermal necrosis, activation of the release of basic fibroblast growth factor, and inhibition of transforming growth factor $\beta 1$ [1, 2]. The combined laser therapy additionally decreases the accumulation of fibroblast cells in the scar tissue and stimulates the production of reticular collagen fibers [10, 11]. Treatment with the combined 585 nm PDL and 1064 nm Nd:YAG laser is noninvasive, minimally uncomfortable, and requires no anesthesia.

Jung et al. compared a PDL and a combined PDL/Nd:YAG laser in the treatment of acne vulgaris and found that the combined PDL/Nd:YAG laser was significantly better than the PDL in reducing noninflammatory acne lesion counts 8 weeks after the treatment; an improvement was also observed in the treatment of inflammatory acne lesions, though it was not statistically significant [16]. Trelles et al. described the efficiency of the PDL/Nd:YAG laser combination in the treatment of leg veins [18]. Berlin et al. treated cutaneous photoaging symptoms with a combined PDL/Nd:YAG laser. Their examinations indicated the greatest improvements in

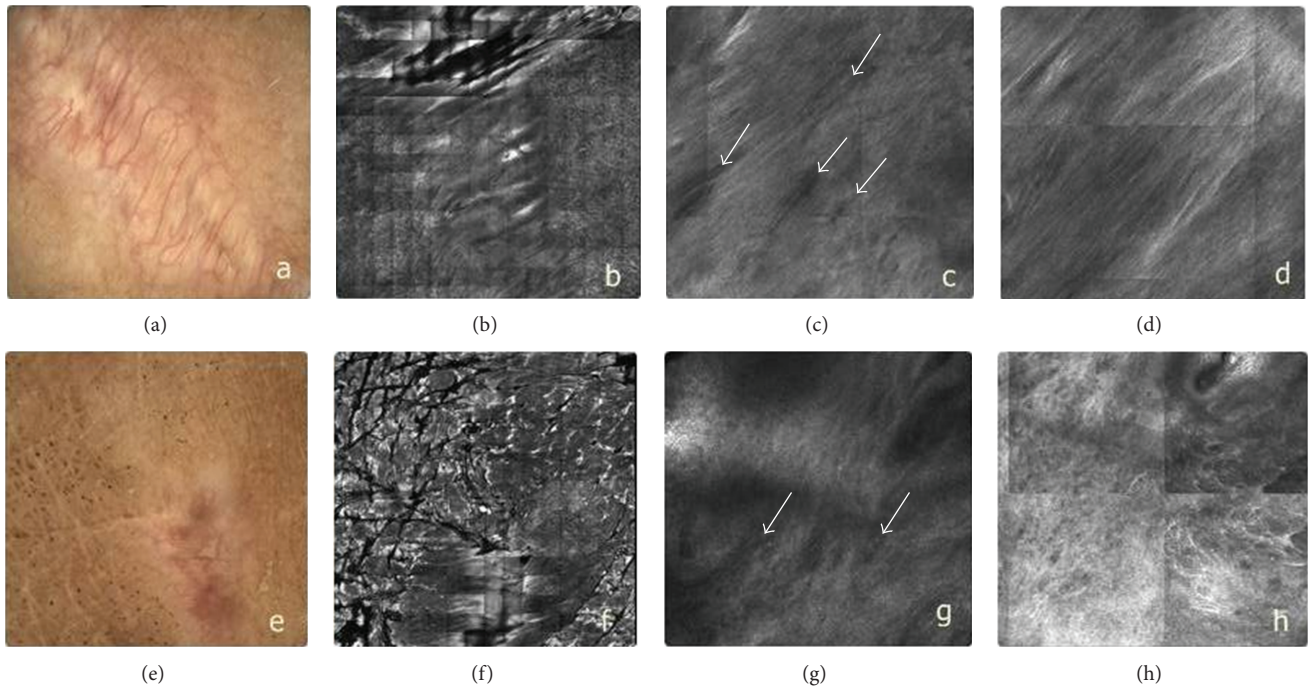

Figure 5: Effects of a single combined 585/1064 nm laser treatment on the blood vessels and collagen fibers (abdomen). The untreated areas ((a), (b), (c), and (d)) and treated areas ((e), (f), (g), and (h)) are indicated. Control area: the dermatoscopic picture revealed high vascularity in the scar tissue ((a) Bar = 92.96 μm). The RCM picture of the scar and its surroundings indicated that the scar is only slightly depressed ((b) Bar = 132.59 μm); there are numerous, parallel collagen fibers with numerous dilated vessels (arrows) among them (c) and numerous parallel collagen fibers ((d) Bar = 132.59 μm). Treated area: the dermatoscopic picture shows low vascularity in the scar tissue (e). The RCM picture of the scar and its surroundings demonstrated that the scar is depressed relative to the normal skin ((f) Bar = 70.10 μm); there were collagen fibers regular and elongated and a few narrow vessels (arrows) among them ((g) Bar = 138.68 μm) and regular and elongated collagen fibers ((h) Bar = 129.54 μm).

telangiectasias and diffuse erythema, with slightly less change in epidermal pigmentation and lentigines. The combined sequential PDL/Nd:YAG laser can be used safely and effectively in facial photorejuvenation [17].

Nouri et al. compared the effectiveness of the 585 nm versus the 595 nm PDL in the treatment of new surgical scars. Both lasers improved the cosmetic appearance of the scars statistically. However, 585 nm appeared to be the better wavelength, as it substantially normalized the height in a significant number of the scars, in addition to the vascularity and pliability. It also emerged that both short (450 μs) and long (1.5 ms) 585 nm pulses were safe and effective in improving the quality and cosmetic appearance of surgical scars starting on the day of suture removal. No significant difference was detected between the results with the different pulse durations. The cryogen-cooled 585 nm and 595 nm PDL was used with a spot size of 10 mm or 7 mm and a pulse duration of 450 μs or 1.5 ms at a fluence of 3.5 J/cm^2 to treat surgical scars starting on the day of suture removal [12–14].

In previous publications, the most significant improvements were found in vascularity and pliability after therapy with the 585 nm or 595 nm PDL [12–15].

Bencini et al. have described the long-term effects of carbon dioxide (CO_2) laser treatment on skin aging after fractional laser therapy lasting 6 weeks to 3 months at least. Epidermal changes and collagen remodeling were evaluated by *in vivo* confocal microscopy [22]. Recently, Sattler et al. treated healthy probands with fractional carbon dioxide laser; then the optical follow-ups were performed using confocal laser scanning microscopy and optical coherence tomography right after laser application and during the following 3 weeks. Both of these techniques were able to visualize the therapeutical effects of the laser therapy, suggesting that noninvasive methods could be used to evaluate the efficacy of laser treatments [23].

The aim of the present study was to investigate the efficacy of the combined 585/1064 nm laser treatment of surgical scars and to evaluate the short-term effects by *in vivo* confocal microscopy and the long-term effects by VSS. Surgical scar treatment with the combined PDL/Nd:YAG laser therapy starting on the day of suture removal has not been reported previously.

In our study, one half of each of the postoperative linear scars immediately after suture removal was treated three times at monthly intervals with the combined 585/1064 nm laser and the cosmetic appearances of the treated and untreated scar halves were compared. The VSS parameters indicated a significant improvement at the final assessment relative to the control. Our results are in concordance with recent data of other authors on the topic.

When additional surgical scars ($n = 7$ scars) were similarly treated only once with the combined 585/1064 nm laser, dermatoscopy and RCM one week later demonstrated an improvement in the treated area, which exhibited only low numbers of narrow horizontal vessels and decreased amounts of collagen fibers, the orientations of which were not uniformly parallel. We examined both parts of the scar by dermatoscopy and RCM one week later since the high temperature applied induces occlusion and absorption of abnormal blood vessels in the scar tissue area, which results in artificial ischemia, inhibiting nutrient supply to the wound. We eliminated the subjectivity of the independent examiner; therefore, the evaluation of changes in vascularisation and rearrangement of collagen bundles was measured using RCM. We found that RCM was suitable for the monitoring of wound healing with or without the combined 585/1064 nm laser treatment. In conclusion, the combined PDL/Nd:YAG laser proved to be safe and effective in improving the cosmetic appearance ($n = 39$ scars) of surgical scars in patients with skin types I–IV, starting on the day of suture removal, and this improvement was confirmed at the structural level ($n = 7$) by *in vivo* confocal microscopy. RCM proved to a valuable tool for monitoring the efficacy of laser treatment of the scars.

Conflict of Interests

The authors declare that there is no conflict of interests regarding the publication of this paper.

Acknowledgments

The authors would like to thank Dr. Attila Bebes for his constructive criticism and helpful suggestions during the preparation of this paper. They thank Éva Viharosné Dósa-Rácz for the statistical analysis and Dr. János Varga and Dr. Gábor Mohos for enrolling the patients into the study. The authors thank Andrea Gyimesi and Klára Molnárné Rónyai for their technical assistance. This work was supported by TAMOP-4.2.2.A-11/1/KONV-2012-0035 research Grant.

References

[1] C. Tziotzios, C. Profyris, and J. Sterling, "Cutaneous scarring: pathophysiology, molecular mechanisms, and scar reduction therapeutics: part II. Strategies to reduce scar formation after dermatologic procedures," *Journal of the American Academy of Dermatology*, vol. 66, no. 1, pp. 13–24, 2012.

[2] S. A. Eming, T. Krieg, and J. M. Davidson, "Inflammation in wound repair: molecular and cellular mechanisms," *Journal of Investigative Dermatology*, vol. 127, no. 3, pp. 514–525, 2007.

[3] M. H. Gold, "Dermabrasion in dermatology," *American Journal of Clinical Dermatology*, vol. 4, no. 7, pp. 467–471, 2003.

[4] M. A. Musgrave, N. Umraw, J. S. Fish, M. Gomez, and R. C. Cartotto, "The effect of silicone gel sheets on perfusion of hypertrophic burn scars," *Journal of Burn Care & Rehabilitation*, vol. 23, no. 3, pp. 208–214, 2002.

[5] N. Bouzari, S. C. Davis, and K. Nouri, "Laser treatment of keloids and hypertrophic scars," *International Journal of Dermatology*, vol. 46, no. 1, pp. 80–88, 2007.

[6] M. L. Elsaie, S. Choudhary, M. McLeod, and K. Nouri, "Scars," *Current Problems in Dermatology*, vol. 42, pp. 131–139, 2011.

[7] T. S. Alster and C. Handrick, "Laser treatment of hypertrophic scars, keloids, and striae," *Seminars in Cutaneous Medicine and Surgery*, vol. 19, no. 4, pp. 287–292, 2000.

[8] M. P. Goldman and R. E. Fitzpatrick, "Laser treatment of scars," *Dermatologic Surgery*, vol. 21, no. 8, pp. 685–687, 1995.

[9] H. Nakagawa, O. T. Tan, and J. A. Parrish, "Ultrastructural changes in human skin after exposure to a pulsed laser," *Journal of Investigative Dermatology*, vol. 84, no. 5, pp. 396–400, 1985.

[10] Y.-R. Kuo, S.-F. Jeng, F.-S. Wang et al., "Flashlamp pulsed dye laser (PDL) suppression of keloid proliferation through down-regulation of TGF-β1 expression and extracellular matrix expression," *Lasers in Surgery and Medicine*, vol. 34, no. 2, pp. 104–108, 2004.

[11] R. R. Anderson and J. A. Parrish, "Selective photothermolysis: precise microsurgery by selective absorption of pulsed radiation," *Science*, vol. 220, no. 4596, pp. 524–527, 1983.

[12] K. Nouri, G. P. Jimenez, C. Harrison-Balestra, G. W. Elgart, and H. Chan, "585-nm pulsed dye laser in the treatment of surgical scars starting on the suture removal day," *Dermatologic Surgery*, vol. 29, no. 1, pp. 65–73, 2003.

[13] K. Nouri, M. P. Rivas, M. Stevens et al., "Comparison of the effectiveness of the pulsed dye laser 585 nm versus 595 nm in the treatment of new surgical scars," *Lasers in Medical Science*, vol. 24, no. 5, pp. 801–810, 2009.

[14] K. Nouri, M. L. Elsaie, V. Vejjabhinanta et al., "Comparison of the effects of short- and long-pulse durations when using a 585-nm pulsed dye laser in the treatment of new surgical scars," *Lasers in Medical Science*, vol. 25, no. 1, pp. 121–126, 2010.

[15] T. D. Conologue and C. Norwood, "Treatment of surgical scars with the cryogen-cooled 595 nm pulsed dye laser starting on the day of suture removal," *Dermatologic Surgery*, vol. 32, no. 1, pp. 13–20, 2006.

[16] J. Y. Jung, Y. S. Choi, M. Y. Yoon, S. U. Min, and D. H. Suh, "Comparison of a pulsed dye laser and a combined 585/1,064-nm laser in the treatment of acne vulgaris," *Dermatologic Surgery*, vol. 35, no. 8, pp. 1181–1187, 2009.

[17] A. L. Berlin, M. Hussain, and D. J. Goldberg, "Cutaneous photoaging treated with a combined 595/1064 nm laser," *Journal of Cosmetic and Laser Therapy*, vol. 9, no. 4, pp. 214–217, 2007.

[18] M. A. Trelles, R. Weiss, J. Moreno-Moragas, C. Romero, M. Vélez, and X. Álvarez, "Treatment of leg veins with combined pulsed dye and Nd:YAG lasers: 60 patients assessed at 6 months," *Lasers in Surgery and Medicine*, vol. 42, no. 9, pp. 609–614, 2010.

[19] M. A. Altintas, A. A. Altintas, M. Guggenheim et al., "Insight in human skin microcirculation using in vivo reflectance-mode confocal laser scanning microscopy," *Journal of Digital Imaging*, vol. 23, no. 4, pp. 475–481, 2010.

[20] M. Ulrich, S. Lange-Asschenfeldt, and S. Gonzalez, "Clinical applicability of in vivo reflectance confocal microscopy in dermatology," *Giornale Italiano di Dermatologia e Venereologia*, vol. 147, no. 2, pp. 171–178, 2012.

[21] P. Guitera, S. W. Menzies, C. Longo, A. M. Cesinaro, R. A. Scolyer, and G. Pellacani, "In vivo confocal microscopy for diagnosis of melanoma and basal cell carcinoma using a two-step method: analysis of 710 consecutive clinically equivocal cases," *Journal of Investigative Dermatology*, vol. 132, no. 10, pp. 2386–2394, 2012.

[22] P. L. Bencini, A. Tourlaki, M. Galimberti et al., "Nonablative fractional photothermolysis for acne scars: clinical and in vivo microscopic documentation of treatment efficacy," *Dermatologic Therapy*, vol. 25, no. 5, pp. 463–467, 2012.

[23] E. C. E. Sattler, K. Poloczek, R. Kästle, and J. Welzel, "Confocal laser scanning microscopy and optical coherence tomography for the evaluation of the kinetics and quantification of wound healing after fractional laser therapy," *Journal of the American Academy of Dermatology*, vol. 69, no. 4, pp. e165–e173, 2013.

Hindawi Publishing Corporation
BioMed Research International
Volume 2014, Article ID 618206, 10 pages
http://dx.doi.org/10.1155/2014/618206

Clinical Study

Unconventional Use of Intense Pulsed Light

D. Piccolo,[1,2] D. Di Marcantonio,[3] G. Crisman,[4] G. Cannarozzo,[2] M. Sannino,[2] A. Chiricozzi,[3,5] and S. Chimenti[3]

[1] *Department of Dermatology, University of L'Aquila, Via Vetoio, Coppito 2, 67100 L'Aquila, Italy*
[2] *Italian Society of Laser Dermatology (SILD), Via Nicolò dall'Arca 7, 70121 Bari, Italy*
[3] *Department of Dermatology, University of Rome, Tor Vergata, Italy*
[4] *Department of Dermatology, University of Bologna, Italy*
[5] *Laboratory for Investigative Dermatology, The Rockefeller University, New York City, USA*

Correspondence should be addressed to D. Piccolo; domenico.piccolo@univaq.it

Received 6 February 2014; Revised 15 June 2014; Accepted 16 June 2014; Published 3 September 2014

Academic Editor: Silvia Moretti

According to the literature, intense pulsed light (IPL) represents a versatile tool in the treatment of some dermatological conditions (i.e., pigmentation disorders, hair removal, and acne), due to its wide range of wavelengths. The authors herein report on 58 unconventional but effective uses of IPL in several cutaneous diseases, such as rosacea (10 cases), port-wine stain (PWS) (10 cases), disseminated porokeratosis (10 cases), pilonidal cyst (3 cases), seborrheic keratosis (10 cases), hypertrophic scar (5 cases) and keloid scar (5 cases), Becker's nevus (2 cases), hidradenitis suppurativa (2 cases), and sarcoidosis (1 case). Our results should suggest that IPL could represent a valid therapeutic support and option by providing excellent outcomes and low side effects, even though it should be underlined that the use and the effectiveness of IPL are strongly related to the operator's experience (acquired by attempting at least one specific course on the use of IPL and one-year experience in a specialized centre). Moreover, the daily use of these devices will surely increase clinical experience and provide new information, thus enhancing long-term results and improving IPL effectiveness.

1. Introduction

First introduced in 1990s, intense pulsed light (IPL) was obtained by U.S. Food and Drug Administration (FDA) authorization in 1995 for the treatment of lower-limb telangiectasias.

This polychromatic, noncoherent, and broad-spectrum pulsed light source (xenon lamp) is able to emit light of a wavelength between 390 nm and 1200 nm [1]. Its basic principle consists in the absorption of photons by exogenous or endogenous chromophores within the skin; this transfer of energy to the target structures generates heat and subsequent destruction of the target through a process called selective photothermolysis. The wavelength should be selected in dependence of the absorption peak of the target chromophore and the pulse duration should last less than the thermal relaxation time. This limits the diffusion of heat and damage to surrounding structures.

The main chromophores of the skin, such as haemoglobin, melanin, and water, have a broad absorption spectrum. Through the use of a filter, available from 500 nm to 755 nm, it is possible to select the wavelengths suitable for the established treatment. The IPL's pulse duration may be set within a relatively wide range between 1 and 100 milliseconds, depending on the selected device. In addition, a wide range of treatment parameters, including pulse sequence and pulse delay time, can be customized, thus giving users greater versatility and accuracy [1].

Versatility represents a significant advantage for experienced dermatologists, but it could be a serious limit for nonexperienced physicians and for nonmedical staff since an erroneous selection of the setting can cause serious side effects.

In daily practice, the application of a gel is necessary, as well as direct contact between the handpiece and the skin, although this hinders the local immediate response.

Table 1: Clinical data.

	Number of patients	Gender	Mean age (range)
Rosacea	10	5 M, 5 F	51.6 (38–62)
Port wine stain	10	7 M, 3 F	52.1 (8–52)
Disseminated Porokeratosis	10	2 M, 8 F	58.3 (41–70)
Pilonidal cyst	3	3 M	24.6 (18–34)
Seborrheic keratosis	10	6 M, 4 F	61.7 (35–83)
Hypertrophic scar/keloids	5/5	3 M, 2 F/2 M, 3 F	30.2 (21–37)/34.8 (27–43)
Becker's nevus	2	2 M	29 (26–32)
Hidradenitis suppurativa	2	1 M, 1 F	32 (26–38)
Sarcoidosis	1	1 F	26
Total	**58**	**32M, 26F**	**42.7 (8–83)**

The combination of wavelength, pulse duration, delay, and fluence allows the use of IPL devices in the treatment of several dermatological conditions, such as acne vulgaris, pigmentation disorders, vascular lesions, hirsutism, photodamaged skin, scars and birthmarks, and melasma [2–4].

The authors herein suggest many unconventional uses of IPL in the treatment of different dermatological conditions, such as rosacea (10 cases), port-wine stain (PWS) (10 cases), disseminated porokeratosis (10 cases), pilonidal cyst (3 cases), seborrheic keratosis (10 cases), hypertrophic scar (5 cases) and keloid scar (5 cases), Becker's nevus (2 cases), hidradenitis suppurativa (2 cases), and sarcoidosis (1 case).

Acne rosacea or *rosacea* is a chronic dermatitis of unknown aetiology, characterized by erythema, telangiectasias, papules and pustules [5, 6].

Port-wine stain is a common congenital vascular malformation occurring in up to 25% of infants [7–10].

Disseminated porokeratosis is a localized alteration of keratinization. Clinically, one or more atrophic mainly asymptomatic and sometimes mildly itching plaques surrounded by an hyperkeratotic border (histologically defined as a cornoid lamella) are observed due to a rapid proliferation of atypical keratinocytes [11–14].

Pilonidal cyst, also known as *pilonidal sinus* or *sacrococcygeal cyst* (due to its frequent onset in this area), is a cyst containing hair and skin debris [15–19].

Seborrheic keratosis is a benign skin lesion of the epidermis, mainly localized on seborrheic areas, in particular, the face and trunk. The most common clinical presentation is a lesion with warty or squamous crusted surface of variable size, coloured yellow-brown or dark-brown with blackish specks, with soft consistency [20, 21].

Hypertrophic scars and keloids are a serious physical and psychological dermatological condition for patients. Despite the several studies performed on metabolisms and treatment of wounds and scars, the exact pathogenesis of keloids and hypertrophic scars remains unknown and this makes therapies even more complicated [22].

Becker's nevus is a mostly male-predominant birthmark hyperpigmentation, presenting with a unilateral (rarely bilateral), benign hypermelanotic patch usually sited on the shoulder, chest, or lower back. Grouped brown spots with a bizarre border are the common presentation, with hypertrichosis in half of the cases [23, 24].

Hidradenitis suppurativa is a common disease, also known as acne inversa, which leads to a chronic relapsing suppurative inflammation of regions where apocrine glands occur, that is, axilla, inguinal folds, perineum, genitalia, and periareolar region. Several predisposing, triggering, and etiologic factors have been encountered (androgenic dysfunction, obesity, etc.); thus, authors agree that aetiology is still unclear. Commonly, the follicles into which the apocrine glands open are plugged by keratin and infections, mainly caused by anaerobic organisms which develop the following stasis and cause cysts that are extremely painful to palpation [25–27].

Sarcoidosis is both a systemic and a dermatologic syndrome of unknown etiology which can affect the skin as well the lymph nodes and viscera. The lesions can be single or multiple and can range from macules to large plaques and nodules. Cutaneous involvement is referred to in up to 25% of patients with systemic sarcoidosis. Plaques, maculopapular eruptions, subcutaneous nodules, and lupus pernio can be observed as well as cutaneous manifestations [28–33].

2. Material and Methods

58 consecutive patients (32 males and 26 females, mean age 42.7—range 8–83) presenting with nine different dermatological disorders were treated with IPL as an unconventional approach (Table 1). The aim of the study was to verify the efficacy of IPL by comparing the obtained results with results achieved through conventional treatment options (according to the literature) using either clinical or dermoscopic pictures before and after each session. Notably, dermoscopy conducted before treatment confirmed its usefulness in confirming diagnosis and in highlighting specific characteristics of each condition, such as number and calibre of blood vessels, distribution of pigment, and presence of crusts or hairs; thus, it also represents a valid method for outcome assessments [34]. An IPL device (Deka M.E.L.A. Srl, Calenzano, Florence, Italy) with two different handpieces for 500 nm and 550 nm filters was used and set according to the skin type and clinical characteristics of each patient. Dermoscopic images were made in all cases before, immediately after and at distance from each treatment using a special lens for dermoscopy (DermLite Foto, 3GEN LLC, San Juan Capistrano, CA, USA) connected to a digital camera (Canon PowerShot A360).

Table 2: IPL setting for each off-label dermatological disease treated.

	Filters	Number of pulses	Pulse duration	Delay	Fluence	Number of sessions
Rosacea erythematotelangiectatic component	500	2	5–10 msec	10 msec	12–16 J/cm^2	Up to 4
Rosacea papulopustular component	550	2	5–10 msec	10 msec	10–12 J/cm^2	Up to 5
Port wine stain	500	2	5–10 msec	10 msec	13–16 J/cm^2	Up to 5
Disseminated porokeratosis	550	2	5–10 msec	10 msec	10–12 J/cm^2	Up to 4
Pilonidal cyst	550	3	5 msec	20 msec	7–9 J/cm^2	Up to 3
Seborrheic keratosis	550	2	5–10 msec	10 msec	10–12 J/cm^2	2
Hypertrophic scar and keloid pigmented component	550	2	5–10 msec	10 msec	10–12 J/cm^2	Up to 5
Hypertrophic scar and keloid vascular component	500	2	5–10 msec	10 msec	14–17 J/cm^2	Up to 6
Becker's nevus hair removal	550	2-3	5 msec	10–20 msec	7–9 J/cm^2	Up to 4
Becker's nevus pigmented component	550	2	5–10 msec	10 msec	9–12 J/cm^2	Up to 5
Hidradenitis suppurativa hair removal	550	2-3	5 msec	10–20 msec	7–9 J/cm^2	Up to 4
Hidradenitis suppurativa inflammatory component	550	2	5–10 msec	10 msec	8–10 J/cm^2	Up to 5
Sarcoidosis	500	2	5–10 msec	10 msec	12–16 J/cm^2	Up to 4

A soothing cream, a gentle cleansing, and a photoprotection (SPF50) solution were prescribed to each patient after each session.

In the following, the authors describe the IPL scheme treatments and the results obtained for each dermatological condition. Each patient has been informed that at least two sessions up to six sessions, with intervals of approximately 20–30 days, are needed to gain significant results.

Rosacea. Ten patients (5 females and 5 males) aged between 38 and 62 years (average age 51.6 years) with Fitzpatrick phototype II-III presented with rosacea, 6 with an erythematotelangiectatic form, 3 with papules and pustules, and only one with rhinophyma.

The telangiectatic component was treated with the 500 nm handpiece, while the papulopustular component was subsequently treated with the 550 nm handpiece (Table 2).

Port-Wine Stain. Ten patients (7 males and 3 females) aged between 8 and 52 years (average age 22.1 years) with Fitzpatrick phototype II-III were treated for the presence of a PWS. Lesions were sited on the malar part of the face (3 cases), on the nose (2 cases), on the glabella (1 case), on the upper lip (1 case), on the forehead (1 case), on the posterior part of the neck (1 case), and on the posterior upper-right limb (1 case), respectively. Table 2 shows the IPL setting used in these cases.

Disseminated Porokeratosis. Ten patients (8 females and 2 males) aged between 41 and 70 years (average age 58.3 years) with Fitzpatrick phototypes II–IV were treated for the presence of multiple disseminated, atrophic, and slightly itchy plaques with a hyperkeratotic border. The lesions were mainly located on the lower extremities (50%), on the upper extremities (40%), and on the back (10%). Protocol shown on Table 2 has been successfully applied to these patients.

Pilonidal Cyst. Three patients (3 males) 18, 22, and 34 years old (average age 24.6 years) presented with a recurrent, inflamed, sore, and swollen cyst localized in the sacrococcygeal region. The lesion of the oldest patient had already been surgically treated. IPL action on hair follicles is well known and we thus suggested the use of this device with the aim of destroying hairs encapsulated within the cyst and hairs in the surrounding area. The anti-inflammatory properties of IPL proved to be effective in reducing the risk of recurrence. We decided to treat the lesion according to the protocol shown on Table 2.

Seborrheic Keratosis. Ten patients (6 males and 4 females) aged between 35 and 83 years (average age 61.7 years) with Fitzpatrick phototypes I–III were treated for the presence of multiple disseminated small seborrheic keratoses sited on the face (30%), on the chest (25%), and on the back (45%).

Figure 1: Rosacea: significant results with a significant reduction in vessel number and size and a complete disappearance of papules have been achieved after 4 IPL sessions.

All lesions were treated at intervals of 15–20 days for a total of 4 sessions per case according to the protocol shown in Table 2.

Dermoscopic images were obtained for each case before (also for diagnostic purpose), immediately after, and at a distance from each treatment using the same equipment described above.

Hypertrophic Scars and Keloids. Ten patients, 5 presenting with hypertrophic scars (3 males and 2 females aged between 21 and 37 years, average age 30.2 years) and 5 presenting with keloids (3 females and 2 males aged between 27 and 43 years, average age 34.8 years), were treated with both 500 nm (vascular component) and 550 nm (pigmented component) wavelength handpieces. The first sessions with the 550 nm handpiece were carried out for the pigmented component where present. Whereupon, successive treatments with the 500 nm handpiece have been made for treating the vascular component (Table 2).

At least 30 days of rest are required before the subsequent session and a few months are needed to obtain very positive results.

Becker's Nevus. A 32-year-old man presented with Becker's nevus sited on his left shoulder blade. Clinically, a hypertrichotic brown patch with irregular edges of 12 cm × 9 cm in size was observed. Successively, a 26-year-old man presented with Becker's nevus without hypertrichosis of 8,5 cm × 8 cm in size and sited on his upper-right chest. In the first case, we decided to first use a 550nm wavelength handpiece with the aim of removing the hair components (Table 2).

After four sessions of IPL at intervals of 40 days, we performed two additional sessions with the aim of treating the hyperpigmented component (Table 2). Only the protocol shown in Table 2 was applied to the second patient since the hypertrichotic component was not present.

Hidradenitis Suppurativa. One 38-year-old man, previously treated in a surgical way (clinical stage II (Hurley's staging system) and sartorius score of 36), and one 26-year-old woman presented with hidradenitis suppurativa of the axillary region, bilateral (clinical stage I (Hurley's staging system) and sartorius score of 24).

After four sessions of IPL at intervals of 15–20 days, we performed two additional sessions with 2 pulses of 5 ms and 10 ms separated by a delay of 10 ms and a fluence of 9 J/cm^2 with the aim of treating the inflammatory component (Table 2).

Sarcoidosis. A 26-year-old female presented with three painful, firm, and vascularized nodules sited on the anterior and posterior parts of the pinna and on the helix. Through histopathological examination, a diagnosis of sarcoidosis was posed. The patient had already undergone intralesional corticosteroid therapy without results. Thus, we suggested using the IPL device with the aim of hitting the very prominent (especially on dermoscopic evaluation) vascular component within the lesions.

3. Results

In this study, we obtained good outcomes for all the treated patients, who were affected by different dermatological conditions. Our results are summarized as follows.

Rosacea. Patients required from 2 to 5 sessions, at intervals of approximately 20–30 days, to gain significant results, even though a moderate reduction in vessel number and size and a partial disappearance of papules were observed subsequent to the second session (Figure 1). A 12-month follow-up revealed the complete absence of recurrences and the persistence of the achieved outcomes in 7 of 10 patients (70%) whereas the other 3 patients required a new treatment within the year for the slight relapse of the papulopustular component.

Port-Wine Stain. The results were already visible after the end of the first session. Dermoscopy performed before treatment highlighted the number, calibre, and depth of the target vessels. Superficial vessels were hit with greater accuracy by IPL and dermoscopic examinations revealed a change in vessel colour from red to blue immediately after treatment. In cases of high numbers of vessels, erosions and crusts can follow treatment sessions for several days. The number of the treatments required to gain significant results depended on the depth and site of the PWS.

Three out of 10 patients (30%) obtained excellent results (disappearance of PWS), 6 of 10 (60%) obtained good results (disappearance of almost 70% of treated vessels), and only one (10%) obtained a moderate result (disappearance of about 30% of the lesion) (Figure 2). The obtained results, confirmed

Figure 2: Port-wine stain: after 4 IPL sessions, the patient gained excellent results.

Figure 3: Disseminated porokeratosis: after 4 treatments, an important reduction of the hyperkeratotic edge and a reduction in the intensity of melanin have been observed.

by dermoscopy, were stable after a follow-up period ranging from 1 to 3 years.

Disseminated Porokeratosis. All treated patients showed interesting results, despite the fact that the histology confirmed the persistence of cornoid lamella. In fact, one patient who had shown significant improvements after four sessions presented at the follow-up visit with an important reduction of the hyperkeratotic edge and a reduction in the intensity of melanin (Figure 3); a punch biopsy was performed and the histopathologic examination revealed the persistence of a cornoid lamella.

Pilonidal Cyst. A complete resolution was achieved by the third session (80 days after the first visit) in 3 patients treated. (Figure 4) After a follow-up period of 5 years, for the first patient treated, and one year, for the other two, no recurrence has been observed.

Seborrheic Keratosis. Superficial and small seborrheic keratoses responded well to IPL, whereas larger and/or deeper lesions may require a CO_2 laser or other treatment. Dermoscopy is useful either to confirm diagnosis or to demonstrate a change in lesion colour from brown to grey immediately after treatment, thus predicting a good response to the treatment. Seborrheic keratosis was usually resolved with a mild inflammation and a complete recovery within 30 days after an average of two treatments (Figure 5).

Hypertrophic Scars and Keloids. Dermoscopic images revealed a significant reduction of vascular component in the thicker areas. Scars flattened and became smaller after three sessions. (Figures 6 and 7) All in all, good results were achieved, even though lengthy treatment (several months) is needed. The obtained results were stable during the follow-up. In one out of 5 cases of keloids, the lesion has resumed its growth phase.

Becker's Nevus. A progressive hair removal and a reduction of the hyperpigmented area were achieved to the good satisfaction of both patients (Figure 8).

Hidradenitis Suppurativa. At the end of the suggested scheme protocol, hidradenitis suppurativa was completely removed in both its inflammatory and painful components; hair removal was also achieved (Figure 9).

Sarcoidosis. A significant reduction of the vascular component and in the consistency of the lesions was achieved, thus leading to pain disappearance (Figure 10).

4. Discussion

In this study, we report on our good results achieved with almost all 58 patients affected by different dermatological conditions. With the aim of providing more exhaustive details, we will briefly discuss each condition separately.

Figure 4: Pilonidal cyst: a complete resolution was achieved by the third session.

Figure 5: Hidradenitis suppurativa: complete resolution of pustular-papules progressive hair removal after 3 IPL treatments, bilaterally. Clinical stage I (Hurley's staging) and sartorius score of 24.

(a)

(b)

Figure 6: Seborrheic keratosis: (a) significant reduction of multiple seborrheic keratoses of the face after 2 IPL sessions, (b) seborrheic keratoses of the back disappeared after 2 IPL sessions.

Figure 7: Hypertrophic scar: significant reduction of vascular component in the thicker areas before and after 3 IPL treatments.

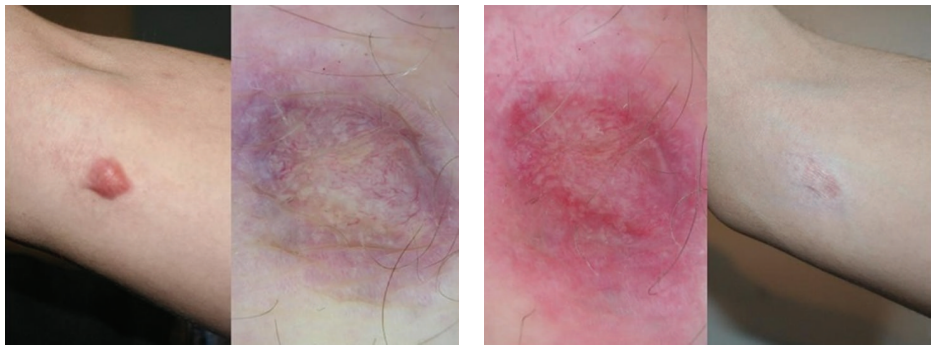

Figure 8: Keloid: scar after three sessions of IPL. Dermoscopy performed immediately after the first treatment showed a variation of the color from red-blue to red.

Rosacea. Treatment of clinical manifestation of rosacea usually involves lasers such as argon, pulsed dye, Nd:YAG, CO_2, and KTP, frequently causing burns, pain, and outcomes such as scars and significant hyperpigmentation due to incautious assessment of the lasers' photophysical parameters.

The ability to choose the duration of pulses makes IPL a versatile tool in the treatment of rosacea. The possibility of different filter settings (515, 550, 560, 570, and 590 nm) allows a wider selection of the range colour of the vascular system. A surface of 2.8 cm^2 can be treated with a single shot, in contrast to the pulse dye laser (1.96 cm^2 or 0.78 cm^2) and argon (3 mm^2). The larger surface offers greater efficiency, in terms of reducing treatment sessions, and less discomfort for the patient. Because it is able to divide the energy into two or three pulses with different delays between one pulse and the next, IPL allows the skin to cool down with minimal side effects [5].

Since the treatment is relatively unpainful, it can be carried out in the absence of anaesthesia. Immediate response usually presents as a slight erythema and a purple colouring which spontaneously resolves within 24–96 hours [5].

In a pilot study conducted by Mark et al., a 30% reduction of blood flow, a 29% reduction of telangiectasias, and a 21% reduction of erythema have been observed after five sessions of IPL. Taub et al. noticed a reduction of 83% of erythema, a reduction of 75% of flushing, and an improved skin texture [5, 6]. A 2008 study performed by Papageorgiou et al. noted the effectiveness of IPL in the treatment of rosacea disease of phase I. It showed a significant improvement of erythema, telangiectasias, and flushing. Severity was reduced and persistent results at 6 months with minimal side effects were obtained [2]. Reduction in the mechanical integrity of connective tissue of the dermis surface, responsible for passive dilatation of the blood vessels and thus resulting in erythema, telangiectasia, release of inflammatory mediators, and the formation of inflammatory papules and pustules, seems to play a key role in the treatment of rosacea. Moreover, IPL can improve rosacea through the ablation of its abnormal vessels and through the collagen remodelling of the dermis.

Furthermore, IPL determines a significant reduction of inflammation and in the number of active sebaceous glands, thus blocking, with great effectiveness, the altered process of keratinization [6].

In our study, all patients achieved significant results with 2 to 5 sessions of treatment.

Port-Wine Stain. Lasers such as the pulse dye laser, Nd:YAG, alexandrite, and the diode laser are the most used ones in the treatment of PWS [7, 8].

Currently, the first-choice treatment for PWS is represented by the pulsed dye laser; unfortunately, it cannot completely remove PWS. The energy emitted reaches only superficial vessels, thus resulting in a decreased amount of available light to hit the deeper ones (shadow effect). Because of this effect, hyper- and hypopigmentation and atrophic and hypertrophic scars may result after treatment [10]. When a PWS, especially with nodular component, is treated with an external light source, the main goal is to reach the vessels localized at the lower surface. IPL, thanks to its variability of pulse and fluence and to its possibility to divide the energy

Figure 9: Becker's nevus: a progressive hair removal and a reduction of the hyperpigmented area were achieved to the good satisfaction of the patient.

Figure 10: Sarcoidosis: significant reduction of the nodules with diminution of the painful sensation after 3 IPL treatments.

into different pulses, allows an additional heating which leads to coagulation of blood vessels of different diameter and different depth [1, 8]. Raulin et al. reported a 70–99% resolution of pink-coloured PWS after 2.9 treatments, of red PWS after about 1.4 treatments, and of purple PWS after an average of 2.4 sessions. In a study by Ozdemir et al., 37 patients with PWS were evaluated with results of up to 100% in 7 patients and 70–99% in 14 patients. In fact, IPL can be considered an effective treatment option. However, IPL systems require considerable experience and should be conducted with the aid of a good dermoscopy in order to determine the type of vessels to treat [34].

Disseminated Porokeratosis. Potential therapies include topical 5-fluorouracil, oral retinoids, CO_2 laser, pulse dye laser, Nd:YAG, cryotherapy, dermabrasion, surgical excision, and imiquimod, or a combination of several therapies simultaneously [11–14].

In cases of superficial actinic porokeratosis, IPL proves to be a valid therapeutic option by determining a destruction of the pigment without risk of scarring or other side effects.

Pilonidal Cysts and Hidradenitis Suppurativa. According to the literature, laser technology applied in such cases includes CO_2 laser and Nd:YAG. For its photocoagulative action, CO_2 laser treatment produces a precise wound with minimal blood loss, leaving a surgical field clean and dry, but it is able to coagulate large vessels and requires a long recovery period [16–19].

IPL may represent a valid option for such lesions. The broad light spectrum is absorbed by the hair shaft, generates heat, and destroys the hair follicle. IPL acts on the melanin of the hair follicle causing necrosis of the follicle within the cyst. Similarly, it acts on the hairs of the surrounding area in order to reduce recurrence. Moreover, IPL has proven to be a powerful anti-inflammatory treatment able to eliminate the chronic inflammation within the cyst [19]. In 2011, Highton et al. selected 18 patients affected by HS and treated one axilla, groin, or inframammary area with intense pulsed light two

times per week for 4 weeks using a harmony laser, whereas the contralateral side received no treatment and was used as a control. A significant improvement in the mean examination and its persistence at 12 months led patients to report high levels of satisfaction. No concurrent improvement on the untreated control side has been observed. This small study suggests that intense pulsed light may be an effective treatment for HS. Although only a few data have been reported so far, results suggest efficacy and safety and the absence of side effects [26].

Seborrheic Keratosis. In previous studies, lasers have been demonstrated to be effective in the treatment of seborrheic keratosis, such as alexandrite (755 nm) and diode laser [21].

No studies on the use of pulsed light for the treatment of seborrheic keratosis have been published so far. Thanks to its broad spectrum of action, it is possible to select the specific wavelength to act selectively on the melanin pigment of seborrheic keratosis. Immediately after the treatment, a change in colour from brown to grey is observed at dermoscopic evaluation and this represents a sign of success of the performed procedure [34]. Subsequently, keratosis tends to disappear completely without residual erythema. The treatment is, however, limited to superficial and small seborrheic keratoses.

Hypertrophic Scars and Keloids. The pulse dye laser has been reported to produce long-term improvements in the appearance of hypertrophic scars. A very recent pilot study has demonstrated the effectiveness of IPL in wound healing after suture removal. The basic mechanism is not yet fully understood but most probably an action on vascular proliferation, essential for the growth of collagen, and on pigmentation resulting from scar formation is involved [22]. Despite the wide use of IPL in various skin diseases, only a few studies demonstrating its effectiveness on hypertrophic scars have been published to date. Wavelengths around 1200 nm are absorbed by the water within the dermis thus triggering a reaction that leads to cytokine stimulation of collagen fibres of types I and III and elastin. The absorption peak of the collagen fibres is found to be from 400 nm to 600 nm. The heating of the collagen fibres by the IPL leads to their contraction, with a clinically detectable improvement in the texture. The IPL, in contrast to other treatments, is not invasive and has very few side effects. Bellew et al. have shown that the IPL is as effective as the long pulse dye laser (595 nm), resulting in a greater softness of the scar. Kontoe et al. reported an improvement of more than 75% in the pigmentation of hypertrophic scars, 50% higher than that in the scars from asphalt, and 50% reduction in the size and thickness of hypertrophic scars. This is probably due to the inhibition of the action of the vessel caused by IPL on scar tissue and on the subsequent proliferation of collagen [22].

Becker's Nevus. Trelles et al. compared the effectiveness of the Erbium:YAG laser with the Nd:YAG laser in 22 Becker's nevus patients, 11 for each group. Up to now, there have been no studies on the treatment of Becker's nevus with IPL. Such treatment is able to produce synchronized single or multiple pulses with the possibility of varying the pulse duration. We can then select the appropriate wavelength, taking into account the main absorption spectrum of the pigmented structures (between 400 nm and 600 nm) and the right pulse duration to act efficiently on the hair follicle. We can operate on both components with excellent results. [23, 24].

Sarcoidosis. In his systematic review on the use of pulsed dye laser in the treatment of inflammatory skin diseases published in 2013, Erceg A reported on five case reports of PDL treatment for cutaneous sarcoidosis/lupus pernio [28–33]. In our experience, IPL has been proven to have a significant effect on the vascular component of granulomata. Even though IPL could not definitely treat cutaneous sarcoidosis, a great improvement of patients' pain and symptoms could be achieved.

5. Conclusions

According to the literature, the effectiveness of IPL has now been well demonstrated. Its versatility, in contrast with many single-laser spectrums, has led to its rapid spread in different clinical scenarios, while the wide range of wavelengths allows us to use these devices for a broader range of clinical conditions. However, we would like to underline how the use and effectiveness of the IPL are strongly related to the operator's experience. Apart from facilitating excellent outcome, the broad spectrum of wavelengths used and the high number of parameters can affect the final result and increase the risk of side effects. The daily use of these devices will surely increase clinical experience and provide new information, thus enhancing long-term results and improving IPL effectiveness.

Conflict of Interests

The authors declare that there is no conflict of interests regarding the publication of this paper.

References

[1] D. H. Ciocon, A. Boker, and D. J. Goldberg, "Intense pulsed light: What works, what's new, what's next," *Facial Plastic Surgery*, vol. 25, no. 5, pp. 290–300, 2009.

[2] P. Babilas, S. Schreml, R. M. Szeimies, and M. Landthaler, "Intense pulsed light (IPL): a review," *Lasers in Surgery and Medicine*, vol. 42, no. 2, pp. 93–104, 2010.

[3] G. Zoccali, D. Piccolo, P. Allegra, and M. Giuliani, "Melasma treated with intense pulsed light," *Aesthetic Plastic Surgery*, vol. 34, no. 4, pp. 486–493, 2010.

[4] P. Myers, P. Bowler, and S. Hills, "A retrospective study of the efficacy of intense pulsed light for the treatment of dermatologic disorders presenting to a cosmetic skin clinic," *Journal of Cosmetic Dermatology*, vol. 4, no. 4, pp. 262–266, 2005.

[5] C. A. Schroeter, S. Haaf-von Below, and H. A. M. Neumann, "Effective treatment of rosacea using intense pulsed light systems," *Dermatologic Surgery*, vol. 31, no. 10, pp. 1285–1289, 2005.

[6] P. Papageorgiou, W. Clayton, S. Norwood, S. Chopra, and M. Rustin, "Treatment of rosacea with intense pulsed light: significant improvement and long-lasting results," *British Journal of Dermatology*, vol. 159, no. 3, pp. 628–632, 2008.

[7] G. Li, T. Lin, Q. Wu, Z. Zhou, and M. H. Gold, "Clinical analysis of port wine stains treated by intense pulsed light," *Journal of Cosmetic and Laser Therapy*, vol. 12, no. 1, pp. 2–6, 2010.

[8] A. J. Burns and J. A. Navarro, "Role of laser therapy in pediatric patients," *Plastic and Reconstructive Surgery*, vol. 124, no. 1, supplement, pp. 82e–92e, 2009.

[9] M. Ozdemir, B. Engin, and I. Mevlitoğlu, "Treatment of facial port-wine stains with intense pulsed light: a prospective study," *Journal of Cosmetic Dermatology*, vol. 7, no. 2, pp. 127–131, 2008.

[10] A. Sevila, E. Nagore, R. Botella-Estrada et al., "Videomicroscopy of venular malformations (port-wine stain type): Prediction of response to pulsed dye laser," *Pediatric Dermatology*, vol. 21, no. 5, pp. 589–596, 2004.

[11] J. Levitt, J. J. Emer, and P. O. Emanuel, "Treatment of porokeratosis of Mibelli with combined use of photodynamic therapy and fluorouracil cream," *Archives of Dermatology*, vol. 146, no. 4, pp. 371–373, 2010.

[12] R. Hartman, R. Mandal, M. Sanchez, and J. A. Stein, "Porokeratosis plantaris, palmaris, et disseminata," *Dermatology Online Journal*, vol. 16, no. 11, article 22, 2010.

[13] S. Venkatarajan, T. M. Leleux, D. Yang, T. Rosen, and I. Orengo, "Porokeratosis of Mibelli: successful treatment with 5 percent topical imiquimod and topical 5 percent 5-fluorouracil," *Dermatology Online Journal*, vol. 16, no. 12, article 10, 2010.

[14] M. Itoh and H. Nakagawa, "Successful treatment of disseminated superficial actinic porokeratosis with Q-switched ruby laser," *Journal of Dermatology*, vol. 34, no. 12, pp. 816–820, 2007.

[15] E. A. Badawy and M. N. Kanawati, "Effect of hair removal by Nd:YAG laser on the recurrence of pilonidal sinus," *Journal of the European Academy of Dermatology and Venereology*, vol. 23, no. 8, pp. 883–886, 2009.

[16] Y. Oram, F. Kahraman, Y. Karincaoğlu, and E. Koyuncu, "Evaluation of 60 patients with pilonidal sinus treated with laser epilation after surgery," *Dermatologic Surgery*, vol. 36, no. 1, pp. 88–91, 2010.

[17] A. V. Benedetto and A. T. Lewis, "Pilonidal sinus disease treated by depilation using an 800 nm diode laser and review of the literature," *Dermatologic Surgery*, vol. 31, no. 5, pp. 587–591, 2005.

[18] N. S. Sadick and J. Yee-Levin, "Laser and light treatments for pilonidal cysts," *Cutis*, vol. 78, no. 2, pp. 125–128, 2006.

[19] V. Jain and A. Jain, "Use of lasers for the management of refractory cases of hidradenitis suppurativa and pilonidal sinus," *Journal of Cutaneous and Aesthetic Surgery*, vol. 5, no. 3, pp. 190–192, 2012.

[20] D. Mehrabi and R. T. Brodell, "Use of the alexandrite laser for treatment of seborrheic keratoses," *Dermatologic Surgery*, vol. 28, no. 5, pp. 437–439, 2002.

[21] G. R. Culbertson, "532-nm diode laser treatment of seborrheic keratoses with color enhancement," *Dermatologic Surgery*, vol. 34, no. 4, pp. 525–527, 2008.

[22] O. O. Erol, A. Gurlek, G. Agaoglu, E. Topcuoglu, and H. Oz, "Treatment of hypertrophic scars and keloids using intense pulsed light (IPL)," *Aesthetic Plastic Surgery*, vol. 32, no. 6, pp. 902–909, 2008.

[23] R. Alhusayen, N. Kanigsberg, and R. Jackson, "Becker nevus on the lower limb: case report and review of the literature," *Journal of Cutaneous Medicine and Surgery*, vol. 12, no. 1, pp. 31–34, 2008.

[24] C. Raulin, M. P. Schönermark, B. Greve, and S. Werner, "Q-switched ruby laser treatment of tattoos and benign pigmented skin lesions: a critical review," *Annals of Plastic Surgery*, vol. 41, no. 5, pp. 555–565, 1998.

[25] K. M. Mitchell and D. E. Beck, "Hidradenitis suppurativa," *Surgical Clinics of North America*, vol. 82, no. 6, pp. 1187–1197, 2002.

[26] L. Highton, W. Chan, N. Khwaja, and J. K. G. Laitung, "Treatment of hidradenitis suppurativa with intense pulsed light: a prospective study," *Plastic and Reconstructive Surgery*, vol. 128, no. 2, pp. 459–465, 2011.

[27] Y. Endo, A. Tamura, O. Ishikawa, and Y. Miyachi, "Perianal hidradenitis suppurativa: early surgical treatment gives good results in chronic or recurrent cases," *British Journal of Dermatology*, vol. 139, no. 5, pp. 906–910, 1998.

[28] A. Erceg, E. M. J. G. de Jong, P. C. M. van de Kerkhof, and M. M. B. Seyger, "The efficacy of pulsed dye laser treatment for inflammatory skin diseases: a systematic review," *Journal of the American Academy of Dermatology*, vol. 69, no. 4, pp. 609.e8–615.e8, 2013.

[29] M. M. Goodman and K. Alpern, "Treatment of lupus pernio with the flashlamp pulsed dye laser," *Lasers in Surgery and Medicine*, vol. 12, no. 5, pp. 549–551, 1992.

[30] S. Cliff, R. H. Felix, L. Singh, and C. C. Harland, "The successful treatment of lupus pernio with the flashlamp pulsed dye laser," *Journal of Cosmetic and Laser Therapy*, vol. 1, no. 1, pp. 49–52, 1999.

[31] R. D. Holzmann, S. Astner, T. Forschner, and G. Sterry, "Scar sarcoidosis in a child: case report of successful treatment with the pulsed dye laser," *Dermatologic Surgery*, vol. 34, no. 3, pp. 393–396, 2008.

[32] S. Roos, C. Raulin, H. Ockenfels, and S. Karsai, "Successful treatment of cutaneous sarcoidosis lesions with the flashlamp pumped pulsed dye laser," *Dermatologic Surgery*, vol. 35, no. 7, pp. 1139–1140, 2009.

[33] M. Ekbäck and L. Molin, "Effective laser treatment in a case of lupus pernio," *Acta Dermato-Venereologica*, vol. 85, no. 6, pp. 521–522, 2005.

[34] D. Piccolo, *The Usefulness of Dermoscopy in Laser and Intense Pulsed Light Treatments*, Remo Sandron, Florence, Italy, 2012.

Hindawi Publishing Corporation
BioMed Research International
Volume 2014, Article ID 903589, 14 pages
http://dx.doi.org/10.1155/2014/903589

Review Article

Clinical Nonlinear Laser Imaging of Human Skin: A Review

Riccardo Cicchi,[1,2] Dimitrios Kapsokalyvas,[2] and Francesco Saverio Pavone[1,2,3]

[1] *National Institute of Optics (INO), National Research Council (CNR), Largo E. Fermi 6, 50125 Florence, Italy*
[2] *European Laboratory for Non-Linear Spectroscopy (LENS), University of Florence, Via Nello Carrara 1, 50019 Sesto Fiorentino, Italy*
[3] *Department of Physics, University of Florence, Via Giovanni Sansone 1, 50019 Sesto Fiorentino, Italy*

Correspondence should be addressed to Riccardo Cicchi; rcicchi@lens.unifi.it

Received 24 April 2014; Accepted 11 July 2014; Published 28 August 2014

Academic Editor: Piero Campolmi

Nonlinear optical microscopy has the potential of being used *in vivo* as a noninvasive imaging modality for both epidermal and dermal imaging. This paper reviews the capabilities of nonlinear microscopy as a noninvasive high-resolution tool for clinical skin inspection. In particular, we show that two-photon fluorescence microscopy can be used as a diagnostic tool for characterizing epidermal layers by means of a morphological examination. Additional functional information on the metabolic state of cells can be provided by measuring the fluorescence decay of NADH. This approach allows differentiating epidermal layers having different structural and cytological features and has the potential of diagnosing pathologies in a very early stage. Regarding therapy follow-up, we demonstrate that nonlinear microscopy could be successfully used for monitoring the effect of a treatment. In particular, combined two-photon fluorescence and second-harmonic generation microscopy were used *in vivo* for monitoring collagen remodeling after microablative fractional laser resurfacing and for quantitatively monitoring psoriasis on the basis of the morphology of epidermal cells and dermal papillae. We believe that the described microscopic modalities could find in the near future a stable place in a clinical dermatological setting for quantitative diagnostic purposes and as a monitoring method for various treatments.

1. Introduction

The "gold standard" for tissue diagnostics is the histological examination, which is performed by means of white light optical microscopy on cryosectioned, processed, and labelled slices of tissue. Modern optics provides imaging tools for a noninvasive label-free deep imaging of skin that offer the potential for both tissue diagnostics and therapy follow-up *in vivo* and *in situ*, without the requirement of a biopsy.

Among these optical techniques, two-photon fluorescence (TPF) microscopy [1] is a high-resolution laser scanning imaging technique enabling deep optical imaging of tissues. TPF intrinsically offers several advantages with respect to other laser scanning imaging techniques, including higher spatial resolution, intrinsic optical sectioning capability, reduced photodamage and phototoxicity, and deeper penetration depth within biological tissues [2]. Further, since both cells and extracellular matrix intrinsically contain a variety of fluorescent molecules (NADH, tryptophan, keratins, melanin, elastin, cholecalciferol, and others), biological tissues can be imaged by TPF microscopy without any exogenously added probe [3–5]. By taking advantage of mitochondrial NADH fluorescence, TPF microscopy can be used for a morphological characterization of epithelia, as demonstrated by studies performed on *ex vivo* tissue samples [6, 7], fresh biopsies [8–12] and also *in vivo* on both animals [13] and humans [14–18]. Additional morphological information can be provided by second-harmonic generation (SHG) microscopy [19–29], which can be combined with TPF microscopy using the same laser source. In particular, while TPF reveals the distribution of endogenous fluorophores such as NADH, flavins, elastin, and others, SHG microscopy is offering the direct high-resolution imaging of collagen structures. SHG was already largely used for imaging anisotropic molecules inside cells [19, 20] and tissues [21, 23]. Collagen fibres produce a high SHG signal [22] with which they can be imaged inside skin dermis. Recently, SHG was also used for investigating collagen fibres orientation and their structural changes in healthy tissues as human dermis [10, 24, 28, 30, 31]

or cornea [25, 27, 32] and in the tumour microenvironment [33–35]. Combined TPF-SHG microscopy represent a powerful tool for imaging skin dermis, since the main dermal components, collagen and elastin, can be imaged by SHG and TPF microscopy, respectively [4]. In particular, it has been used for monitoring collagen alteration in dermal disorders [28] or at the tumour-stroma interface [33–35], as well as for monitoring skin aging by measuring the collagen/elastic fibres content [36–38]. Fluorescence lifetime imaging microscopy (FLIM), when performed with nonlinear excitation, is an additional noninvasive microscopy technique enabling the identification of endogenous fluorescence species and their surrounding medium by measuring the decay rate of fluorescence emission [39, 40]. FLIM is useful to study protein localization [41] and fluorescent molecular environment [42]. FLIM was demonstrated to be a powerful technique able to provide functional information about tissue conditions [16, 17, 39, 40, 43–45]. It was successfully used to characterize tissues and to detect cellular differentiation inside epithelia as demonstrated by studies performed on cell cultures [46], fresh biopsies [8, 11, 12], and recently also *in vivo* [18]. Further, functional information on tissue conditions can be revealed by means of time-resolved analysis of NADH emission [46–48]. TPEF-FLIM has been previously applied to the study of the fluorescent properties of both normal and diseased skin [16, 17, 45] and has been demonstrated as an important tool to characterize skin layers specificity [8, 16].

In this paper, after having described materials and methods, we first show how it is possible to differentiate various epidermal layers *in vivo* by using TPF microscopy. In particular, the detection of skin autofluorescence allows direct imaging of cells and their morphological classification based on the cellular and nuclear sizes. Additional functional information, related to the metabolic conditions of cells, can be extracted by analysing the temporal decay of NADH fluorescence by means of FLIM. We found that cells located in the basal layer have the strongest metabolic activity, whereas the activity is reduced when moving towards the epidermal surface. Such approach can be used for characterizing epithelial tissues in various physiologic conditions and has the potential to detect pathologies in a very early stage, as demonstrated by studies performed on cell cultures [46, 49], fresh biopsies [8, 11, 12], and also *in vivo* [18]. In the second part of the paper, we show two different examples demonstrating that nonlinear microscopy can be successfully used for monitoring the effect of a laser-based treatment and for diagnosing and monitoring psoriasis. In particular, combined TPF and SHG microscopy were used *in vivo* for monitoring collagen remodeling after microablative fractional laser resurfacing and for characterizing psoriasis on the basis of the morphology of epidermal keratinocytes and dermal papillae. In the first example, *in vivo* nonlinear imaging was performed at the dermal level on the forearm of healthy subjects before and forty days after microablative fractional laser resurfacing treatment with the aim of characterizing collagen organization. Both qualitative and quantitative analyses demonstrated a stronger collagen synthesis and remodelling on older subjects, whereas the modifications were minimal on younger subjects. The second example focuses on the morphological characterization of both skin epithelium and papillary dermis in psoriasis. The morphological differences that can be observed between healthy and psoriatic skin are already well established by histopathological examination. In the example shown, these morphological differences were visualized *in vivo* by means of nonlinear imaging. In particular, in psoriasis we observed a drastically different morphology of epithelium with respect to healthy skin that includes a thickening of corneum layer, a disorganization of corneocytes, and a more sparse arrangement of keratinocytes. Differences were observed also at the dermal level in terms of an increased density and penetration depth of dermal papillae in psoriasis with respect to healthy skin. Morphological and architectural information were quantified and could be used for monitoring their course during a systemic treatment. The imaging modalities presented here represent promising tools to be used for both diagnostic and therapy follow-up purposes in dermatology and they could find a stable place in a clinical dermatological setting in the near future.

2. Materials and Methods

2.1. Experimental Setup. The experimental setup for imaging is a custom-made compact flexible nonlinear laser scanning microscope to be used for *in vivo* skin inspection. The system is mainly composed of four parts: the laser source and the optical system on the bench; the 7-mirror articulated arm; the microscope head; and the multispectral detector (see Figure 1(a)). The laser source is a Chameleon Ultra II (Coherent, Santa Clara, CA, US) pulsed Ti:Sapphire laser emitting 140 fs pulses at 80 MHz repetition rate, tunable in the range 690 nm–1080 nm. The output beam passes through a polarization-based system for power adjustment, made with a rotating half-waveplate and a polarizer, before being collimated by a telescope. An electronic shutter SH05 (Thorlabs, Newton, NJ, US) allows minimizing the exposure of the sample. Laser beam is then coupled to the articulated arm (El.En. Group, Calenzano, Italy), which is made by three titanium tubes connected through couples of mirrors, mounted on ball-bearings-based 45-degree mounts. This solution allows moving the microscope head maintaining the laser beam aligned and centered inside the arm itself. The laser beam is sent to the microscope head, composed of three metallic plates that divide it into three levels. In the lower level we placed detectors electronics, galvomirrors driver C280 (Galvoline, Rome, Italy), and a stepping motor for focusing M-111.DG (Physik Insytrumente, Karlsruhe, Germany). In the midlevel (scanning plate) we have the scanning head G1222 (Galvoline, Rome, Italy), a beam expander, a dichroic mirror 685DCXRU (Chroma Technology Corporation, Rockingham, VT, US), and the objective lens. Fluorescence (and/or SHG) light is reflected by the dichroic mirror to the upper level (detection plate) through a hole in which a laser blocking filter E700SP-2P (Chroma Technology Corporation, Rockingham, VT, US) is inserted. On the upper level (detection plate), there are two detection systems. The former is composed of a photomultiplier tube H7422 (Hamamatsu, Hamamatsu City,

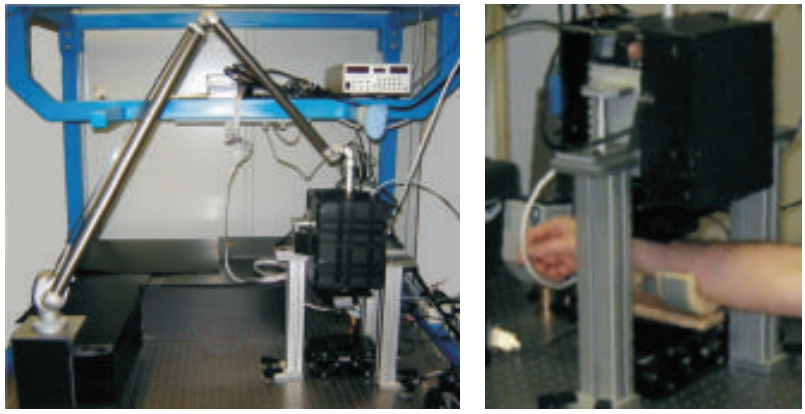

(a) (b)

Figure 1: Experimental setup. (a) Photo of the custom nonlinear microscope experimental setup. (b) Detail of the forearm mounting stage.

Japan) and is based on photocurrent integration. The latter is based on single photon counting and is made by an objective lens Plan10x (Nikon, Tokyo, Japan) to collect light and to couple it into a multimode optical fibre (OF), connected to the multispectral detector (Multi-PMT). The insertion of a narrow band-pass filter HQ420BP (Chroma Technology Corporation, Rockingham, VT, US) in the detection path allows exclusively detecting SHG. The multispectral detector PML-Spec (Becker-Hickl GmbH, Berlin, Germany) is composed of a diffraction grating with 600 lines/mm and a 16-channel multianode photomultiplier strip with 200 ps FWHM pulses that allows time- and spectral-resolved detection. A special custom mount, placed on the optical bench, allows placing the forearm under the microscope for *in vivo* examination (see Figure 1(b)).

The experimental setup used for microablative fractional laser resurfacing is a SmartXide DOT (Deka, El.En. Group, Calenzano, Italy) providing pulsed illumination in a raster fashion in order to perform fractional ablation of skin. The experiments were performed using a laser power of 20 W, a pixel dwell time of 1 ms, and a spacing of 0.5 mm over a 15 mm by 15 mm treated area. The volunteers were treated in the volar part of the forearm.

2.2. Data Acquisition and Processing. Two objective lenses can be mounted on the microscope: PlanFluor 40x (Zeiss, Jena, Germany), oil immersion, NA1.3, and WD 0.16 mm, or XLUM 20x (Olympus Corporation, Tokyo, Japan), water immersion, NA0.9, and WD 2 mm. Acquisition and control are performed using a PC and two synchronized I/O boards: a PCI-MIO-16E (National Instruments, Austin, TX, US); a SPC-730 (Becker-Hickl GmbH, Berlin, Germany). The two boards are synchronized by an electronic timing board E-6502 (National Instruments, Austin, TX, US) providing a common trigger. The output settings are controlled by custom-made software developed in LabView 7.1 (National Instruments, Austin, TX, US) ambient. The visualization of the acquired FLIM images is accomplished using dedicated software SPCM 1.1 (Becker-Hickl GmbH, Berlin, Germany). Image pixels exponential fits, deconvolution, and fluorescence decay analyses are performed using the software SPC-Image 2.8 (Becker-Hickl GmbH, Berlin, Germany) using a double-exponential decay model. Graphs and histograms were prepared in Microcal Origin Pro 8.0 (OriginLab Co., Northampton, MA, US).

TPF images in the epidermis were typically acquired using the 40x objective lens, 740 nm as excitation wavelength, a resolution of 512 × 512 pixels (corresponding to a field of view of about 200 μm), using a pixel dwell time of 20 μs, and a power in the 20 mW–50 mW range, depending on the depth of recording. FLIM images were acquired using the same laser power and wavelength, with 128 × 128-pixel spatial resolution (corresponding to 100 μm field of view), a pixel dwell time of 0.2 ms, and an integration time of approximately 40 s per image.

SHG images in the dermis were typically acquired using the 20x objective lens, 900 nm as excitation wavelength, a resolution of 512 × 512 pixels (corresponding to a field of view of about 400 μm), using a pixel dwell time of 20 μs, and a power in the 30 mW–60 mW range, depending on the depth of recording. FLIM images were acquired using the same laser power and wavelength, with 128 × 128-pixel spatial resolution (corresponding to 200 μm field of view), a pixel dwell time of 0.2 ms, and an integration time of approximately 40 s per image. Spectral images were acquired in blocks of 16 spectral images (420 nm–620 nm spectral range) with 64 × 64-pixel spatial resolution, 64 μm field of view dimension, using a pixel dwell time of 0.2 ms and an integration time of approximately 40 s per image block.

2.3. Examined Volunteers. The study on FLIM imaging of the epidermis (Section 3.1) included 2 healthy Caucasian male volunteers (31 and 32 years old). The study on fractional laser resurfacing (Section 3.2) included 9 healthy Caucasian volunteers (5 males, 4 females, age range: 27–79 years). Examined volunteers were divided into three groups according to their age: Group I (3 volunteers, age < 35 years), Group II (3 volunteers, 35 years < age < 60 years), and Group III (3 volunteers, age > 60 years). The study on psoriasis

(Section 3.3) included 8 Caucasian volunteers, 5 healthy and 3 affected with psoriasis. All the studies were approved by the Institutional Review Board of the University of Florence and conducted according to the tenets of the Declaration of Helsinki. Written informed consents were obtained from all participants after detailed explanation of the study.

3. Results

3.1. In Vivo Imaging and Characterization of Epidermal Layers. *In vivo* imaging of the epidermis with subcellular spatial resolution can be performed by using TPF microscopy. Images of the various epidermal layers (Figures 2(a)–2(c)) were acquired by using a water immersion objective lens (NA 1.2) and an excitation wavelength of 740 nm. Signal was collected in the whole spectral range without any filtering in order to have a signal-to-noise ratio as high as possible. Cells are clearly distinguishable from the images and they appear with a fluorescent cytoplasm and a dark nucleus. Further, an analysis based on morphology enables discriminating various epidermal layers. In particular, our attention was focused on epidermal layers containing living cells. As expected, granular layer (Figure 2(a)) showed cells larger in dimension, with a characteristic content of highly fluorescent granuli, and emitting a lower average fluorescence with respect to other epidermal cells. Then, going deeper into skin (spinous layer), cells appear smaller in size, more round in shape and they are in average more fluorescent as well as tightly packed (Figure 2(b)) with respect to the upper layer. This trend is maintained when imaging deeper in the basal layer (Figure 2(c)) which contains the smaller epidermal cells having the largest metabolic activity. This feature corresponds to a higher fluorescent signal coming from this layer, as shown in Figure 2(c). Further, at this depth, images start exhibiting some extremely bright spots, probably corresponding to melanin granuli. Even if the probability of generating reactive oxygen species by prolonged multiphoton excitation inside skin has already been demonstrated to be not higher than normal sun exposure [50], at this depth we preferred to limit the acquisition only to few images because basal layer is the most absorbing region inside skin. Moreover, in order to limit the absorption to a minimum dose, images of epidermis were taken from the inner forearm which is one of the less pigmented regions of the body.

A layer-by-layer analysis of epidermis using FLIM was performed in skin of a healthy male volunteer who agreed to participate in the study. Mean lifetime distributions were calculated from images acquired at 20 μm, 40 μm, and 60 μm depth from skin surface, approximately corresponding to granular, spinous, and basal layer, respectively (Figures 3(a)–3(f)). For these measurements, the excitation wavelength was set to 740 nm, which is good for exciting NADH autofluorescence, and the detection was in the 420 nm–620 nm range. Other tissue intrinsic fluorophores can be excited and detected in the same range because two-photon absorption spectra of intrinsic fluorophores are overlapping. The cellular mean lifetime distribution of the three layers is plotted in Figure 3(g). The distributions of spinous and basal layers are well separated whereas the distribution obtained from the granular layer can be considered a mix of the previous two. The mean fluorescence lifetime for all the investigated layers is in the range of 1 ns, which is in good agreement with previous measurements performed on keratinocytes [11, 32, 33]. Even if other similar FLIM measurements on skin have already been performed in previous studies, they were more devoted to the differentiation between cells in healthy and cancer tissue such as healthy skin versus BCC [32] or melanocytic nevus versus melanoma [33]. Here we mainly focus on a layer-by-layer differentiation in healthy skin. The measured differentiation among skin layers in terms of fluorescence lifetime can be related to the differentiation in terms of proteins and cytokeratins content. In fact, in all the examined layers, even if the main contribution of tissue autofluorescence should arise from NADH, FAD, keratin, melanin, and cholecalciferol, the observed differences could be due not only to a different relative abundance of the molecules listed above, but also to the cytokeratin content in each layer. In particular, granular layer is characterized by the presence of loricrin and profilaggrin; spinous layer by cytokeratins 1 and 5; basal layer by cytokeratins 5 and 14. A spectroscopic and lifetime analysis on all these purified molecules would not help in clarifying this point because fluorescence lifetime of the same molecules should differ when measured in the tissue environment. For lifetime components ratio distributions, a different distribution was found for the three layers. In particular, as shown in Figure 3(h) the distribution center moves to higher value when increasing depth. If we consider that NADH autofluorescence is responsible for the main contribution to endogenous TPF signal, the ratio can be related with tissue metabolism in terms of bound-to-free NADH. In fact, fluorescence lifetime is able to determine if a fluorescent molecule is in its free or protein-bound state. NADH has a short lifetime in its free state and a much longer lifetime in its protein-bound state [47, 48]. The fluorescence lifetime of protein-bound NADH depends on the molecule to which it is bound and the changes in the binding site of NADH, connected with tumour development, can be potentially probed by measuring its lifetime. All these features can be used to optically monitor the metabolic state of a tissue and to potentially detect cancer in a very early stage on the basis of the fluorescence lifetime components ratio, as demonstrated by Skala and coauthors on cultivated living tissues [49, 51]. When moving from skin surface to the inside, epidermal cells differentiate: deeper located cells are smaller in dimension, younger in age and they have higher metabolic activity. The result shown in Figure 3(h) can be interpreted as a confirmation of this effect, because basal cells were found having the largest ratio, corresponding to a higher metabolic activity. Hence, a detailed characterization and differentiation of various epidermal layers, useful for diagnostics, can be obtained by analyzing the decay of NADH autofluorescence using FLIM. In particular, the mean fluorescence lifetime of NADH and the ratio of fast to slow fluorescence lifetime components can be taken as indicator of the metabolic state of cells. Considering that an altered metabolic activity of cells is very often precursor of a diseased state, these two

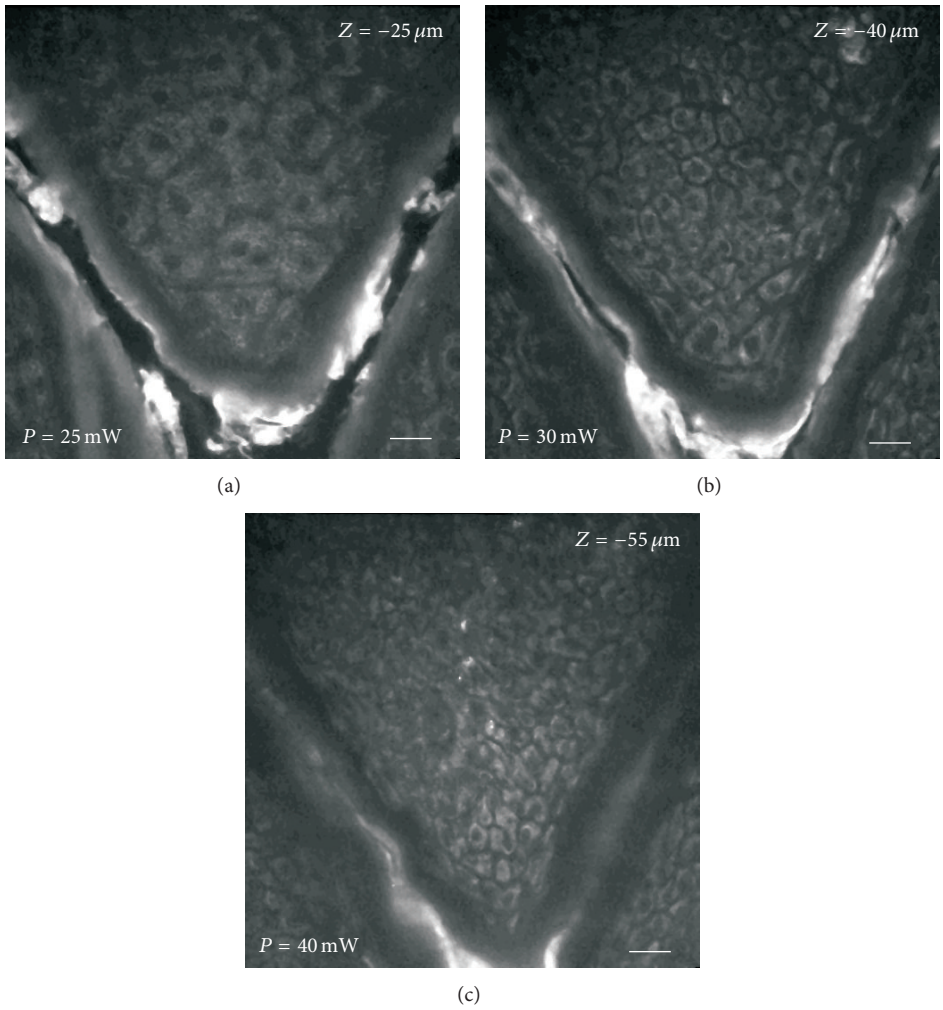

Figure 2: Morphological examination of epidermis. TPF image of NADH autofluorescence acquired from the epidermis of a healthy male volunteer at 25 μm depth from skin surface (a), 40 μm depth from skin surface (b), and 55 μm depth from skin surface (c). The images are approximately corresponding to granular layer (a), spinous layer (b), and basal layer (c). Laser power, measured after the objective, is indicated in the down-left corner of each image. Excitation wavelength: 740 nm. Field of view: 200 μm. Scale bar: 20 μm.

parameters offer the potential to be used for diagnosing altered physiological conditions in a very early stage.

3.2. Noninvasive Follow-Up of Collagen Remodeling after Fractional Laser Resurfacing. A microscopic observation of the effects on collagen caused by microablative laser resurfacing treatment was performed by using SHG microscopy. SHG images were acquired in the dermis of volunteers at depths of 80 μm, 130 μm, and 180 μm from skin surface. A qualitative nonblinded microscopic analysis was performed by visual examination of SHG images acquired immediately before and 40 days after treatment (Figure 4). The acquired SHG images were visually examined for extracting information on collagen fibres and amorphous component appearance that are related to skin aging. In particular, as the age increases we expect an increase in collagen fibres thickness and density, a decrease of the amorphous component (mainly composed of hyaluronic acid and glycosaminoglycans) that affects tissue hydration [52]. Collagen can be directly visualized on SHG images, whereas the increased scattering that gives to the images a more "cloudy" appearance can indirectly give an indication about the amorphous component abundance [38].

For Group I (age < 35 years), in the images acquired after treatment (Figures 4(d), 4(e), and 4(f)) we did not observe any significant modification with respect to the corresponding images acquired before treatment (Figures 4(a), 4(b), and 4(c)). Both the collagen and the amorphous component show a similar appearance before and after the treatment. For Group II (35 years < age < 60 years, Figures 4(g)–4(l)), we observed a slight increase of collagen fibres density after treatment; the amorphous component increases as demonstrated by a more "cloudy" appearance of the images. For Group III (age > 60 years, Figures 4(m)–4(r)), collagen fibres strongly increase in density, the amorphous component undergoes a drastic improvement, and both the epidermal thickness and the number of dermal papillae increase. In this group, all the observed features are in

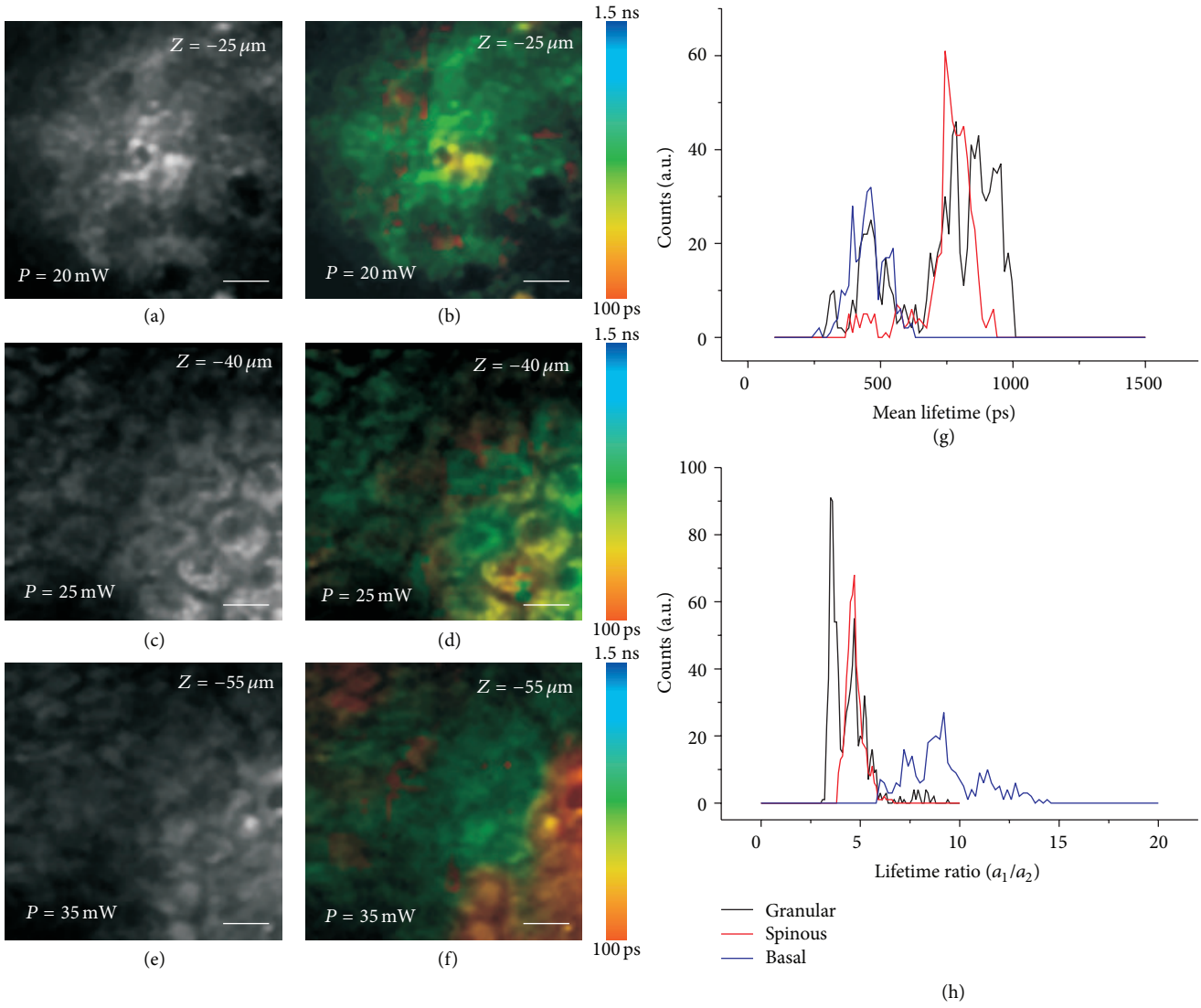

Figure 3: Layer-by-layer characterization of epidermis. TPF image of NADH autofluorescence and the corresponding FLIM images representing mean lifetime map acquired from the epidermis of a healthy male volunteer at 25 μm depth from skin surface ((a), (b)), 40 μm depth from skin surface ((c), (d)), and 55 μm depth from skin surface ((e), (f)). The images are approximately corresponding to granular layer ((a), (b)), spinous layer ((c), (d)), and basal layer ((e), (f)). Images were acquired in the epidermis of a healthy male volunteer by using an excitation wavelength of 740 nm. Laser power, measured after the objective, is indicated in the down-left corner of each image. Field of view: 60 μm. Scale bar: 6 μm. Mean cellular lifetime distribution (g) and mean cellular lifetime components ratio (h) of the 3 different epidermal layers obtained after system response deconvolution and double-exponential fitting.

agreement with a rejuvenating effect. Even if the effectiveness of the treatment seems to increase with age, as confirmed by the following quantitative analysis, a better statistics on a larger number of volunteers would be beneficial to confirm this tendency.

A quantitative microscopic analysis, aimed at evaluating treatment effectiveness, was performed using the so-called second-harmonic to autofluorescence aging index of dermis (SAAID) [10, 36–38]. The SAAID defines a normalized ratio between SHG and TPF, so that it can be used for monitoring skin photoaging based on the ratio between collagen and elastic fibres. In fact, whereas collagen fibres should decrease with aging, elastic fibres should increase, causing a decrease of the SAAID with age. Hence, we expected an increase of the SAAID after treatment. SAAID images of the three examined groups are represented in Figure 5(a). SAAID analysis was performed on all the acquired spectral images, and the results were averaged and plotted in graphs (Figures 5(b), 5(c), and 5(d)). It has to be noted that before treatment the average SAAID level of Group III is always lower than that of the second group, which is in turn lower than that one of the first group, confirming that this parameter decreases with increasing age, as observed in other studies aimed at monitoring skin photoaging [36–38, 53, 54]. When comparing SAAID levels before and after treatment, the results show a negligible increase on young volunteers of

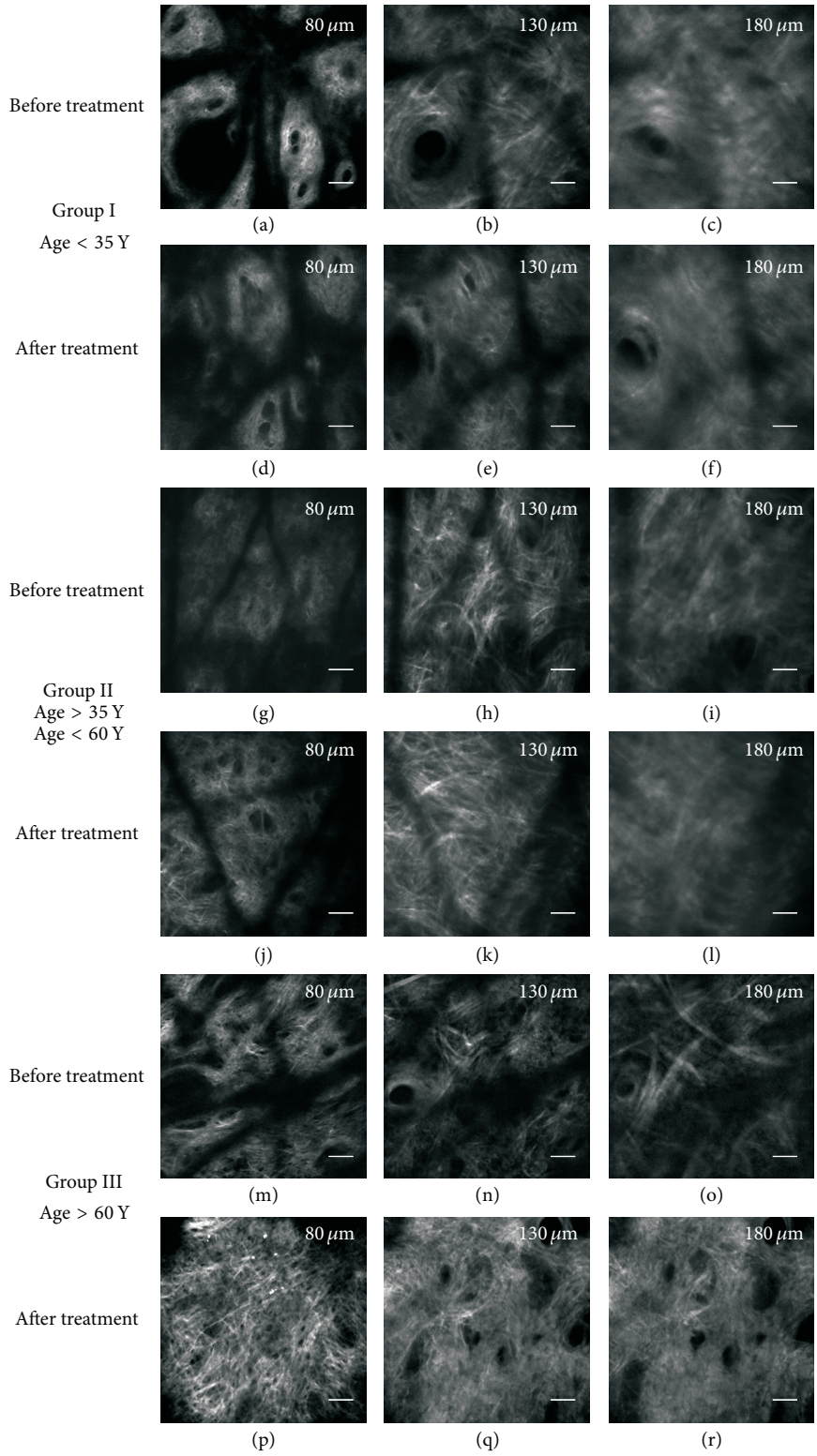

Figure 4: SHG imaging of collagen after laser resurfacing. SHG images of human dermis taken at 80 μm, 130 μm, and 180 μm from skin surface on the inner forearm of healthy volunteers before and 40 days after microablative fractional laser resurfacing treatment. On the top, representative images of Group I (age < 35 years) taken before ((a), (b), and (c)) and 40 days after ((d), (e), and (f)) the treatment. In the middle, representative images of Group II (35 years < age < 60 years) taken before ((g), (h), and (i)) and 40 days after ((j), (k), and (l)) treatment. At the bottom, representative images of Group III (age > 60 years) taken before ((m), (n), and (o)) and 40 days after ((p), (q), and (r)) treatment. Field of view: 400 μm. Scale bars: 40 μm. Figure modified from [38].

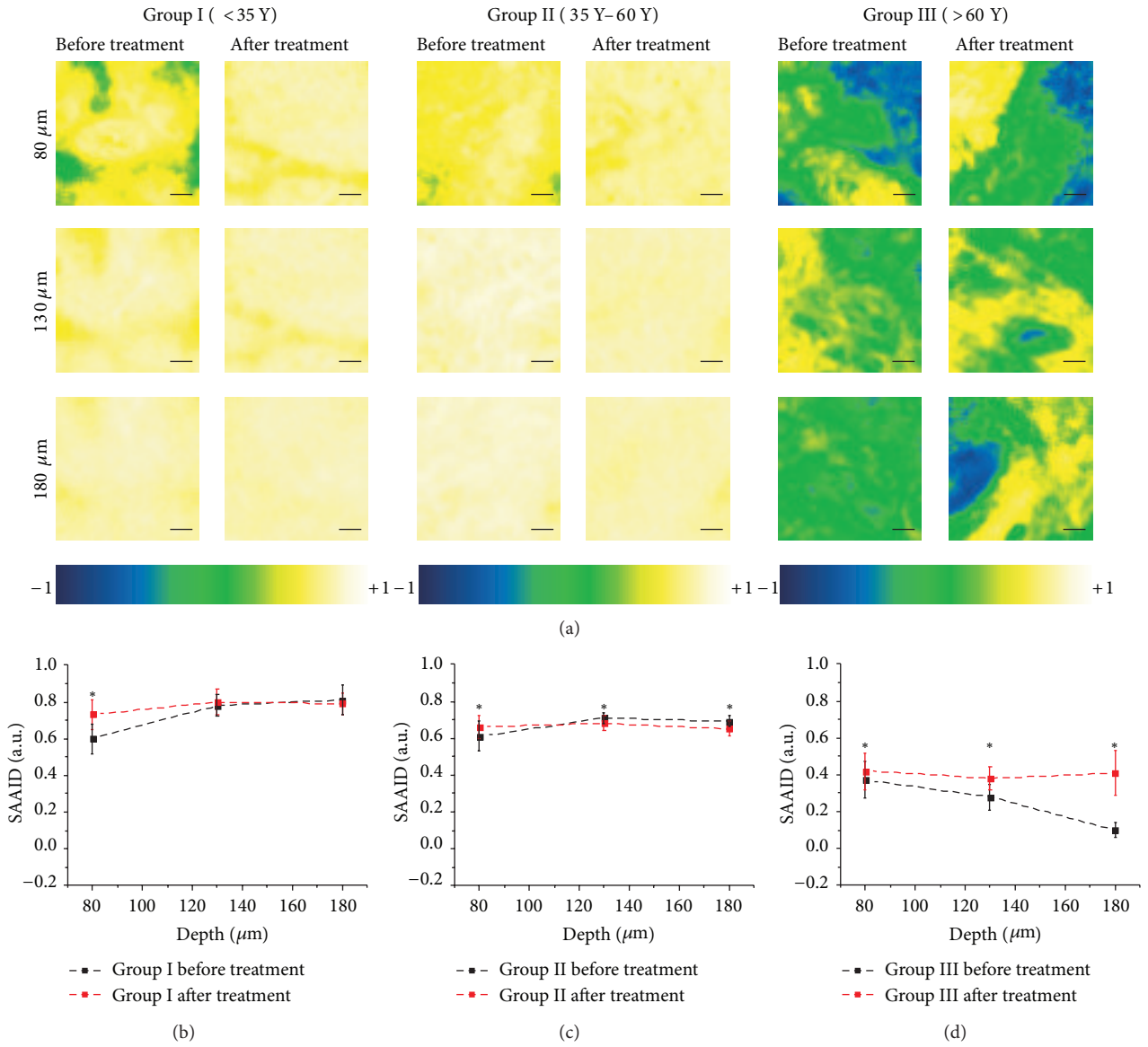

Figure 5: SAAID analysis of dermis after laser resurfacing. (a) SAAID images of human dermis at 80 μm, 130 μm, and 180 μm from skin surface before and after microablative fractional laser resurfacing treatment. On the left, representative SAAID images of Group I (age < 35 years) taken before (left column) and 40 days after (right column) treatment. In the middle, representative SAAID images of Group II (35 years < age < 60 years) taken before (left column) and 40 days after (right column) treatment. On the right, representative SAAID images of Group III (age > 60 years) taken before (left column) and 40 days after (right column) treatment. Scale bars: 40 μm. Color-coded scales for SAAID are plotted beneath each of the three groups of figures. SAAID score versus depth of recording for (b) Group I before (black) and after (red) treatment; (c) Group II before (black) and after (red) treatment; (d) Group III before (black) and after (red) treatment. Data are averaged on all the acquired data sets. The error bars correspond to the standard deviation of measured data. The SAAID mean values before and after treatment were found to be statistically different (indicated with *) or not statistically different (no *) at the 0.05 level after a two-sample statistical t-test ($P = 0.05$). Figure derived from [38].

Group I (age < 35 years, Figure 5(b)), a very small increase on Group II (35 years < age < 60 years, Figure 5(c)), and a strong increase on Group III (age > 60 years, Figure 5(d)). Even if the increase is small, in Group II the SAAID exhibits a statistically significant variation (after a two-sample statistical t-test at the 0.05 level) when comparing images before and after treatment. In Group III SAAID is increasing after treatment, exhibiting statistically significant variations (after a two-sample statistical t-test at the 0.05 level). This confirms the fact that the treatment has stronger effect on more aged subjects. This result is in agreement with the visual observation described in the previous section, where the difference between the youngest and the oldest volunteers in terms of treatment effectiveness was clearly distinguishable from the images. In conclusion, SAAID analysis allowed better delineation of treatment effectiveness versus age.

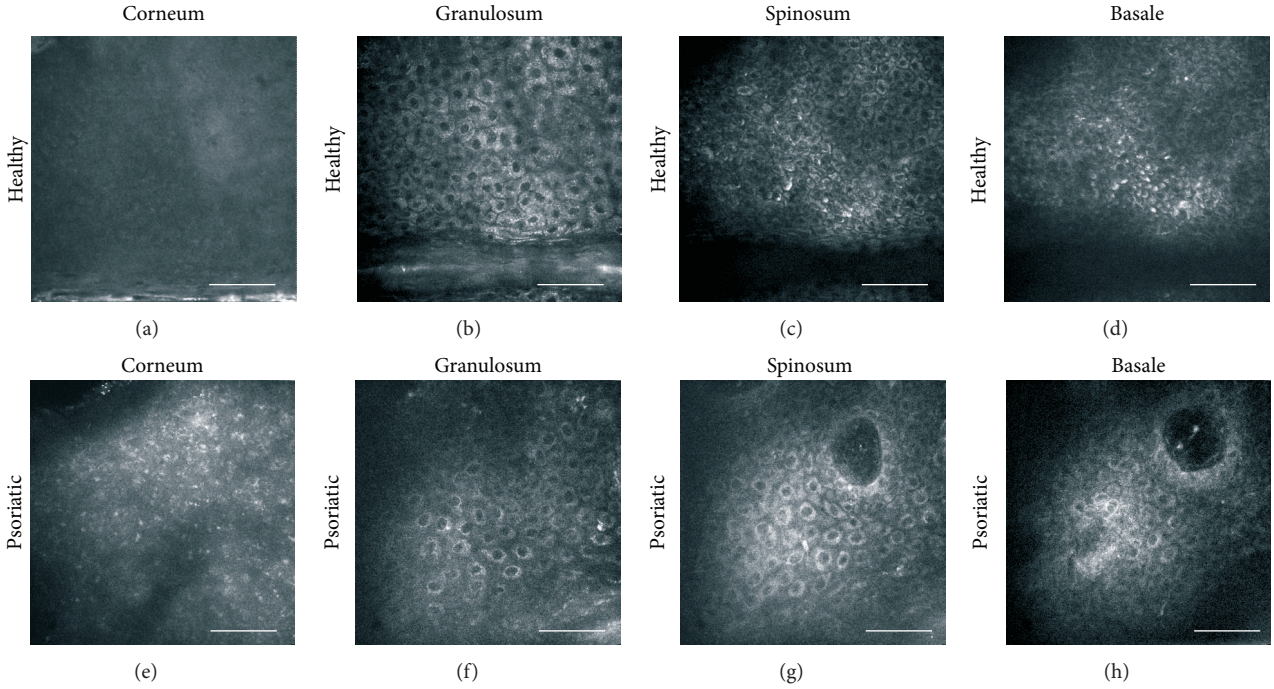

Figure 6: TPF imaging of healthy and psoriatic epidermis. Two-photon autofluorescence images of the layers of the epidermis. The images come from the dorsal forearm of a healthy ((a)–(d)) and a psoriatic ((e)–(h)) skin. Scale bars: 50 μm. Figure modified from [55].

3.3. In Vivo Clinical Investigation of Psoriasis. The microscopic imaging of psoriatic skin was performed on the dorsal forearm of the volunteers [55]. Imaging of the epidermis and of the dermis was performed under different conditions, as reported in the Materials and Methods section. TPF images of the epidermis were acquired using the excitation wavelength of 740 nm, which is adequate for exciting NADH fluorescence, and a power in the 10 mW–40 mW range, depending on the depth of recording. SHG images of the dermis were acquired using the excitation wavelength of 900 nm and a power in the 20 mW–60 mW range, depending on the depth of recording.

Two typical image stacks, respectively, from a healthy and psoriatic epidermis are shown in Figure 6. The images correspond to the acquisition from a 30-year-old healthy male (Figures 6(a)–6(d)) and from a 35-year-old female with psoriasis (Figures 6(e)–6(h)). Imaging starts at a depth located immediately below skin surface for safety and practical reasons. In healthy skin, the fluorescence originating from the corneum layer is very strong (Figure 6(a)) and it appears to be uniform without a characteristic morphology. On the other hand, in psoriatic skin the fluorescence level is lower and a characteristic punctuated pattern appears (Figure 6(e)). The physiological origin of this signal is still under evaluation. This atypical morphology of corneum layer is probably because psoriatic keratinocytes are not completely differentiated. This morphology was confirmed by the acquisitions in the other cases of psoriasis but it was never observed in healthy skin. Hence, it could be considered as a characteristic feature of psoriasis. At the depth of stratum granulosum, typical big cells with the characteristic granular morphology in the cytoplasm are found in healthy epidermis (Figure 6(b)), whereas this layer is very thin and in some cases is even absent in psoriatic skin. Here, psoriatic cells (Figure 6(f)) have a very small cytoplasmic area. Moving down to the stratum spinosum, in healthy skin cells are densely packed and have the characteristic spiny morphology (Figure 6(c)). This is a relatively extended layer with cellular morphology and size similar to those of the stratum granulosum, with the only difference of a more uniform fluorescence. On the other hand, at this depth psoriatic cells (Figure 6(g)) appear with a very small cytoplasmic area and bigger nuclei compared to healthy cells. The packing is very sparse with big distances between adjacent cells. In the healthy stratum basale (Figure 6(d)) cells have even smaller size, they are densely packed, and they emit a strong fluorescence. In psoriatic skin (Figure 6(h)), this layer is not clearly distinguishable in a single optical section due to its typical wavy morphology and deep epidermal proliferation. Nevertheless, it is possible to identify basal cells by looking around the formation of the dermal papillae. Here cells show a very small cytoplasmic area and their packing is even denser compared to stratum spinosum. Another characteristic feature of psoriatic skin at this depth is the presence of dermal papillae that infiltrate deep inside the epidermis (Figures 6(g)-6(h)). On the other hand, in healthy skin a papilla infiltrating inside the epidermis can be observed only occasionally and it never protrudes so near to the surface.

Imaging of the papillary dermis was performed using SHG microscopy in both healthy and psoriatic skin. Three images from a typical image stack acquired from the dorsal forearm of a healthy 30-year-old male are presented in

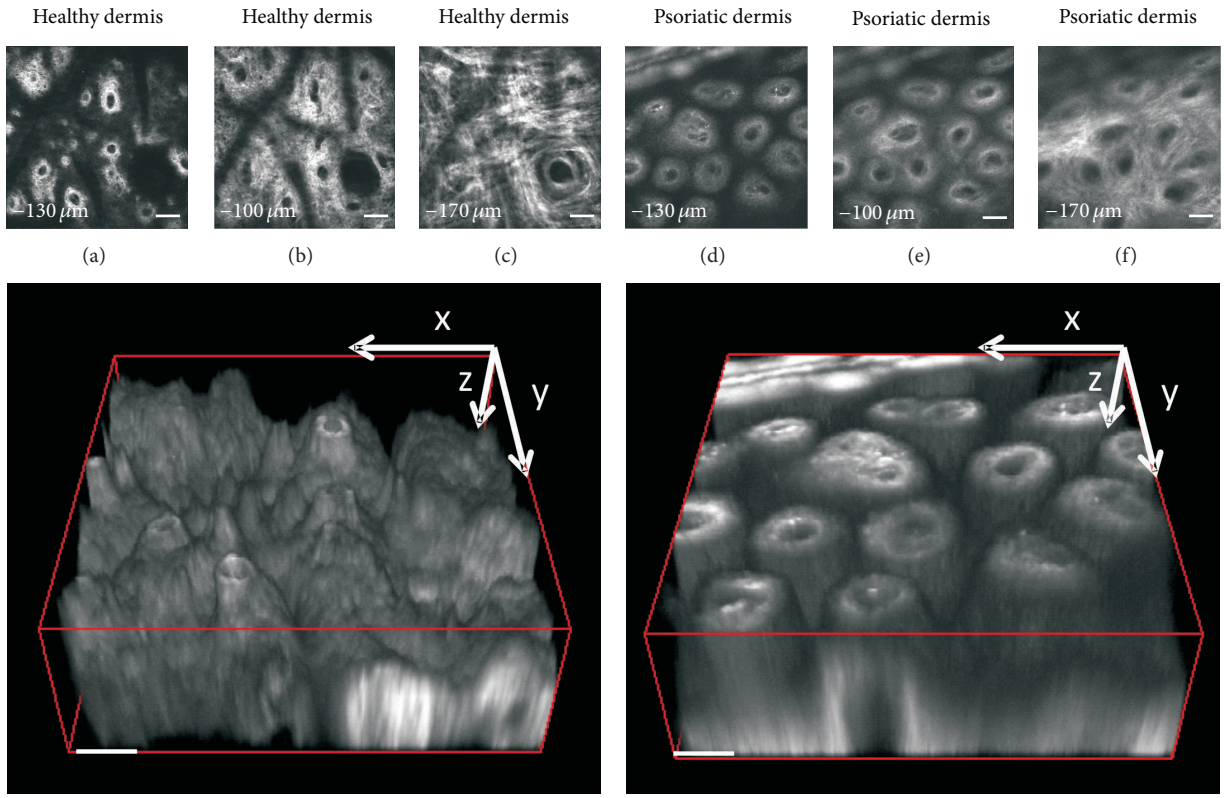

Figure 7: SHG imaging of healthy and psoriatic dermis. ((a)–(c)) SHG images from healthy papillary dermis. ((d)–(f)) SHG images from psoriatic papillary dermis. Scale bars: 50 μm. ((g)-(h)) 3D reconstruction of the dermal layer of healthy (g) and psoriatic (h) skin lesion. The volumes are rotated 30° in the y-z plane. (g) The papillae in healthy skin are short, typically 30 μm, and with small diameter, around 29 μm. (h) Psoriatic papillae dimensions are bigger with typical lengths more than 100 μm and a diameter of around 65 μm. (Scale bars: 50 μm.) Figure modified from [55].

Figures 7(a)–7(c). Imaging starts at a depth of about 85 μm from the surface and it goes deeper. In the first dermal layers, collagen fibres have a small diameter (around or less than 1 μm), a curly appearance and they form a very complex and dense network. At this depth, dermal papillae dominate the images and their density is high. Dark regions around papillae are occupied by epidermal cells proliferating inside dermis. At a depth of 150 μm from skin surface most of the dermal papillae disappear in the dense collagen network. When moving deeper, collagen fibres gradually increase in size and the collagen network appears with a better contrast. The network is less complex and the direction of the fibres is more ordered. At the depth of 180 μm the quality of the image starts to degrade due to scattering. Three images from a typical image stack acquired from the dorsal forearm of a psoriatic 35-year-old female are presented in Figures 7(d)–7(f). Similarly to healthy skin, imaging starts at a depth of about 85 μm from the surface and it goes deeper. By observing the formation of papillae in the first dermal layers, we noted that the density of papillae is higher compared to healthy skin. The presence of papillae is still evident also when moving deeper into the tissue, where the space around them starts to be filled with collagen. At a depth of 170 μm from the skin surface, dermis starts having a similar morphology with respect to healthy skin. However, the fine collagen network of interwoven curly fibres below the dermoepidermal junction that is seen in healthy skin is not visible in psoriasis.

From the acquired images, it looks like the formation of papillae in psoriasis starts at depths around 170 μm below the skin surface, whereas in healthy skin the formation starts at a depth of around 115 μm. The characteristic feature of psoriatic skin (Figures 7(d)–7(f)) is the elongated dermal papillae. This feature becomes better visible in the 3D reconstruction of this part of the skin. Volume stacks with 5 μm step are recorded and used to produce the 3D reconstruction. The result is presented in Figures 7(g) and 7(h) where the 3D reconstruction of the papillae is shown for both healthy and psoriatic skin. Examination of the 3D reconstruction revealed that papillae in psoriasis have a length of around 100 μm, which is much longer than the length of papillae in healthy skin, which is around 30 μm. In addition, in psoriasis dermal papillae are larger in diameter compared to healthy skin. A quantitative evaluation of this feature was obtained by measuring the cross-sectional surface occupied by dermal papillae at around 10 μm below their tip in both healthy and psoriatic skin. Considering the fact that the shape of the

cross-section of a papilla is closer to an ellipse than to a circle, we characterized the papilla size based on their surface rather than on their diameter. Then, a typical diameter was extrapolated by considering the size of the diameter of a circle that would occupy the same surface of the measured ellipse. This calculation provided the following results: a papilla in healthy skin had a mean surface of $650 \pm 50\,\mu m^2$, approximately corresponding to a diameter of $29 \pm 9\,\mu m$; a papilla in psoriasis had a mean surface of $3300 \pm 400\,\mu m^2$, approximately corresponding to a diameter of $64 \pm 22\,\mu m$. In conclusion, the length of the dermal papillae is at least 3 times longer in psoriasis and almost doubled in diameter compared to healthy skin.

4. Discussion

In this review, we highlighted the capability of nonlinear microscopy for clinical dermatological imaging of both epidermis and dermis *in vivo*. In particular, both cellular epidermis and dermal collagen morphology can be noninvasively imaged and characterized by means of TPF and SHG microscopy, respectively. These two techniques are able to noninvasively provide high-resolution images of skin morphology that can be used for diagnostic purposes.

Although skin morphology can be noninvasively imaged with high resolution by other laser scanning imaging techniques, such as confocal reflectance microscopy [56–68], the nonlinear approach offers several advantages with respect to the confocal reflectance. First, the nonlinear dependence of the signal on the excitation light intensity allows selectively exciting only molecules located in an extremely confined volume around the focal point. The direct consequence is an intrinsically high spatial resolution in comparison with other conventional microscopy techniques that employ similar excitation wavelengths. Second, a confocal pinhole rejecting out-of-focus light is not required in nonlinear microscopy, allowing for a 3D scanning of the specimen using a reduced exposure with respect to confocal microscopy. Third, every biological tissue intrinsically contains a certain amount of fluorescent molecules and SHG emitters that can be excited using nonlinear microscopy. This allows not only imaging the morphology of a biological tissue without adding any probe, but also extracting functional information. Finally, the use of particular contrast methods based on nonlinear excitation, such as SHG and FLIM, allows a more specific identification of molecular species in skin, such as collagen in dermis and other nucleotides in epidermis. The selective imaging and spectroscopy of these molecules can provide information about the physiologic condition of the tissue and hence they can be used for both diagnostic and therapy follow-up purposes.

As demonstrated in this review, additional characterization and differentiation of various epidermal layers, useful for diagnostics, can be obtained by analyzing the decay of NADH autofluorescence using FLIM. In particular, the mean fluorescence lifetime of NADH and the ratio of fast to slow fluorescence lifetime components can be taken as indicator of the metabolic state of cells. Considering that an altered metabolic activity of cells is very often precursor of a diseased state, these two parameters offer the potential to be used for diagnosing altered physiological conditions in a very early stage.

The potential clinical dermatological applications of nonlinear microscopy are not limited to skin diagnostics, but they extend also to treatment follow-up. In this review, we demonstrated the capability of nonlinear microscopy for imaging dermis *in vivo* after microablative fractional laser resurfacing treatment. In particular, for the first time nonlinear microscopy was used *in vivo* with the final goal of monitoring a laser-based treatment [38]. The obtained results have shown that nonlinear microscopy is able noninvasively providing a quantitative measurement of the efficacy of the resurfacing treatment. The production of new collagen, as well as an increase in the amount of dermal amorphous component, was found within 40 days from the laser treatment. The effects caused by the treatment can be evaluated qualitatively by visual examination of SHG images of collagen, and quantitatively by measuring the relative amount of SHG and TPF signals, through the SAAID index. The SAAID analysis demonstrated a strong treatment effectiveness in older subjects, whereas the effect was found to be negligible in young and minimal in middle-age subjects.

These nonlinear imaging techniques were additionally used for *in vivo* revealing the characteristic micromorphology of psoriasis at both epidermal and dermal levels. In the epidermis, psoriatic cells have very small cytoplasmic area and they are sparsely packed compared to healthy cells. Further, the more pronounced epidermal proliferation and the dilated papillae of the dermis, typical of psoriasis, were imaged at high resolution. A 3D reconstruction of dermal papillae revealed the great difference of psoriatic skin morphology, where dilated and elongated dermal papillae can be observed. A quantitative measurement demonstrated that the length of dermal papillae is 60% longer in psoriasis and almost doubled in size compared to healthy skin. Imaging and characterization of psoriasis with such a detail is not required for diagnostics. However, during the past years there has been a great effort in the research for the treatment of this disease [69–71]. These therapies have risks that could be reduced if the effect of a treatment can be timely assessed. Currently the severity of psoriasis and the effect of a treatment are evaluated by the Psoriasis Area and Severity Index (PASI) [72]. A potential quantitative monitoring of a treatment effect on psoriasis could be based on the measurement of the nucleus to cytoplasm ratio in epidermis and on papillae size in dermis. Correlation of the measured values with the well-established PASI during the course of a treatment could provide a means of comparison and evaluation of the proposed methodologies. Apart from monitoring the effect of an experimental treatment, the presented imaging techniques could be used for the personalization of existing treatments.

5. Conclusion

In conclusion, the methodologies described here could become a powerful tool to be used in a dermatological clinic

for both early diagnosis and therapy follow-up purposes. New emerging technologies for ultrafast pulsed laser sources, potentially cheaper than the usual solid state Ti:Sapphire oscillator, can help nonlinear laser scanning microscopy to become more and more popular among medical doctors with the final goal of being recognized as a standard clinical imaging method. On the basis of the results described here and of several other successful dermatological applications experienced *in vivo* by means of nonlinear microscopy in recent years [16–18, 37, 38, 45, 53, 54], we believe that in the near future nonlinear laser scanning microscopy will find a stable place in the clinical dermatological setting.

Abbreviations

TPF: Two-photon fluorescence
SHG: Second-harmonic generation
FLIM: Fluorescence lifetime imaging microscopy
SAAID: Second-harmonic to autofluorescence aging index of dermis.

Conflict of Interests

The authors declare that there is no conflict of interests regarding the publication of this paper.

Acknowledgments

The authors acknowledge the following medical and technical experts: N. Bruscino, P. Campolmi, F. Prignano, G. Cannarozzo, M. Troiano, C. Morini, and T. Lotti for dermatological collaboration; V. Maio and D. Massi for medical collaboration; M. Giuntini, M. De Pas, A. Montuori, R. Ballerini, and A. Hajeb for electronic and mechanical support. The research leading to these results has received funding from Fondazione Pisa in the framework of the project "Diagnostic technology for the post-operative monitoring of pediatric brain tumors," from the European Union Seventh Framework Programme (FP7/2007–2013) under Grant Agreements nos. 228334 and 284464 and from the Italian Ministry for Education, University and Research in the framework of the Flagship Project NANOMAX. Furthermore, financial support by the Ente Cassa di Risparmio di Firenze (private foundation) is acknowledged.

References

[1] W. Denk, J. H. Strickler, and W. W. Webb, "Two-photon laser scanning fluorescence microscopy," *Science*, vol. 248, no. 4951, pp. 73–76, 1990.

[2] F. Helmchen and W. Denk, "Deep tissue two-photon microscopy," *Nature Methods*, vol. 2, no. 12, pp. 932–940, 2005.

[3] A. Zoumi, A. Yeh, and B. J. Tromberg, "Imaging cells and extracellular matrix in vivo by using second-harmonic generation and two-photon excited fluorescence," *Proceedings of the National Academy of Sciences of the United States of America*, vol. 99, no. 17, pp. 11014–11019, 2002.

[4] W. R. Zipfel, R. M. Williams, R. Christiet, A. Y. Nikitin, B. T. Hyman, and W. W. Webb, "Live tissue intrinsic emission microscopy using multiphoton-excited native fluorescence and second harmonic generation," *Proceedings of the National Academy of Sciences of the United States of America*, vol. 100, no. 12, pp. 7075–7080, 2003.

[5] W. R. Zipfel, R. M. Williams, and W. W. Webb, "Nonlinear magic: multiphoton microscopy in the biosciences," *Nature Biotechnology*, vol. 21, no. 11, pp. 1369–1377, 2003.

[6] L. H. Laiho, S. Pelet, T. M. Hancewicz, P. D. Kaplan, and P. T. C. So, "Two-photon 3-D mapping of ex vivo human skin endogenous fluorescence species based on fluorescence emission spectra," *Journal of Biomedical Optics*, vol. 10, no. 2, Article ID 024016, 2005.

[7] R. Cicchi and F. S. Pavone, "Non-linear fluorescence lifetime imaging of biological tissues," *Analytical and Bioanalytical Chemistry*, vol. 400, no. 9, pp. 2687–2697, 2011.

[8] R. Cicchi, D. Massi, S. Sestini et al., "Multidimensional nonlinear laser imaging of Basal Cell Carcinoma," *Optics Express*, vol. 15, no. 16, pp. 10135–10148, 2007.

[9] J. Paoli, M. Smedh, A. Wennberg, and M. B. Ericson, "Multiphoton laser scanning microscopy on non-melanoma skin cancer: morphologic features for future non-invasive diagnostics," *Journal of Investigative Dermatology*, vol. 128, no. 5, pp. 1248–1255, 2008.

[10] R. Cicchi, S. Sestini, V. de Giorgi, D. Massi, T. Lotti, and F. S. Pavone, "Nonlinear laser imaging of skin lesions," *Journal of Biophotonics*, vol. 1, no. 1, pp. 62–73, 2008.

[11] R. Cicchi, A. Crisci, A. Cosei et al., "Time- and spectral-resolved two-photon imaging of healthy bladder mucosa and carcinoma in situ," *Optics Express*, vol. 18, no. 4, pp. 3840–3849, 2010.

[12] R. Cicchi, A. Sturiale, G. Nesi et al., "Multiphoton morpho-functional imaging of healthy colon mucosa, adenomatous polyp and adenocarcinoma," *Biomedical Optics Express*, vol. 4, no. 7, pp. 1204–1213, 2013.

[13] J. A. Palero, H. S. de Bruijn, A. van der Ploeg van den Heuvel, H. J. C. M. Sterenborg, and H. C. Gerritsen, "Spectrally resolved multiphoton imaging of in vivo and excised mouse skin tissues," *Biophysical Journal*, vol. 93, no. 3, pp. 992–1007, 2007.

[14] B. R. Masters, P. T. C. So, and E. Gratton, "Optical biopsy of in vivo human skin: multi-photon excitation microscopy," *Lasers in Medical Science*, vol. 13, no. 3, pp. 196–203, 1998.

[15] B. R. Masters and P. T. C. So, "Confocal microscopy and multiphoton excitation microscopy of human skin in vivo," *Optics Express*, vol. 8, no. 1, pp. 2–10, 2001.

[16] K. König and I. Riemann, "High-resolution multiphoton tomography of human skin with subcellular spatial resolution and picosecond time resolution," *Journal of Biomedical Optics*, vol. 8, no. 3, pp. 432–439, 2003.

[17] E. Dimitrow, I. Riemann, A. Ehlers et al., "Spectral fluorescence lifetime detection and selective melanin imaging by multiphoton laser tomography for melanoma diagnosis," *Experimental Dermatology*, vol. 18, no. 6, pp. 509–515, 2009.

[18] K. König, "Clinical multiphoton tomography.," *Journal of Biophotonics*, vol. 1, no. 1, pp. 13–23, 2008.

[19] L. Moreaux, O. Sandre, S. Charpak, M. Blanchard-Desce, and J. Mertz, "Coherent scattering in multi-harmonic light microscopy," *Biophysical Journal*, vol. 80, no. 3, pp. 1568–1574, 2001.

[20] P. J. Campagnola and L. M. Loew, "Second-harmonic imaging microscopy for visualizing biomolecular arrays in cells, tissues

and organisms," *Nature Biotechnology*, vol. 21, no. 11, pp. 1356–1360, 2003.

[21] P. J. Campagnola, A. C. Millard, M. Terasaki, P. E. Hoppe, C. J. Malone, and W. A. Mohler, "Three-dimensional high-resolution second-harmonic generation imaging of endogenous structural proteins in biological tissues," *Biophysical Journal*, vol. 82, no. 1, pp. 493–508, 2002.

[22] S. Roth and I. Freund, "Second harmonic generation in collagen," *The Journal of Chemical Physics*, vol. 70, no. 4, pp. 1637–1643, 1979.

[23] R. M. Williams, W. R. Zipfel, and W. W. Webb, "Interpreting second-harmonic generation images of collagen I fibrils," *Biophysical Journal*, vol. 88, no. 2, pp. 1377–1386, 2005.

[24] P. Stoller, K. M. Reiser, P. M. Celliers, and A. M. Rubenchik, "Polarization-modulated second harmonic generation in collagen," *Biophysical Journal*, vol. 82, no. 6, pp. 3330–3342, 2002.

[25] P. Matteini, F. Ratto, F. Rossi et al., "Photothermally-induced disordered patterns of corneal collagen revealed by SHG imaging," *Optics Express*, vol. 17, no. 6, pp. 4868–4878, 2009.

[26] F. Vanzi, L. Sacconi, R. Cicchi, and F. S. Pavone, "Protein conformation and molecular order probed by second-harmonic-generation microscopy," *Journal of Biomedical Optics*, vol. 17, no. 6, Article ID 060901, 2012.

[27] P. Matteini, R. Cicchi, F. Ratto et al., "Thermal transitions of fibrillar collagen unveiled by second-harmonic generation microscopy of corneal stroma," *Biophysical Journal*, vol. 103, no. 6, pp. 1179–1187, 2012.

[28] R. Cicchi, D. Kapsokalyvas, V. de Giorgi et al., "Scoring of collagen organization in healthy and diseased human dermis by multiphoton microscopy," *Journal of Biophotonics*, vol. 3, no. 1-2, pp. 34–43, 2010.

[29] R. Cicchi, C. Matthäus, T. Meyer et al., "Characterization of collagen and cholesterol deposition in atherosclerotic arterial tissue using non-linear microscopy," *Journal of Biophotonics*, vol. 7, no. 1-2, pp. 135–143, 2014.

[30] T. Yasui, Y. Tohno, and T. Araki, "Characterization of collagen orientation in human dermis by two-dimensional second-harmonic-generation polarimetry," *Journal of Biomedical Optics*, vol. 9, no. 2, pp. 259–264, 2004.

[31] Y. Sun, W. Chen, S. Lin et al., "Investigating mechanisms of collagen thermal denaturation by high resolution second-harmonic generation imaging," *Biophysical Journal*, vol. 91, no. 7, pp. 2620–2625, 2006.

[32] M. Han, G. Giese, and J. F. Bille, "Second harmonic generation imaging of collagen fibrils in cornea and sciera," *Optics Express*, vol. 13, no. 15, pp. 5791–5797, 2005.

[33] E. Brown, T. McKee, E. DiTomaso et al., "Dynamic imaging of collagen and its modulation in tumors *in vivo* using second-harmonic generation," *Nature Medicine*, vol. 9, no. 6, pp. 796–800, 2003.

[34] S. J. Lin, S. Jee, C. Kuo et al., "Discrimination of basal cell carcinoma from normal dermal stroma by quantitative multiphoton imaging," *Optics Letters*, vol. 31, no. 18, pp. 2756–2758, 2006.

[35] P. P. Provenzano, K. W. Eliceiri, J. M. Campbell, D. R. Inman, J. G. White, and P. J. Keely, "Collagen reorganization at the tumor-stromal interface facilitates local invasion," *BMC Medicine*, vol. 4, article 38, 2006.

[36] S. J. Lin, R. Wu, H. Tan et al., "Evaluating cutaneous photoaging by use of multiphoton fluorescence and second-harmonic generation microscopy," *Optics Letters*, vol. 30, no. 17, pp. 2275–2277, 2005.

[37] M. J. Koehler, K. König, P. Elsner, R. Bückle, and M. Kaatz, "In vivo assessment of human skin aging by multiphoton laser scanning tomography," *Optics Letters*, vol. 31, no. 19, pp. 2879–2881, 2006.

[38] R. Cicchi, D. Kapsokalyvas, M. Troiano et al., "In vivo non-invasive monitoring of collagen remodelling by two-photon microscopy after micro-ablative fractional laser resurfacing," *Journal of Biophotonics*, 2013.

[39] P. J. Tadrous, "Methods for imaging the structure and function of living tissues and cells: 2. Fluorescence lifetime imaging," *Journal of Pathology*, vol. 191, no. 3, pp. 229–234, 2000.

[40] P. J. Tadrous, J. Siegel, P. M. W. French, S. Shousha, E. Lalani, and G. W. H. Stamp, "Flourescence lifetime imaging of unstained tissues: early results in human breast cancer," *The Journal of Pathology*, vol. 199, no. 3, pp. 309–317, 2003.

[41] Y. Chen and A. Periasamy, "Characterization of two-photon excitation fluorescence lifetime imaging microscopy for protein localization," *Microscopy Research and Technique*, vol. 63, no. 1, pp. 72–80, 2004.

[42] K. M. Hanson, M. J. Behne, N. P. Barry, T. M. Mauro, E. Gratton, and R. M. Clegg, "Two-photon fluorescence lifetime imaging of the skin stratum corneum pH gradient," *Biophysical Journal*, vol. 83, no. 3, pp. 1682–1690, 2002.

[43] P. I. H. Bastiaens and A. Squire, "Fluorescence lifetime imaging microscopy: spatial resolution of biochemical processes in the cell," *Trends in Cell Biology*, vol. 9, no. 2, pp. 48–52, 1999.

[44] R. Cubeddu, A. Pifferi, P. Taroni et al., "Fluorescence lifetime imaging: an application to the detection of skin tumors," *IEEE Journal on Selected Topics in Quantum Electronics*, vol. 5, no. 4, pp. 923–929, 1999.

[45] E. Dimitrow, M. Ziemer, M. J. Koehler et al., "Sensitivity and specificity of multiphoton laser tomography for in Vivo and ex vivo diagnosis of malignant melanoma," *Journal of Investigative Dermatology*, vol. 129, no. 7, pp. 1752–1758, 2009.

[46] M. C. Skala, K. M. Riching, D. K. Bird et al., "In vivo multiphoton fluorescence lifetime imaging of protein-bound and free nicotinamide adenine dinucleotide in normal and precancerous epithelia," *Journal of Biomedical Optics*, vol. 12, no. 2, Article ID 024014, 2007.

[47] J. R. Lakowicz, H. Szmacinski, K. Nowaczyk, and M. L. Johnson, "Fluorescence lifetime imaging of free and protein-bound NADH," *Proceedings of the National Academy of Sciences of the United States of America*, vol. 89, no. 4, pp. 1271–1275, 1992.

[48] D. Li, W. Zheng, and J. Y. Qu, "Time-resolved spectroscopic imaging reveals the fundamentals of cellular NADH fluorescence," *Optics Letters*, vol. 33, no. 20, pp. 2365–2367, 2008.

[49] M. C. Skala, K. M. Riching, A. Gendron-Fitzpatrick et al., "In vivo multiphoton microscopy of NADH and FAD redox states, fluorescence lifetimes, and cellular morphology in precancerous epithelia," *Proceedings of the National Academy of Sciences of the United States of America*, vol. 104, no. 49, pp. 19494–19499, 2007.

[50] F. Fischer, B. Volkmer, S. Puschmann et al., "Risk estimation of skin damage due to ultrashort pulsed, focused near-infrared laser irradiation at 800 nm," *Journal of Biomedical Optics*, vol. 13, no. 4, Article ID 041320, 2008.

[51] M. C. Skala, K. M. Riching, D. K. Bird et al., "*In vivo* multiphoton fluorescence lifetime imaging of protein-bound and free nicotinamide adenine dinucleotide in normal and precancerous epithelia," *Journal of Biomedical Optics*, vol. 12, no. 2, Article ID 024014, 2007.

[52] I. Ghersetich, T. Lotti, G. Campanile, C. Grappone, and G. Dini, "Hyaluronic acid in cutaneous intrinsic aging," *International Journal of Dermatology*, vol. 33, no. 2, pp. 119–122, 1994.

[53] M. J. Koehler, S. Hahn, A. Preller et al., "Morphological skin ageing criteria by multiphoton laser scanning tomography: non-invasive in vivo scoring of the dermal fibre network," *Experimental Dermatology*, vol. 17, no. 6, pp. 519–523, 2008.

[54] M. J. Koehler, A. Preller, N. Kindler et al., "Intrinsic, solar and sunbed-induced skin aging measured in vivo by multiphoton laser tomography and biophysical methods," *Skin Research and Technology*, vol. 15, no. 3, pp. 357–363, 2009.

[55] D. Kapsokalyvas, R. Cicchi, N. Bruscino et al., "In-vivo imaging of psoriatic lesions with polarization multispectral dermoscopy and multiphoton microscopy," *Biomedical Optics Express*, vol. 5, pp. 2405–2419, 2014.

[56] S. González, M. Rajadhyaksha, G. Rubinstein, and R. R. Anderson, "Characterization of psoriasis in vivo by reflectance confocal microscopy," *Journal of Medicine*, vol. 30, no. 5-6, pp. 337–356, 1999.

[57] M. Huzaira, F. Rius, M. Rajadhyaksha, R. R. Anderson, and S. González, "Topographic variations in normal skin, as viewed by *in vivo* reflectance confocal microscopy," *Journal of Investigative Dermatology*, vol. 116, no. 6, pp. 846–852, 2001.

[58] S. González and Z. Tannous, "Real-time, in vivo confocal reflectance microscopy of basal cell carcinoma," *Journal of the American Academy of Dermatology*, vol. 47, no. 6, pp. 869–874, 2002.

[59] L. T. Wang, J. T. Demirs, M. A. Pathak, and S. González, "Real-time, in vivo quantification of melanocytes by near-infrared reflectance confocal microscopy in the guinea pig animal model," *Journal of Investigative Dermatology*, vol. 119, no. 2, pp. 533–535, 2002.

[60] S. González, Y. Gilaberte-Calzada, A. González-Rodríguez, A. Torres, and M. C. Mihm Jr., "In vivo reflectance-mode confocal scanning laser microscopy in dermatology," *Advances in Dermatology*, vol. 20, pp. 371–387, 2004.

[61] T. Yamashita, T. Kuwahara, S. González, and M. Takahashi, "Non-invasive visualization of melanin and melanocytes by reflectance-mode confocal microscopy," *Journal of Investigative Dermatology*, vol. 124, no. 1, pp. 235–240, 2005.

[62] A. L. C. Agero, K. J. Busam, C. Benvenuto-Andrade et al., "Reflectance confocal microscopy of pigmented basal cell carcinoma," *Journal of the American Academy of Dermatology*, vol. 54, no. 4, pp. 638–643, 2006.

[63] A. Scope, C. Benvenuto-Andrade, A. C. Agero et al., "In vivo reflectance confocal microscopy imaging of melanocytic skin lesions: consensus terminology glossary and illustrative images," *Journal of the American Academy of Dermatology*, vol. 57, no. 4, pp. 644–658, 2007.

[64] S. González and Y. Gilaberte-Calzada, "In vivo reflectance-mode confocal microscopy in clinical dermatology and cosmetology," *International Journal of Cosmetic Science*, vol. 30, no. 1, pp. 1–17, 2008.

[65] S. González, "Confocal reflectance microscopy in dermatology: promise and reality of non-invasive diagnosis and monitoring," *Actas Dermo-Sifiliograficas*, vol. 100, supplement 2, pp. 59–69, 2009.

[66] M. Ulrich, S. Lange-Asschenfeldt, and S. Gonzalez, "Clinical applicability of in vivo reflectance confocal microscopy in dermatology," *Giornale Italiano di Dermatologia e Venereologia*, vol. 147, no. 2, pp. 171–178, 2012.

[67] M. Ulrich, S. Lange-Asschenfeldt, and S. Gonzalez, "The use of reflectance confocal microscopy for monitoring response to therapy of skin malignancies," *Dermatology Practical & Conceptual*, vol. 2, no. 2, Article ID 0202a10, 2012.

[68] M. Venturini, M. Arisi, A. Zanca et al., "In vivo reflectance confocal microscopy features of cutaneous microcirculation and epidermal and dermal changes in diffuse systemic sclerosis and correlation with histological and videocapillaroscopic findings," *European Journal of Dermatology*, 2014.

[69] M. A. Lowes, A. M. Bowcock, and J. G. Krueger, "Pathogenesis and therapy of psoriasis," *Nature*, vol. 445, no. 7130, pp. 866–873, 2007.

[70] E. D. O. Roberson and A. M. Bowcock, "Psoriasis genetics: breaking the barrier," *Trends in Genetics*, vol. 26, no. 9, pp. 415–423, 2010.

[71] W. Weger, "Current status and new developments in the treatment of psoriasis and psoriatic arthritis with biological agents," *British Journal of Pharmacology*, vol. 160, no. 4, pp. 810–820, 2010.

[72] P. I. Spuls, L. L. A. Lecluse, M. N. F. Poulsen, J. D. Bos, R. S. Stern, and T. Nijsten, "How good are clinical severity and outcome measures for psoriasis: quantitative evaluation in a systematic review," *Journal of Investigative Dermatology*, vol. 130, no. 4, pp. 933–943, 2010.

Hindawi Publishing Corporation
BioMed Research International
Volume 2014, Article ID 384646, 10 pages
http://dx.doi.org/10.1155/2014/384646

Research Article

A Medical Manipulator System with Lasers in Photodynamic Therapy of Port Wine Stains

Xingtao Wang,[1] Chunlai Tian,[1] Xingguang Duan,[2] Ying Gu,[3] and Naiyan Huang[3]

[1] *State Nuclear Power Technology Research & Development Centre, Floor 7, Building A, South Area of Future Science and Technology Park, Beiqijia Town, Changping District, State Nuclear Power Research Institute, Beijng 102209, China*
[2] *Intelligent Robotics Institute, Beijing Institute of Technology, 5 Nandajie, Zhongguancun, Haidian, Beijing 100081, China*
[3] *Department of Laser Medicine, Chinese People Liberation Army General Hospital, 28 Fuxing Road, Haidian, Beijing 100853, China*

Correspondence should be addressed to Xingtao Wang; wangxingtao@snptrd.com

Received 23 April 2014; Revised 24 June 2014; Accepted 15 July 2014; Published 14 August 2014

Academic Editor: Silvia Moretti

Port wine stains (PWS) are a congenital malformation and dilation of the superficial dermal capillary. Photodynamic therapy (PDT) with lasers is an effective treatment of PWS with good results. However, because the laser density is uneven and nonuniform, the treatment is carried out manually by a doctor thus providing little accuracy. Additionally, since the treatment of a single lesion can take between 30 and 60 minutes, the doctor can become fatigued after only a few applications. To assist the medical staff with this treatment method, a medical manipulator system (MMS) was built to operate the lasers. The manipulator holds the laser fiber and, using a combination of active and passive joints, the fiber can be operated automatically. In addition to the control input from the doctor over a human-computer interface, information from a binocular vision system is used to guide and supervise the operation. Clinical results are compared in nonparametric values between treatments with and without the use of the MMS. The MMS, which can significantly reduce the workload of doctors and improve the uniformity of laser irradiation, was safely and helpfully applied in PDT treatment of PWS with good therapeutic results.

1. Introduction

Port wine stains (PWS), also known as birthmarks, are a congenital expansion and malformation of the superficial dermal capillary network [1]. The morbidity rate is as high as 3–5‰ [2]. Most of PWS appear in the skin of the head, face, and neck; some appear on the legs and arms (Figure 1). PWS not only affects patients on functional aspects, but also influences patients' psychological health [3–5].

According to the histopathological changes of PWS, the main difficulty of the treatment is that the expanded and deformed capillary network in the superficial dermis should be dispelled to eliminate abnormal red lesion, while the epidermis and deep tissue should not be damaged to avoid scaring [2]. Conventional treatments, including skin grafting, irradiation, and chemical peels, are not ideal with respect to scaring and pigmentation.

Photodynamic therapy (PDT), which was started as a novel antitumor therapy in the early 1980s, is a type of laser-based treatment for PWS. In 1990, Professor Ying Gu began to study the PDT treatment of PWS and established a new PDT program for PWS. The effective rate can reach up to 98% [2, 4, 6, 7]. In the PDT treatment of PWS, a "photosensitizer" drug (such as hematoporphyrin monomethyl ether), which is highly concentrated inside PWS vessels and diffuses little to normal tissue, is injected intravenously. Then the PWS lesion is irradiated by laser. The photosensitizer is excited by the laser, producing singlet oxygen and other toxic chemical substances which will destroy the malformed vascular. The toxic chemical species are only generated in malformed vascular and have only little damage to normal skin [8].

In the PDT treatment of PWS, the correct laser power density and a uniform laser irradiation on the PWS lesion are very important to get good therapeutic effectiveness.

Figure 1: PWS symptom. (a) PWS in face. (b) PWS in neck. (c) PWS in arm and hand. (d) PWS in leg.

Unfortunately, the power density of a laser spot is a Gauss distribution (Figure 2), which is uneven. For a given lesion, the laser irradiation of the central area is too high, which may cause skin burns, while the laser power density of other areas is too low, which may affect the therapeutic effectiveness. So, a uniform laser radiation, which means every section of the PWS lesion receives the same quantity of laser radiation during the PDT process which is used. A uniform radiation can be obtained by operating the laser fiber in such a way that the centre of the laser spot is kept in motion over the lesion. The operating doctor has to move the laser fiber to produce an even irradiation on the lesion and avoid skin burn (Figure 3).

The process of treating a single lesion takes about 30 to 60 minutes. This long duration manual operation is a high work load to doctors with low efficiency and accuracy. Therefore, a medical manipulator system (MMS) was developed to assist doctors in clinical treatment. Until now, 296 PWS cases have been treated using the MMS; the therapeutic results are comparable to the results of the traditional treatment. Clinical trials show that the MMS is effective and useful in PDT treatment of PWS.

2. Materials and Methods

2.1. Medical Manipulator System. The MMS consists of four main components, as shown in Figure 4:

(1) a PC-based workstation providing overall control using a human-computer interface, an image processing module, and an expert database subsystem;

(2) a PDT device, which produces a laser beam and controls the treatment parameters, such as the laser power density and the irradiation time;

(3) a medical manipulator to operate the laser fiber automatically;

(4) a binocular vision system used as guidance and surveillance of the MMS.

2.2. Medical Manipulator. Manipulators in medical application should be safe and convenient for doctors to use [9]. Based on the analysis of treatment requirements and the application environment in Chinese PLA General Hospital (known as Beijing 301 Hospital), a novel 7-DOF medical

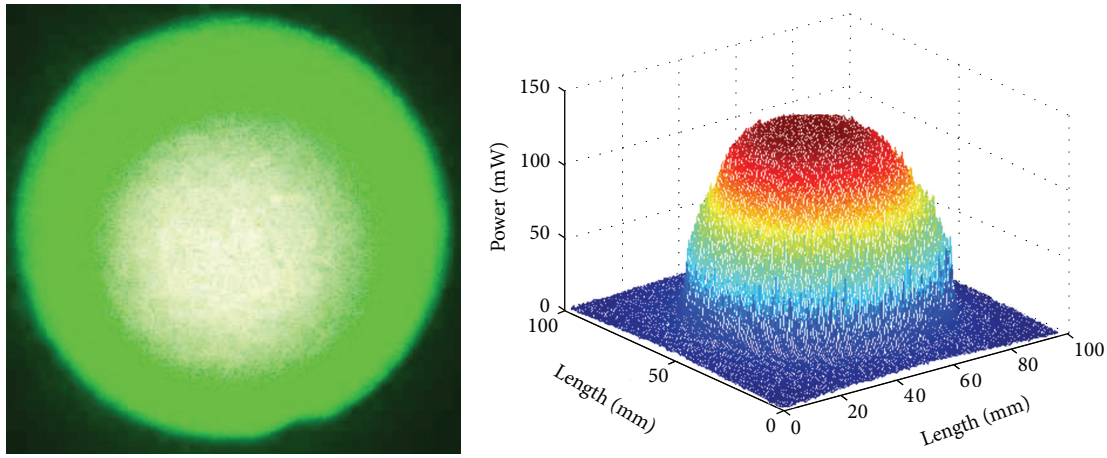

(a) (b)

Figure 2: The uneven power density distribution of laser spot. (a) Laser beam image. (b) Gray handled image with MATLAB.

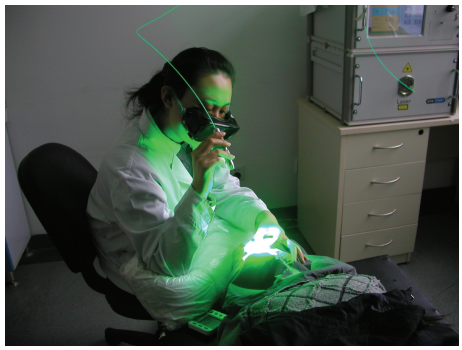

Figure 3: The manual operation of laser fiber by doctor.

Figure 4: The medical manipulator system.

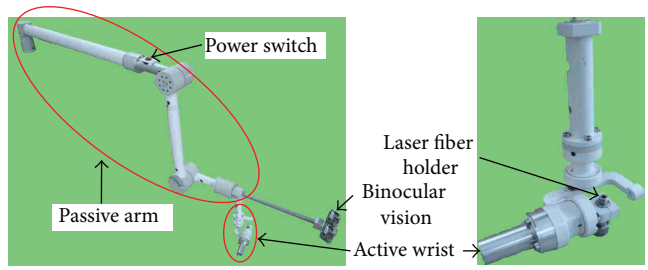

Figure 5: The mechanism of medical manipulator.

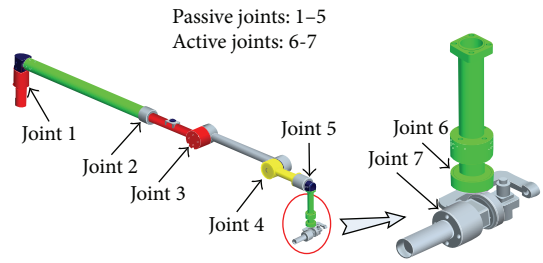

Figure 6: The seven-DOF arrangement of medical manipulator.

manipulator with passive and active joints is developed (Figure 5). The medical manipulator consists of a passive arm and an active wrist. There are 5 passive joints in the arm corresponding to 5 degrees of freedom (DOF) and 2 active joints in the wrist corresponding to 2 DOF. The DOF arrangement of the medical manipulator is shown in Figure 6.

2.3. Passive Arm. The 5-DOF passive arm can be adjusted manually. Once adjusted, it will hold the active wrist stationary. The arm consists of one translational DOF (Joint 2) and four rotational DOF (Figure 6). In each rotational DOF, there is an electromagnetic brake. If the power switch is pressed, all the electromagnetic brakes lose power, and the passive joints can simultaneously be freely and quickly adjusted. Once the power switch is released, the joints will be locked firmly into place again by the electromagnetic brakes (Figure 7).

The passive arm was tested by several doctors in the Department of Laser Medicine of the PLA General Hospital. According to the results, the passive arm is easy to operate, is stable to hold, and self-locks firmly; fulfilling these

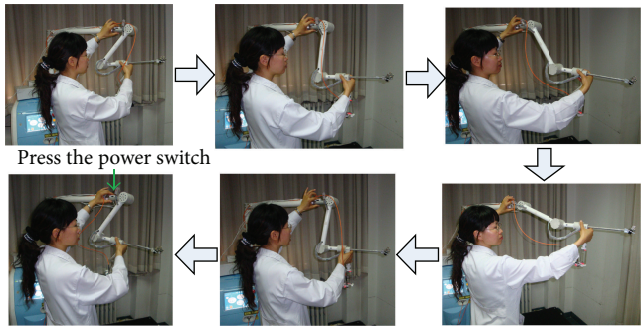

Figure 7: The operation of passive arm.

requirements shows that it meets all the clinical treatment requirements.

2.4. Active Wrist. Each of the DOF in the active wrist is controlled by DC servo motors. There are two rotational DOF, and the laser fiber is held by wrist joint 7 (Figure 6).

In order to simplify the movement of medical manipulator, the PWS lesion is approximated to lie on a plane. By adjusting the passive arm manually, the active wrist is positioned above the PWS lesion with the guidance of binocular vision. Figure 8 shows the kinematics model of the medical manipulator.

By analysing the doctors' movement of the laser fiber during a traditional treatment, the trajectory of the laser spot's centre can be simplified and decomposed into two movements. The first is a circular movement along the circumferential direction of the lesion. The other is a swinging movement along the radial direction of the lesion. Using this analysis, three treatment modes were designed to simulate the doctors' manual operation (Figure 9).

(1) Treatment mode 1: the centre of laser spot scans the lesion's perimeter. After a complete revolution, the perimeter is decreased by a specified scale and another revolution is made.

(2) Treatment mode 2: while the laser scans the lesion border, the "swing joint" of the active wrist swings along the radial direction of the lesion.

(3) Treatment mode 3: a circle, which includes the lesion zone, is used to approximate the lesion border. The laser moves identically to treatment mode 2.

2.5. Safety System. The safety system (Figure 10) was developed to avoid risks to patients under any circumstances. Besides the supervision of doctors and the use of the binocular vision system, several safety precautions were proposed including software, electrical design, and mechanical means [10–12].

(1) After the passive arm is operated, if the minimum distance between the active wrist and the PWS lesion is 40 mm or less, the MMS is locked by the hardware and the software.

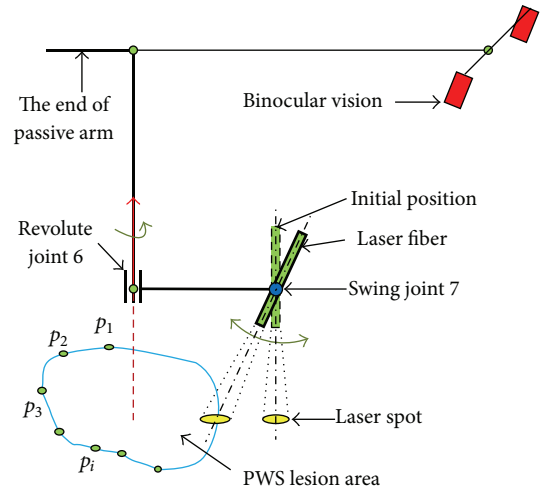

Figure 8: The kinematics model of medical manipulator.

(2) In the software program a speed limit, a position limit, and a watch dog timer are applied. Furthermore, the response time limit is set in the communication handshaking procedure between the DSP controller and the PC user software. If both of them have not received a response signal from the other within the set time (50 ms for the MMS) due to a freeze-up, runaway, or other errors, the power will be shut off.

(3) Fuses are implemented to limit the current supplied to each servo motor.

(4) A hall position switch is attached at each active wrist joint to limit the position.

(5) The binocular vision system positions the PWS lesion and supervises the patient. If the patient moves tempestuously, an alarm is given.

(6) By pressing the emergency stop button, doctor can stop the MMS at any time in case of an emergency.

(7) Each servo motor is equipped with a brake so that the active joints will be locked if power is lost.

2.6. Clinical Treatment of PDT for PWS with MMS

2.6.1. Data Collection. The MMS was applied in a clinical PDT treatment of PWS in the Chinese PLA General Hospital in 2010. A total of 296 PWS lesions were treated in patients with various ages, PWS lesion sites, and disease extents. The patients were 74 male (39.8%) and 112 were female (60.2%). The patient's ages ranged from 3 to 42 years. Some of the patients had multiple lesions (diameter > 8 cm or in more than one anatomic planes), and some of them had single lesion (diameter < 8 cm and in one anatomic plane) [5, 8]. None of the patients had received previous treatment with a complete medical record.

So far, there are no standard classification criteria for PWS. In this paper, the classification criteria which wereadopted in [3, 5, 13–15] were used to classify PWS lesions

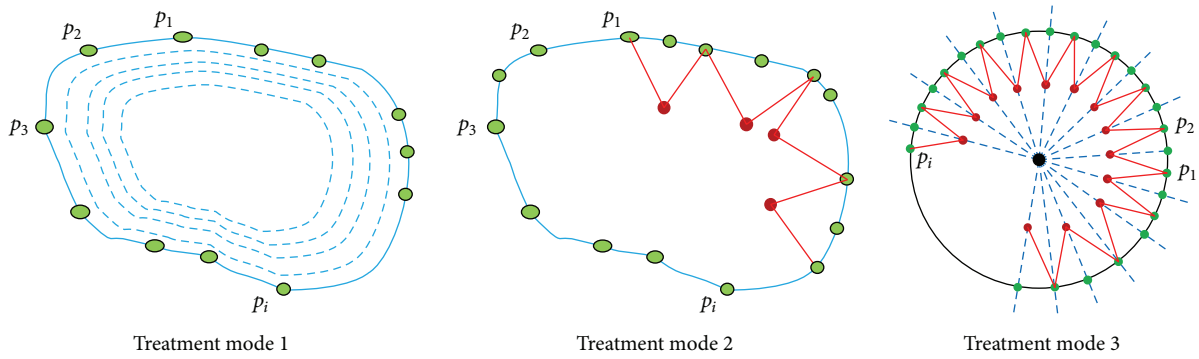

Figure 9: Treatment modes of medical manipulator assisted PDT for PWS.

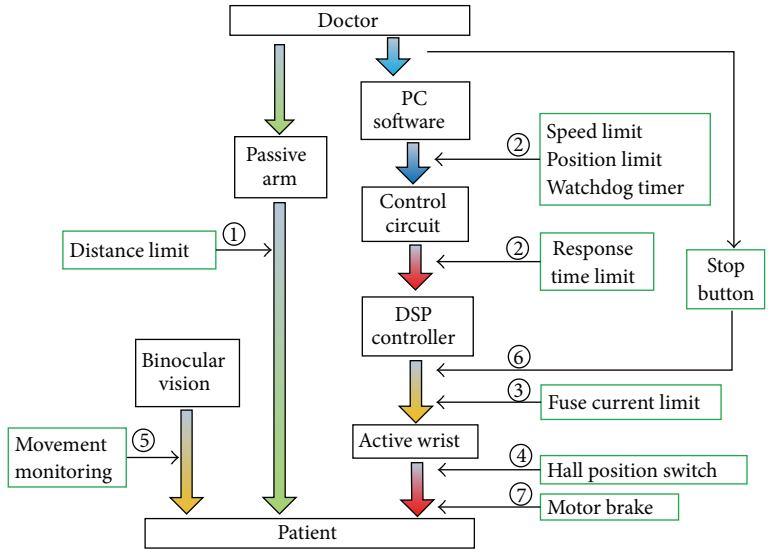

Figure 10: The safety precautions of MMS.

into five types: Type I: pink, flat; Type II: light red, flat; Type III: dark red, flat; Type IV: purple, slightly thicker, and Type V: significantly thicker or nodular [5]. PWS lesion distribution is shown in Table 1. There are 29 (9.8%), 46 (15.6%), 117 (39.5%), 77 (26.0%), and 27 (9.1%) lesions, respectively, for each type.

2.6.2. Treatment Protocols of MMS Assisted PDT Treatment of PWS. In the treatment, a PDT device (produced by Beijing Newraysing Laser Tech Co. Ltd.; power output of 5 W) was used to provide a continuous KTP laser with a wavelength of 532 nm. The laser was delivered through an optic fiber with a flat cut tip, which was held by the active wrist. The laser beam showed quasi-Gaussian output; the power density was 80–100 mW/cm^2.

As shown in Figure 11, after a routine allergy test, the doctor selected the lesion of the patient and protected normal skin around lesion by applying black cloth. The patient was then injected intravenously with a photosensitizer, after which the laser irradiation was performed immediately. The doctor operated the passive arm, so that the laser fiber was positioned perpendicular to the surface of the PWS lesion. The binocular vision system measured the position of the lesion and then transferred the information to workstation. The PDT device delivered the laser spot which was automatically guided by the active wrist to generate a uniform irradiation over the entire lesion. With the assistance of the MMS, the doctor had more time and energy during the treatment to diagnose the lesion response and carry out treatment accordingly. The laser irradiation lasted 20–50 minutes with a total energy density of 120–300 J/cm^2.

The doctors can select different treatment modes in the human-computer interface. Simultaneously, the binocular vision system monitors the whole operation and the safety system of MMS guarantees patient safety during the treatment.

3. Results and Discussion

3.1. Criterions of Therapeutical Evaluation and Follow-Up. Until now, there are no standard evaluation criteria to assess the therapeutical effectiveness of the PDT treatment of PWS. In this paper, the criteria, which is introduced in [3, 5, 13–15] and is widely used by other physicians for PWS PDT

Table 1: Clinical characteristic.

Number of Patients	Number of Lesions	Gender		Age	Lesion type				
		Male	Female		I	II	III	IV	V
186	296	74 (39.8%)	112 (60.2%)	3–42	29 (9.8%)	46 (15.6%)	117 (39.5%)	77 (26.0%)	27 (9.1%)

Table 2: The statistical results of traditional and MMS assisted PDT treatment of PWS.

Grades	Traditional PDT treatment of PWS		MMS assisted PDT treatment of PWS	
	Number of lesions	Percentage (%)	Number of lesions	Percentage (%)
I	128	6.6	15	5.1
II	746	38.3	124	41.9
III	923	47.4	145	49.0
IV	145	7.4	11	3.7
V	7	0.3	1	0.3
Total of lesions	1949		296	

evaluation, is adopted to assess the clinical outcomes of the MMS assisted PDT treatment of PWS. Therapeutic responses are recorded and defined in five grades: Grade I excellent: colour is close to normal skin colour and no scar formation; Grade II good: marked blanching, thicker lesion become flat, no scar formation; Grade III fair: partial blanching, thicker lesion becomes moderately flat; Grade IV poor: slight blanching, thicker lesion becomes slightly flat; and Grade V: no change.

The follow-up time ranged from 6 months to 3 years. The lesions were examined visually by experts of the Chinese PLA General Hospital. Photographs of pretreatment and posttreatment conditions were taken and evaluated. By comparing the lesion color after treatment to the lesion color before treatment, the grade of therapeutic responses was determined and recorded by the same doctor, who is unfamiliar with the patient group. Other responses, such as side-effects and scar formations, were also recorded.

3.2. Treatment Outcomes. Each of the patients showed different degrees of edema after treatment, but no scaring or pigmentation was observed. All of the PWS lesions showed different degrees of improvement. The clinical outcomes displayed good therapeutic results. Parts of the patients' representative photographs of before and after the PDT treatment using the MMS can be seen in Figure 12.

3.3. Statistical Analysis. The mechanism of PDT treatment involves the complex interactions of various factors including light, photosensitizer, oxygen, and diseased tissue. The qualitative research of a single factor cannot reveal the overall therapeutic effect of the PDT treatment of PWS [16]. The statistical comparison of nonparametric values was used to evaluate the treatment response between the MMS assisted and the traditional PDT treatment of PWS [5, 13].

As mentioned above, the therapeutic outcomes were graded as excellent, good, fair, poor, or no change. As shown in Table 2, there were 15 lesions (5.1%) which achieved excellent response, 124 lesions (41.9%) which showed good results, fair response appeared in 145 lesions (49.0%), in 11 lesions (3.7%) poor results were observed, and 1 lesion (0.3%) showed no change. In [3], the Chinese PLA General Hospital reported 1949 PWS lesions in 1385 patients treated by PDT. Excellent results were achieved in 128 lesions (6.6%), 746 lesions (38.3%) yielded good results, 923 lesions (47.4%) showed moderate results, 145 lesions (7.4%) showed poor results, and in 7 lesions (0.3%) no visible change was observed.

As shown in Figure 13, the percentage of Grade I and Grade IV outcomes in the MMS assisted treatment are lower than those in traditional treatment. Accordingly, the percentage rate of Grade II and Grade III are higher in the MMS assisted treatment, and the percentage rates of Grade V are the same.

Given the statistical analysis, although there was no significant improvement of the MMS assisted treatment method compared to the traditional treatment method, the therapeutic effectiveness of the MMS assisted treatment was almost as good as the results of traditional treatment. In particular, there were more lesions which achieved good and fair responses in the MMS assisted treatment. Considering that the traditional treatment group was achieved by experts with more than 10 years of experience in PWS-PDT treatment, the therapeutic effectiveness achieved by the MMS was also an acceptable positive result with the significant advantage of reducing doctors' work load, improving laser irradiation uniformity, and the possibility of tirelessly continuous long-time work. Therefore, the MMS is useful in assisting doctors for PDT treatment of PWS.

3.4. Discussion. Factors, such as depth and size of the lesion, type and dose of the photosensitizer, laser wavelength, interval time between drug injection and laser irradiation, and laser irradiation dose can make different degrees of influence on the results of PWS-PDT treatment. The following factors correlated with the clinical effect are summarized [5].

(1) Depth and size of PWS lesion: a good response can be obtained when the lesion depth is less than 830 μm and poor or no response is achieved at 1000 μm or

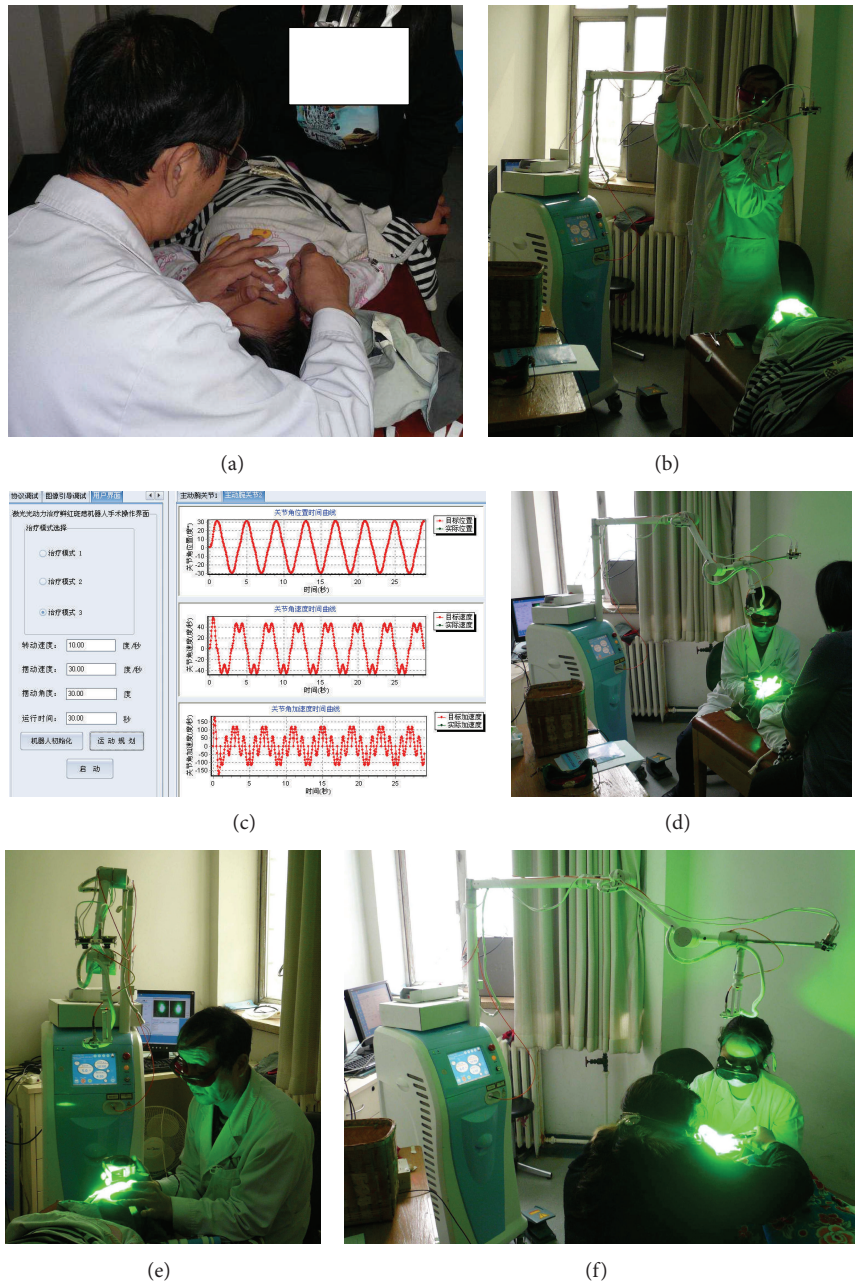

FIGURE 11: The clinical treatment with MMS. (a) Lesion selection and patient protection. (b) Passive arm operation. (c) The human-computer interface. (d) Active wrist operating the laser fiber. (e) Lesion response diagnosis. (f) Another case of MMS assisted PDT treatment of PWS.

deeper. Larger lesions, particularly those extended to the lip, showed poor response.

(2) Anatomical location of PWS lesion: generally, lesions in the forehead, lateral aspect of the cheek, neck, chest, and shoulder often showed good responses.

(3) Type and dose of photosensitizer: as discussed by Gu et al. [15], different photosensitizers have different characteristics depending on the PWS lesion. The photodynamic effect can be enhanced if a higher drug dose is used, but there is a possibility of poisoning the patient.

(4) Energy and fluence rate of the laser: for children and lightly colored superficial lesions, a lower fluence rate should be used in order to avoid scar formation. For thick, dark, and deep lesions, higher fluence rates should be used in order to reach the deeper lesion.

(5) Uniformity of laser irradiation: in order to avoid overexposing and to prevent overheating and scaring, it is critical to insure an even light distribution.

(a) (b)

Figure 12: The clinical outcome of MMS assisted PDT treatment for PWS. (a) Before treatment. (b) After treatment.

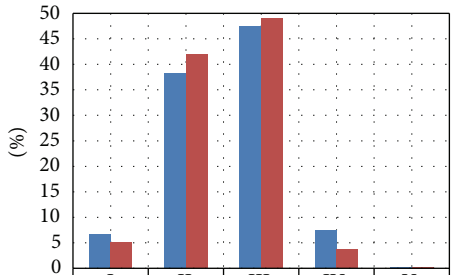

	I	II	III	IV	V
Traditional treatment	6.6	38.3	47.4	7.4	0.3
MMS assisted treatment	5.1	41.9	49	3.7	0.3

Figure 13: The statistical comparison of traditional and MMS assisted PDT treatment of PWS.

(6) Experience of doctors: during the course of treatment, the irradiation time and dose of the laser can be adjusted according to the lesion's reaction and the tissue temperature. The sensitivity to the PDT treatment is quite different for various PWS patients. The treatment experience of doctors is very important to make correct judgments, especially for the first treatment.

(7) Posttreatment care: patients should avoid strong light for half to one month after the therapy. Edema and scabs should be carefully taken care of. The result of the posttreatment phase also affects the therapeutical effectiveness of the PWS-PDT treatment.

The complex influencing factors of the PWS-PDT treatment might explain why there are some poor and no change responses, and why the percentage of Grade I results is lower than in the traditional treatment. Although the MMS can only optimize some of the listed factors, considering the advantages (discussed following) of the MMS and the therapeutical evaluation (discussed above), the MMS is feasible and useful in assisting doctors giving PDT treatment for PWS.

The advantages and limitations of MMS are summarized below.

Advantages

(1) Improving the uniformity of laser irradiation: the MMS has the same advantages as a medical robot: high positioning accuracy, firm grip, and smooth movement. In the MMS, a binocular vision system can position the PWS lesion precisely; the medical manipulator can firmly hold the laser fiber and operate it smoothly and with high accuracy. The MMS improves the uniformity of laser irradiation which ensures that every section of the PWS lesion receives the same quantity of laser radiation during the PDT process. Additionally, the system avoids overexposing or overheating the lesion.

(2) Lightening doctors' workload: the laser fiber is automatically operated by an active wrist in the MMS, which lightens the doctors' workload. This makes it possible for the doctor to devote more energy to diagnose the lesion's response and pay more attention on the patient's comfort during the PDT treatment, which is clinically favorable.

(3) Treating more patients: the MMS can operate the laser fiber continuously without rest, so that doctors have the opportunity to take care of a larger amount of patients.

(4) Reducing influence of personal factors: in a conventional manually operated treatment, laser irradiation of a PWS lesion is arbitrary and nonuniform. In the MMS assisted treatment, the movement of the laser fiber can be quantified, which reduces the impact of human factors and is good for therapeutical evaluation.

Limitations

(1) A major problem is that if the patient suddenly moves too much, the binocular vision system will lose the position of the PWS lesion. The positioning algorithm is not stable enough under the condition of high-intensity laser irradiation.

(2) The workspace of the active wrist is limited. Sometimes, during a clinical treatment, the laser fiber interfered with the active wrist during the swinging movement, especially when the PWS lesion had a large surface area.

(3) The active wrist does not have enough DOF. It is not possible for a patient to lie on a bed motionless throughout the treatment. Due to pain or an uncomfortable posture, the PWS lesion was turned a certain angle by the movement of patient. Two DOF are not enough to follow the lesion movement automatically.

(4) During the clinic treatment, doctors needed more time to prepare the MMS. The human-computer interface was not convenient enough for doctors to use. The process of operating the MMS is still complex; the initial position of laser spot needed to be manually adjusted by doctors using the computer interface.

4. Conclusions

In this paper, a medical manipulator system is put forward to assist doctors for the PDT treatment of PWS. The uniformity of laser irradiation can be improved by precise and stable movement of a medical manipulator. The doctors' workload can be lightened by operating the laser fiber with the MMS instead of moving it manually. More patients can be treated by the continuous and tireless work of the MMS. Clinical results show that the MMS is useful in PDT treatment of PWS; it can improve the therapeutical effectiveness and doctor satisfaction. The MMS appears to have a promising future, and it hopefully will become an objective and reliable PWS therapy machine in the future.

Conflict of Interests

The authors declare that there is no conflict of interests regarding the publication of this paper.

Acknowledgment

This study was financially supported by High-Tech Research and Development Program of China (863 Project) under Grant no. 2007AA04Z231, and by Staff Independent Innovation Fund of SNPTC (State Nuclear Power Technology Company, China) with no. SNP-KJ-CX-2013-10.

References

[1] W. Ying and G. Ying, "Modern techniques for non-invasive detection of port-wine stain therapeutic outcome: a review," *Chinese Journal of Laser Medicine & Surgery*, vol. 17, no. 1, pp. 60–63, 2008.

[2] N. Y. Huang, *Mathematical Modeling and Verification study on Photodynamic Therapy for Port Wine Stains (D)*, People's Liberation Army General Hospital Postgraduate Medical School, Beijing, China, 2005.

[3] Y. Gu, N. Y. Huang, J. Liang, Y. M. Pan, and F. G. Liu, "Clinical study of 1949 cases of port wine stains treated with vascular photodynamic therapy (Gu's PDT)," *Annales de Dermatologie et de Venereologie*, vol. 134, no. 3, pp. 241–244, 2007, (French).

[4] K. Yuan, Q. Li, W. Yu, and Z. Huang, "Photodynamic therapy in treatment of port wine stain birthmarks—recent progress," *Photodiagnosis and Photodynamic Therapy*, vol. 6, no. 3-4, pp. 189–194, 2009.

[5] Z. P. Qin, K. L. Li, L. Ren, and X. J. Liu, "Photodynamic therapy of port wine stains—a report of 238 cases," *Photodiagnosis and Photodynamic Therapy*, vol. 4, no. 1, pp. 53–59, 2007.

[6] Z. Huang, "Photodynamic therapy in China: over 25 years of unique clinical experience: part one—history and domestic photosensitizers," *Photodiagnosis and Photodynamic Therapy*, vol. 3, no. 1, pp. 3–10, 2006.

[7] D.-Y. Xu, "Research and development of photodynamic therapy photosensitizers in China," *Photodiagnosis and Photodynamic Therapy*, vol. 4, no. 1, pp. 13–25, 2007.

[8] N. Huang, J. Zhu, Y. Wang et al., "Photodynamic therapy for port wine stains assisted by a novel robotic system," in *Optics in Health Care and Biomedical Optics IV*, vol. 7845 of *Proceedings of SPIE*, pp. 1–7, Beijing, China, October 2010.

[9] P. Patrizia, M. Giovanni, G. Rosati, and S. Masiero, "Robotic technologies and rehabilitation: new tools for stroke patients' therapy," *BioMed Research International*, vol. 2013, Article ID 153872, 8 pages, 2013.

[10] H. Koga, Y. Usuda, M. Matsuno et al., "Development of the oral rehabilitation robot WAO-1," in *Proceedings of the 2nd Biennial IEEE/RAS-EMBS International Conference on Biomedical Robotics and Biomechatronics (BioRob '08)*, pp. 556–561, Scottsdale, AZ, USA, October 2008.

[11] H. Koga, Y. Usuda, M. Matsuno et al., "Development of oral rehabilitation robot for massage therapy," in *Proceedings of the 6th International Special Topic Conference on Information Technology Applications in Biomedicine*, pp. 111–114, Tokyo, Japan, November 2007.

[12] J. Solis, Y. Obokawa, H. Ishii, H. Koga, A. Takanishi, and A. Katsumata, "Development of oral rehabilitation robot WAO-1R designed to provide various massage techniques," in *Proceedings of the 11th IEEE International Conference on Rehabilitation Robotics (ICORR '09)*, pp. 457–462, Kyoto, Japan, June 2009.

[13] K. Yuan, Q. Li, W. Yu, D. Zeng, C. Zhang, and Z. Huang, "Comparison of photodynamic therapy and pulsed dye laser in patients with port wine stain birthmarks: a retrospective analysis," *Photodiagnosis and Photodynamic Therapy*, vol. 5, no. 1, pp. 50–57, 2008.

[14] Z. Huang, "Photodynamic therapy in China: over 25 years of unique clinical experience. Part two—clinical experience," *Photodiagnosis and Photodynamic Therapy*, vol. 3, no. 2, pp. 71–84, 2006.

[15] Y. Gu, F. G. Liu, and K. Wang, "A clinic analysis of 1216 cases of port wine stain treated by photodynamic therapy," *Chinese Journal of Laser Medicine & Surgery*, vol. 10, no. 2, pp. 86–89, 2010, (Chinese).

[16] Z. Yang, H. Nai-Yan, and G. Ying, "Advances in research of photodynamic therapy for port wine stain," *Chinese Journal of Laser Medicine & Surgery*, vol. 20, no. 1, 2011, (Chinese).

Hindawi Publishing Corporation
BioMed Research International
Volume 2014, Article ID 354608, 7 pages
http://dx.doi.org/10.1155/2014/354608

Clinical Study

Tattoo-Associated Skin Reaction: The Importance of an Early Diagnosis and Proper Treatment

Andrea Bassi,[1] Piero Campolmi,[1] Giovanni Cannarozzo,[1] Rossana Conti,[1] Nicola Bruscino,[1] Massimo Gola,[1] Stefano Ermini,[2] Daniela Massi,[3] and Silvia Moretti[1]

[1] *Department of Surgery and Translational Medicine, Section of Dermatology, University of Florence Medical School, Hospital P. Palagi, 50125 Florence, Italy*
[2] *Department of Immunology and Allergology, University of Florence Medical School, 50125 Florence, Italy*
[3] *Division of Pathological Anatomy, University of Florence Medical School, 50125 Florence, Italy*

Correspondence should be addressed to Andrea Bassi; bassi76@interfree.it

Received 26 February 2014; Revised 21 June 2014; Accepted 9 July 2014; Published 23 July 2014

Academic Editor: Michael S. Kaminer

Tattoo is going to be a very common practice especially among young people and we are witnessing a gradual increase of numerous potential complications to tattoo placement which are often seen by physicians, but generally unknown to the public. The most common skin reactions to tattoo include a transient acute inflammatory reaction due to trauma of the skin with needles and medical complications such as superficial and deep local infections, systemic infections, allergic contact dermatitis, photodermatitis, granulomatous and lichenoid reactions, and skin diseases localized on tattooed area (eczema, psoriasis, lichen, and morphea). Next to these inflammatory skin reactions we have to consider also the possibility of the development of cutaneous conditions such as pseudolymphomatous reactions and pseudoepitheliomatous hyperplasia. The aim of this study is to underline the importance of an early diagnosis by performing a histological examination especially when we are in front of suspected papulonodular lesions arising from a tattoo, followed by a proper treatment, since cutaneous neoplastic evolution is known to be a rare but possible complication.

1. Introduction

The number of tattooed people has become more prevalent in the last few years for the continuous development of new trends especially among young people. Despite the increasing number of tattooed individuals, there are currently few requirements, little legislation, and few criteria for the safety of tattoos. In Italy, composition of tattoo inks is not regulated by law and their labeling is not compulsory [1]. Frequently, there is no information on packaging, such as expiration date, conditions of use, warnings, or the guarantee of sterility of the contents [2]. Consequently, we are witnessing a gradual increase of numerous potential complications to tattoo placement which are often seen by physicians, but generally unknown to the public [3].

The most common skin reactions to tattoo reported in the literature [4–7] include a transient acute inflammatory reaction due to trauma of the skin with needles and medical complications such as superficial and deep local infections, systemic infections, allergic contact dermatitis, photodermatitis, granulomatous and lichenoid reactions, and skin diseases localized on tattooed area (eczema, psoriasis, lichen, and morphea) (Table 1). These reactions may have different onset of symptoms immediately when the tattoo has been inked into it, days, months, or years later [8–10]. Next to these inflammatory skin reactions we have to consider also the possibility of the development of cutaneous conditions such as pseudolymphomatous reactions [11] and pseudoepitheliomatous hyperplasia [12]. The evolution in neoplastic lymphoma [13, 14], squamous cell carcinoma, and Keratoacanthoma [15] is a rare outcome, since this neoplastic condition usually appears when they are fully evolved and not with "premalignant" condition. Despite that, it is mandatory to perform histological examination when we are in front of suspected papulonodular lesions arising from a tattoo.

The aim of this study is to underline the importance of an early diagnosis and proper treatment of tattoo reactions, since cutaneous neoplastic evolution is known to be a rare

Table 1: Dermatologic disorders and complications after tattooing.

Complications after tattooing	Clinical features	Onset of symptoms
Allergic disorders	Allergic dermatitis	Days to weeks
	Photoallergic reaction	After sun exposure
Skin infections	Erysipelas	First few days
	Gangrene	=
	Sepsis	=
	Impetigo	=
	Ecthyma	=
	Cellulitis	=
	Tetanus	Weeks to years
	Lepra	=
	Syphilis	=
Viral infections	Molluscum contagiosum	Weeks to months
	Verruca vulgaris	=
	Hepatitis B, C	=
	AIDS	=
Mycoses	Tinea cutis glabrae	After weeks
	Zygomycoses	After months
Tumors	Lymphoma	Years
	Carcinoma basocellular	=
	Carcinoma spinocellular	=
	keratoacanthoma	=
	Melanoma	=
Skin disease localized in tattooed area	Psoriasis	Weeks to years
	Lichen planus	=
	Morphea	=
	Pseudolymphoma	=
	Pseudoepitheliomatous hyperplasia	=

but possible complication, even if this process was not found in our experience.

2. Methods

During the period from May 2012 to April 2013, a total of 16 patients (6 women, 10 men) were treated at the Department of Dermatology in Florence for the development of cutaneous reactions secondary to tattoos. All these patients underwent allergological examination by means of patch tests according to the standard SIDAPA series (Italian Society of Allergological, Occupational and Environmental Dermatology) (Table 2(a)) and the International Contact Dermatitis Research Group guidelines, using the IQ chamber method (Chemotechnique Diagnostics, Vellinge, Sweden). Standard allergological examination was supplemented with various metal haptens associated with different tattoo pigments (Table 2(b)). Five patients were tested directly with the pigment used for the tattoo, while it was impossible for the others. A punch biopsy of the skin was performed in all patients for histopathological examination. Cutaneous reactions were documented with photographs taken by a Canon digital camera.

Table 2: (a) The 25 haptens of the Italian SIDAPA series with their own concentrations and (b) the other seven metal haptens with their concentrations and different dyes in which they are contained.

(a)

Thiuram mix	1% pet.
Potassium dichromate	0.5% pet.
Balsam Peru	25% pet.
Phenylisopropyl-p-phenylenediamine	0.1% pet.
Kathon CG	0.01% aqua
p-Phenylenediamine	1% pet.
Lanolin alcohol	30% pet.
Colophony	20% pet.
Neomycin sulfate	20% pet.
Cobalt chloride	1% pet.
Epoxy resin	1% pet.
Formaldehyde	1% aqua
Mercaptobenzothiazole	2% pet.
p-ter-Butylphenol-formaldehyde resin	1% pet.
Nickel sulphate	5% pet.
Disperse yellow 3	1% pet.
Fragrance mix + sorbitan sesquioleate	8% pet.
Paraben mix	16% pet.
Disperse blue 124	1% pet.
Benzocaine	5% pet.
Dibromodicyanobutane	0.3% pet.
Corticosteroid mix	2.01% pet.
Lyral	5% pet.
Mercapto mix	2% pet.
Desoximetasone	1% pet.

(b)

Cadmium chloride	1% pet.	Yellow
Chromium oxide	2% aqua	Green
Mercury metal	0.5% pet.	Red
Copper sulfate	1% aqua	Blue
Ferric oxide	2% pet.	Black
Aluminium chloride	2% pet.	Purple
Zinc metal	1% pet.	White

3. Results

In the above-mentioned period for the 16 patients, the reactions to tattoo were 5 foreign body granulomatous reactions (Figure 1), 4 lichenoid reactions (Figure 2), 2 psoriasis, 1 pseudoepitheliomatous hyperplasia (Figure 3), and 4 pseudolymphomatous reactions of which 3 were on red tattoos and 1 was on a black tattoo (Figures 4 and 5). All the 16 patients were negative for allergological examination with the standard SIDAPA series and the tattoo additional one. Patch testing with the real pigment used for the tattoo in 5 patients was also negative. Histological examination for the foreign body granulomatous reactions revealed granulomatous depositions of exogenous pigment in the background

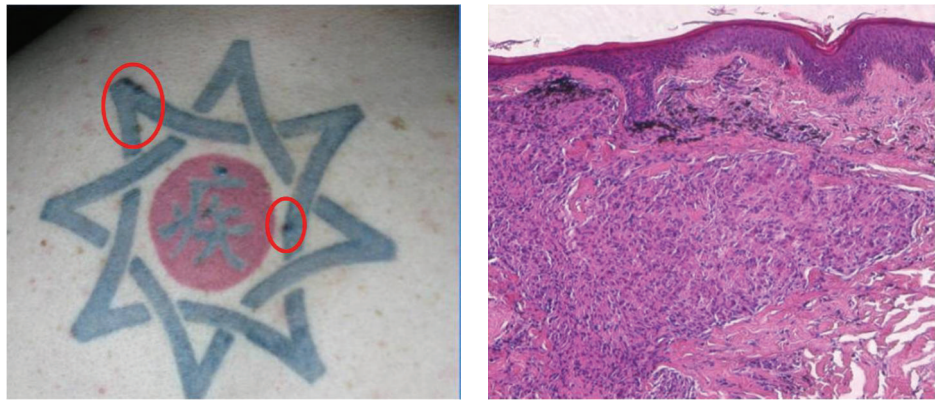

Figure 1: Foreign body granulomatous reaction on a black tattoo and relative histology with granulomatous depositions of exogenous pigment in the background of granulomatous-productive inflammation of the dermal stroma.

Figure 2: Lichenoid reaction on a black tattoo and relative histology with a widespread vacuolar basal epidermic degeneration with a deep dermal lymphohistiocytic infiltrate into a lichenoid pattern, associated with deposition of exogenous pigment.

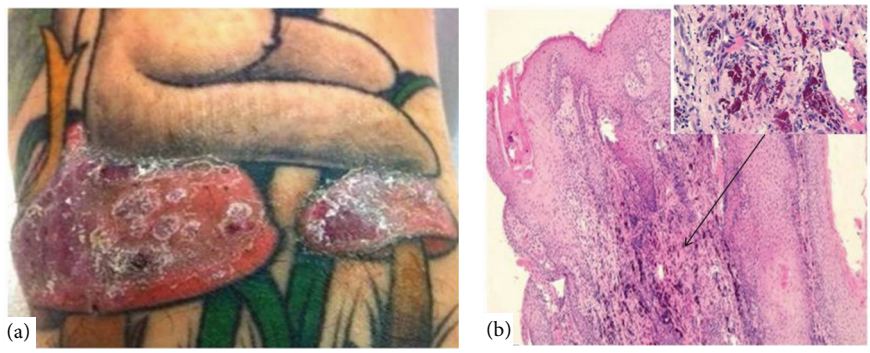

Figure 3: (a) Pseudoepitheliomatous hyperplasia on a red tattoo and relative histology with epidermal pseudoepitheliomatous hyperplasia and follicular hyperkeratosis (H&E, original magnification ×5); (b) the part indicated by the arrow shows an inflammatory infiltrate in the dermis, composed of lymphocytes and plasma cells and dermal exogenous pigment deposition (H&E, original magnification ×40).

of granulomatous-productive inflammation of the dermal stroma. The lichenoid reactions showed a widespread vacuolar basal epidermic degeneration with a deep dermal lymphohistiocytic infiltrate into a lichenoid pattern, associated with deposition of exogenous pigment. The pseudolymphomatous reactions demonstrated the presence of colour (red or black) exogenous pigment in the background of a reactive lymphoid hyperplasia in the superficial and medium dermis. The specimens were analysed by PCR-based IgH chain (FR2A-JH and FR3A-JH segments), T-Cell Receptor gamma and T-Cell Receptor beta clonality detection, and heteroduplex analysis of PCR products revealing polyclonal rearrangement of these regions. Polarizing microscopy showed no signs of birefringence. The pseudoepitheliomatous hyperplasia on the red tattoo showed an epidermal pseudoepitheliomatous hyperplasia and follicular hyperkeratosis with an exogenous red pigment deposition which was demonstrated within the dermis, associated with a mixed inflammatory infiltrate, composed of lymphocytes and plasma cells.

Patients with inflammatory skin reaction (granulomatous, lichenoid, and psoriasis) were treated with topical steroid with rapid improvement of skin lesions. Patients

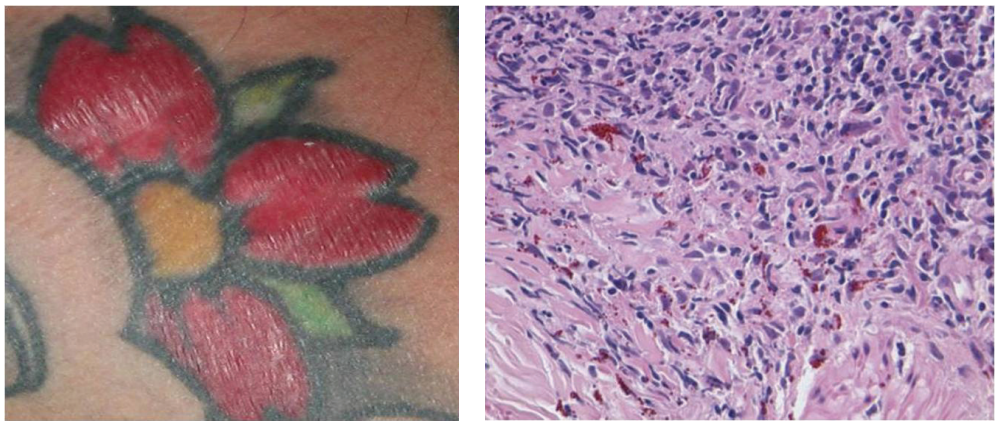

Figure 4: Pseudolymphomatous reaction on a red tattoo and relative histology with the presence of red colour exogenous pigment in the background of a reactive lymphoid hyperplasia in the superficial and medium dermis.

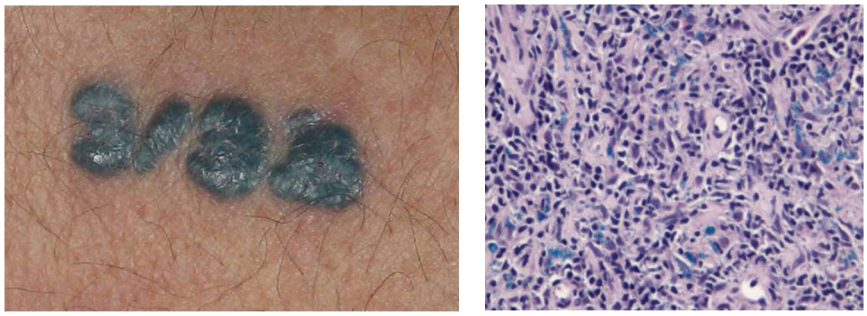

Figure 5: Pseudolymphomatous reaction on a black tattoo and relative histology with the presence of black colour exogenous pigment in the background of a reactive lymphoid hyperplasia in the superficial and medium dermis.

Figure 6: Resolution of the lesions of pseudolymphoma on the red portion of the tattoo after 4 sessions of Q-Switched Nd:YAG laser.

with neoplastic reaction (pseudoepitheliomatous hyperplasia and pseudolymphoma) initially underwent systemic steroid treatment (methylprednisolone acetate 40 mg PO daily) resulting into complete clearance of the lesions, but they reappeared immediately after ten days. Subsequent treatment with Q-Switched Nd:YAG laser (DEKA M.E.L.A, srl, Calenzano, Italy) resulted into almost complete lesion disappearance (Figure 6). Q-Switched Nd:YAG laser was used in two different wavelengths at 1064 nm with a spot size of 3 mm and a fluence of 11–12.5 J/cm^2 and 532 nm with a spot size of 3 mm and a fluence of 3 J/cm^2.

4. Discussion

Tattooing has recently become increasingly popular and not only among young people, giving rise to parallel increase of adverse reactions. With the increasing incidence of tattooing fashion trend in society, physicians should be able to recognize tattoo complications and also appropriately counsel their patients on risks of tattoo placement [16]. Numerous potential complications secondary to tattoo placement have been reported in literature. Tattoo reactions can be divided into three main categories: inflammatory, infectious, and neoplastic. Inflammatory manifestations include focal oedema, pruritus, papules, or nodules at the tattoo site. Histologically they can be classified as lichenoid, eczematoid, foreign body granulomatous, and sarcoidal [17]. Less commonly, psoriasiform, morpheaform, and vasculitic reaction have also been reported [18, 19]. The infectious reaction can be generally distinguished in bacterial, viral or mycotic and they can appear as superficial or with deep skin involvement. Rare but possible reactions are represented by pseudoepitheliomatous hyperplasia and pseudolymphoma. They are not considered as real premalignant conditions. The neoplastic complication described within tattoo pigments includes keratoacanthoma, squamous cell and basal cell carcinoma, leiomyosarcoma, and melanoma. When we observe tattoo malignancies, usually squamous cell carcinoma, they are fully evolved and they do not present as "premalignant" condition. According to the literature, the most frequent tattoo reactions concern allergic contact dermatitis due to delayed hypersensitivity reaction to different pigments contained in the tattoos [20, 21]. The main pigment causing allergic reaction is the red one, due to the presence of mercury and its sulphides [22]. However, nowadays most reactions are not due to the traditional presence of mercury sulphides, but due to new organic pigments (e.g., Pigment Red 181 and Pigment Red 170) [1]. Different from red tattoo, the blue, green, and black tattoos are a less frequent cause of allergic contact dermatitis [23–26]. Actually allergological reactions to temporary henna tattoos due to the *para*-phenylenediamine are very common [27]. The first conclusion of our study showed that the results of these 16 patients for standard series and additional and specific haptens were negative. Therefore we noticed that allergic reactions due to sensitization to haptens contained in tattoos are not very frequent. A possible explanation is that needles used by tattoo artists, passing through the skin and inoculating haptens directly in the dermis, could bypass the normal mechanism of hapten processing. In fact, the first phase of the hapten processing usually occurs in the epidermis, where antigen presenting cells are present in great number, whereas the inoculation of the hapten in the dermis without any adjuvant could escape the first phase of the innate immunity. For example, we can suggest that whereas a typical hypersensitivity reaction, such as the one directed towards p-phenylenediamine, is possibly due to the activation of memory T cells previously activated by occasional contact (i.e., hair dye), it is unlikely that we could have been in contact with substances present in tattoo inks.

Even the most recent subcutaneous vaccinations (such as the flu vaccine) need the presence of adjuvants. Moreover, the nature of the antigen is different, viral particles being more immunogenic than haptens.

Another hypothesis is that tattoo composition is very heterogeneous and in continuous evolution (Table 3), and we have tested solely the SIDAPA standard series and only few metal haptens associated with different tattoo pigments.

The second conclusion is related to the possible development of neoplastic skin manifestation arising from a tattoo. Four of the 16 patients presented a histological examination compatible with a pseudolymphomatous reaction and one patient presented a pseudoepitheliomatous hyperplasia reaction. The pathogenesis of malignancies in tattoos is far from being obvious since it is not clarified if the development of neoplasms in tattoos is coincidental or is somehow due to the tattoo. The trauma induced by the procedure (puncturing the skin) has always been pointed out in the literature as

Table 3: Other possible ingredients and haptens contained in the tattoo ink and pigment colour.

Tattoo ink/pigment color	Ingredient
Black	Iron oxide
	Carbon
	Logwood
Brown	Ochre (ferric oxide)
Red	Cinnabar/mercuric sulfide
	Cadmium red
	Iron oxide/common rust
	Napthol-AS pigment
Yellow	Cadmium yellow
	Ochre
	Curcuma yellow
	Chrome yellow ($PbCrO_4$, often mixed with PbS)
Green	Chromic oxide (Casalis Green or Anadomis Green)
	Lead chromate
	Phthalocyanine dyes
	Ferrocyanides and ferricyanides
Blue	Azure blue
	Cobalt blue
	Cobalt phthalocyanine
	Cobalt aluminate
Violet (purple)	Manganese ammonium pyrophosphate
	Various aluminum salts
	Dioxazine/carbazole
White	Lead carbonate
	Titanium dioxide
	Barium sulfate
	Zinc oxide
Henna	Henna dye and paraphenylenediamine (PPD)

one of the main causes: tattoo pigments do not remain inert in the dermis because a skin inflammatory reaction occurs during the whole life in an attempt to degrade the foreign material, and it is unknown exactly what type of reactions occurs [28]. This inflammatory reaction starts as being local but can become generalized. Trauma is probably not the only factor, since tattoo inks have been shown to contain numerous potentially hazardous and carcinogenic compounds that hypothetically could be tumorigenic [29]. However, the potential carcinogenicity or toxicity related to the pigments/dyes or their byproducts still remains unclear [30]. Unfortunately, only in vitro data are available showing that some azo dyes, under certain circumstances (laser therapy, UV exposure), may lead to the increase of some carcinogenic substances such as 3,3-dichlorobenzidine [30, 31].

An early diagnosis through skin biopsy, especially with papulonodular growth within the tattoo pigment, is mandatory since neoplastic conditions are not immediately recognized with clinical examination only. For that reason, the transformation from a pseudolymphoma into a lymphoma and the transformation from a pseudoepitheliomatous hyperplasia into a squamous cell carcinoma or keratoacantoma are very rare, but not impossible [13–15].

Once a diagnosis has been established, it is important to remove the lesion. For refractory skin eruptions unresponsive to medical therapy, surgical or laser treatment may be considered. In our patients we have used a Q-Switched Nd:YAG laser capable of emitting two different wavelengths at 1064 nm (useful for dark blue and black pigment) and 532 nm (useful for removal of red, orange, and purple tattoo pigments). The Q-Switched Nd:YAG system releases high energy in extremely short times (max 6 ns), producing a "photoacoustic" effect that breaks down the derma cells containing the tattoo pigment. Thanks to the rupturing of the membrane of these cells, the pigment is released and eliminated by the lymphatic system. These short laser emissions allow for confining the thermal effect exclusively to the target—in this case the tattoo pigment—therefore safeguarding the surrounding tissues [32, 33]. Moreover, laser systems allow the best aesthetic results without leaving scars if compared with surgery that sometimes may be more radical but capable of injuring the underlying tissue.

5. Conclusion

The medical literature contains numerous case reports on dermatological reaction after tattoos procedure. Our experience on a small number of patients underlines that the allergic contact reaction is not the most frequent complication after the tattoo procedure. The potential correlation between tattooing and skin cancer is rare but not impossible, though its pathogenesis is still unclear. Our study is subject to several limitations due to the number of patients involved. Further studies should be done to investigate in depth the possible evolution to malignancy. A follow-up of a large cohort of tattooed people would help to assess whether or not tattooing is an independent risk factor for skin malignances. This paper should advise not only dermatologist but also physicians about the possible risk of malignancies in tattoo reactions. In suspected cases, especially in front of papulonodular lesions arising from a tattoo, it is important to perform an early diagnosis through histopathology followed by removal of the lesion.

Conflict of Interests

All authors declare that they have no conflict of interests neither financial nor personal in this work. They also affirm that the paper has not been published previously and is not being considered currently by any other publication.

Authors' Contribution

All authors and contributors have read and approved the paper.

References

[1] E. Cinotti, R. Gallo, and A. Parodi, "Reazioni avverse ai tatuaggi," *Annali Italiani di Dermatologia Allergologica Clinica e Sperimentale*, vol. 66, no. 1, pp. 23–31, 2012.

[2] K. Lehner, F. Santarelli, R. Vasold, B. König, M. Landthaler, and W. Bäumler, "Black tattoo inks are a source of problematic substances such as dibutyl phthalate," *Contact Dermatitis*, vol. 65, no. 4, pp. 231–238, 2011.

[3] A. E. Ortiz and T. S. Alster, "Rising concern over cosmetic tattoos," *Dermatologic Surgery*, vol. 38, no. 3, pp. 424–429, 2012.

[4] S. A. Sanghavi, A. M. Dongre, and U. S. Khopkar, "Tattoo reactions-an epidemic on the surge: a report of 3 cases," *Indian Journal of Dermatology, Venereology and Leprology*, vol. 79, no. 2, pp. 231–234, 2013.

[5] C. Piérard-Franchimont, J. F. Hermanns, and G. E. Piérard, "Skin reactions to tattoo ink," *Revue Médicale de Liège*, vol. 66, pp. 430–433, 2011.

[6] S. M. Wenzel, I. Rittmann, M. Landthaler, and W. Bäumler, "Adverse reactions after tattooing: review of the literature and comparison to results of a survey," *Dermatology*, vol. 226, no. 2, pp. 138–147, 2013.

[7] S. Garcovich, T. Carbone, S. Avitabile, F. Nasorri, N. Fucci, and A. Cavani, "Lichenoid red tattoo reaction: histological and immunological perspectives," *European Journal of Dermatology*, vol. 22, no. 1, pp. 93–96, 2012.

[8] J. Post and P. Hull, "Tattoo reactions as a sign of sarcoidosis," *Canadian Medical Association Journal*, vol. 184, no. 4, p. 432, 2012.

[9] S. A. Sweeney, L. D. Hicks, N. Ranallo, N. S. IV, and A. C. Soldano, "Perforating granulomatous dermatitis reaction to exogenous tattoo pigment: a case report and review of the literature," *The American Journal of Dermatopathology*, vol. 35, no. 7, pp. 754–756, 2013.

[10] F. A. M. Cruz, D. Lage, R. M. Frigério, M. C. Zaniboni, and L. H. F. Arruda, "Reactions to the different pigments in tattoos: a report of two cases," *Anais Brasileiros de Dermatologia*, vol. 85, no. 5, pp. 708–711, 2010.

[11] P. Campolmi, A. Bassi, P. Bonan et al., "Cutaneous pseudolymphoma localized to black tattoo," *Journal of the American Academy of Dermatology*, vol. 65, no. 5, pp. e155–e157, 2011.

[12] T. S. Breza Jr., A. K. O'Brien, and F. L. Glavin, "Pseudoepitheliomatous hyperplasia: an unusual tattoo reaction," *JAMA Dermatology*, vol. 149, no. 5, pp. 630–631, 2013.

[13] O. P. Sangueza, S. Yadav, C. R. White Jr., and R. M. Braziel, "Evolution of B-cell lymphoma from pseudolymphoma: a multidisciplinary approach using histology, immunohistochemistry, and Southern blot analysis," *The American Journal of Dermatopathology*, vol. 14, no. 5, pp. 408–413, 1992.

[14] N. Anandasabapathy, M. Pulitzer, W. Epstein, K. Rosenman, and J. Latkowski, "Pseudolymphoma evolving into diffuse large B-cell lymphoma," *Dermatology Online Journal*, vol. 14, article 22, no. 5, 2008.

[15] N. Kluger, C. Minier-Thoumin, and F. Plantier, "Keratoacanthoma occurring within the red dye of a tattoo," *Journal of Cutaneous Pathology*, vol. 35, no. 5, pp. 504–507, 2008.

[16] E. Juhas and J. C. English, "Tattoo-Associated Complications," *Journal of Pediatric and Adolescent Gynecology*, vol. 26, no. 2, pp. 125–129, 2013.

[17] R. Korner, C. Pfholer, T. Vogt et al., "Histopathology of body art revisited-analysis and discussion of 19 cases," *Journal der Deutschen Dermatologischen Gesellschaft*, vol. 11, pp. 1073–1080, 2013.

[18] M. Mahalingam, E. Kim, and J. Bhawan, "Morphea-like tattoo reaction," *The American Journal of Dermatopathology*, vol. 24, no. 5, pp. 392–395, 2002.

[19] M. Jolly and M. I. Danila, "Tattoo: inflected vasculitis?" *Journal of Clinical Rheumatology*, vol. 13, p. 49, 2007.

[20] M. M. Tang, H. Beltranimelli, and D. Perruchoud, "A tattoo complicated by allergic contact dermatitis and panniculitis," *Journal of the European Academy of Dermatology and Venereology*, vol. 28, no. 1, pp. 127–128, 2014.

[21] J. Vilaplana, J. M. Chimenos, A. I. Ferńndez, N. Pereira-Veigab, and C. Romaguera, "Problems in the diagnosis of contact dermatitis by tattooing," *Exogenous Dermatology*, vol. 1, no. 6, pp. 307–312, 2002.

[22] G. Chapman and C. A. Hildyar, "Two decades later: a delayed red ink tattoo reactions," *BMJ Case Reports*, 2014.

[23] J. Kazandjieva and N. Tsankov, "Tattoos: dermatological complications," *Clinics in Dermatology*, vol. 25, no. 4, pp. 375–382, 2007.

[24] A. Rostenberg Jr., R. A. Brown, and M. R. Caro, "Discussion of tattoo reactions with report of a case showing a reaction to a green color," *AMA Archives of Dermatology and Syphilology*, vol. 62, no. 4, pp. 540–547, 1950.

[25] D. J. Tazelaar, "Hypersensitivity to chromium in a light-blue tattoo," *Dermatologica*, vol. 141, no. 4, pp. 282–287, 1970.

[26] W. D. Tope, J. L. Arbiser, and L. M. Duncan, "Black tattoo reaction: the peacock's tale," *Journal of the American Academy of Dermatology*, vol. 35, no. 3, pp. 477–479, 1996.

[27] F. Z. Lamchahab, B. Guerrouj, S. Benomar et al., "Henna symbolic tatoo and real dermatitis," *Archives de Pediatrie*, vol. 18, no. 6, pp. 653–656, 2011.

[28] N. Kluger, A. Phan, S. Debarbieux, B. Balme, and L. Thomas, "Skin cancers arising in tattoos: coincidental or not?" *Dermatology*, vol. 217, no. 3, pp. 219–221, 2008.

[29] W. Bäumler, R. Vasold, J. Lundsgaard et al., "Chemical used in tattooing and permanent make up products," in *Proceedings of the Workshop on Technical/Scientific and Regulatory Issues on the Safety of Tattoos, Body Piercing and of Related Practices*, D. Papameletiou, D. Schwela, and A. Zenie, Eds., pp. 21–36, European Commission, Ispra, Italy, 2003.

[30] E. Engel, F. Santarelli, R. Vasold et al., "Establishment of an extraction method for the recovery of tattoo pigments from human skin using HPLC diode array detector technology," *Analytical Chemistry*, vol. 78, no. 18, pp. 6440–6447, 2006.

[31] K. M. Müller, I. Schmitz, and L. Hupe-Nörenberg, "Reaction patterns to cutaneous particulate and ornamental tattoos," *Pathologe*, vol. 23, no. 1, pp. 46–53, 2002.

[32] W. Kirby, C. Chen, A. Desai, and T. Desai, "Successful treatment of cosmetic mucosal tattoos via Q-switched laser," *Dermatologic Surgery*, vol. 37, no. 12, pp. 1767–1769, 2011.

[33] E. F. Bernstein and J. M. Civiok, "A continuously variable beam-diameter, high-fluence, Q-switched Nd: YAG laser for tattoo removal: comparison of the maximum beam diameter to a standard 4-mm-diameter treatment beam," *Lasers in Surgery and Medicine*, vol. 45, pp. 621–627, 2013.